TASER: Towards ALMA System on Chip European Receivers

End of Project Report
2025

Status: Pending (*Draft, Pending, Approved, Released, or Obsolete*)

2025/10/24

Prepared By:	
Name(s) and Signature(s)	**Organization**
E. M. Franks, W. McGenn H. Wang	Univ. of Manchester STFC RAL Space
Approved By:	
Name and Signature	**Organization**
D. George	Univ. of Manchester
G. Fuller	Univ. of Manchester
C. De Breuck	ESO
G. Tan	ESO
T. Mroczkowski	Institute of Space Sciences (ICE-CSIC)
H. Wang / P Huggard	STFC

Change Record

Version	Date	Affected Section(s)	Change Request #	Reason/Initiation/Remarks
A	2024-03-01	All		New document.

Contents

TASER Executive Summary

We report on an ESO ALMA development study conducted in 2024 and 2025 by staff at the University of Manchester and STFC Rutherford Appleton Laboratory (RAL), both in the UK. The work was undertaken by Manchester's Advanced Radio Instrumentation Group (ARIG) and RAL's Millimetre Mave technology (MMT) Groups.

This "Towards ALMA System on Chip European Receivers" *TASER* project features four deliverables:

1. Hardware: an integrated low noise amplifier (LNA) and subharmonic sideband separating mixer unit (SHIRM) covering ALMA Band 2 (67-116 GHz) as a proof of concept.
2. A higher frequency sideband separating mixer unit using discrete InGaAs Schottky diodes covering ALMA Bands 4 and/or 5.
3. Based on the above, a feasibility study outlining the practicability of an integrated LNA+mixer design in one MMIC for ALMA Band 4+5.
4. This final report, describing the design, manufacture, and performance achieved throughout the technical development.

An ALMA Band 2 LNA+SHIRM and a Band 4+5 SHIRM were designed, fabricated, and tested at RAL. Measurement of two integrated LNA+SHIRM blocks confirm that integration does not degrade the performance compared with individual components. Noise temperatures of ~80 K (Block A) and ~50 K (Block B) were achieved. When paired with an additional first stage LNA (with 17 dB of gain and 26 K noise temperature as representative), the calculated system noise is 28 and 27 K respectively, showing that the integrated *TASER* LNA+SHIRMs only add 1 and 2 K of noise.

The ALMA Band 4+5 SHIRM units demonstrated robust, balanced sideband performance across devices and LO frequencies. The compact design and low LO power requirement make this mixer highly suitable for future ALMA upgrades.

The feasibility study explored several future integration strategies, including on-chip couplers (30-50 and 40-60 GHz designs and simulations being presented), alternative LNA+SHIRM topologies, and integration of additional components such as triplers, IF amplifiers, and initial LNA stages. In addition, triple cascode mixers (TCM) show a route towards on-MMIC LNA+Mixer integration with promising simulations. Trade-offs between size, performance, and manufacturability were identified, with promising routes for further miniaturisation and improved matching through balanced amplifier and TCM-based approaches.

1. Introduction

Since 2013, the Atacama Large Millimeter/Submillimeter Array (ALMA) telescope has substantially advanced astronomical research in planetary, stellar, and galactic formation. Notably, protoplanetary regions have been imaged, turbulence from galaxy collisions has been detected, and ALMA contributed to significantly improving our understanding of black holes. [1]As such, ALMA has been recognised as a world leading scientific instrument. Technology has progressed since ALMA's inception, and opportunities to improve the performance of the observatory have been identified. Progress in engineering at millimetre/sub-millimetre wavelengths and semiconductor fabrication techniques have the potential to offer receivers which operate at higher temperatures and wider operational bandwidths, reduced noise, higher pixel density, and more. The ESO ALMA Development study ***Towards ALMA System-on-Chip European Receivers (TASER)*** has worked towards developing key technologies for producing compact and integrated receivers for ALMA. The benefits of receiver integration and miniaturisation are, among others, lower operational costs, reduced production/testing/setup labour, and the potential for high density focal plane array (FPA)/phased array feed (PAF) technology. The results of the *TASER* study are important steps towards implementing the ALMA Development Roadmap [2], and beyond, with the aim of enhancing ALMA's status as a leading scientific tool.

In this document, a background to this project and relevant technologies is given in section 2, followed by a breakdown of each of the three work packages in sections 3, 4 and 5 respectively, a section on future outlook in section 6, and finally a summary in section 7. The sections for work packages one and two outline the final designs, testing methods, and performance of their associated deliverables. The section for work package three forms the third deliverable.

2. Background

Over the past ten years, the University of Manchester's (UoM) Advanced Radio Instrumentation Group (ARIG) have designed and developed a suite of Low Noise Amplifiers (LNAs) covering 67 – 116 GHz, initially intended for use in the ALMA Band 2 receivers [3]. The development of these LNAs then led to work with Rutherford Appleton Laboratories (RAL) on the Cryogenic Array Receiver for Users of the Sardinia Observatory (*CARUSO*) multi pixel receiver, which operates from 70 to 116 GHz. The unique development required for the *CARUSO* receiver was the need for close spacing of the pixels to provide adjacent beams on the sky when the receiver is in use. This meant that each of the receiver pixels had to be

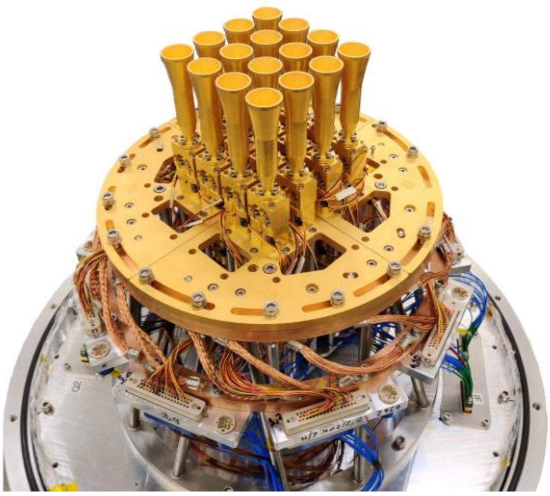

Figure 1 - The *CARUSO* Receiver

contained within the footprint of the feedhorn, as shown in Figure 1 and Figure 2. Therefore, the initial ALMA Band 2 LNA packaging described in [3] had to be miniaturised, along with most of the other receiver components. Due to the short time scale of the *CARUSO* project, the decision was made to individually package each of the components as this would allow complete flexibility to select suitably matched components and to swap components within the pixel if necessary. To achieve this within the required pixel footprint a modified version of the standard UG387/m waveguide flange had to be used.

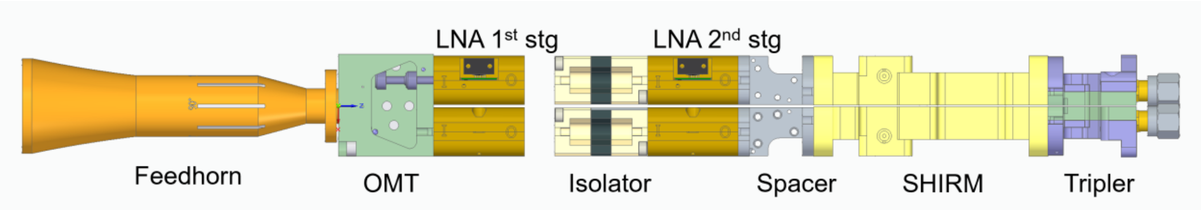

Figure 2 - A *CARUSO* Receiver Chain

Our experience with the *CARUSO* project made it apparent that integration and miniaturisation is an important part of the future of design of high sensitivity, high reliability, broadband and compact receivers for millimetre/sub-millimetre radio telescopes, including for future ALMA upgrades. At high frequencies, and as we look to go to still higher frequencies, it is important to minimise any unnecessary losses or mismatches from the interfaces between component packages. Integrating multiple components into a single package eliminates these interfaces and as such allows the components to be positioned closer. In addition, as multi-pixel receivers such as FPA and PAF based technologies are more in demand due to their speedy survey times [4], the miniaturization of the receivers is of critical importance to allow each of the pixels to be appropriately positioned within the focal plane.

The work in *TASER* builds on the receiver pixel developed in the *CARUSO* project, with the aim to develop the receiver technologies needed for future ALMA upgrades. The most complex components in the receiver pixel are the LNA and Sub Harmonic Image Rejection Mixer (SHIRM), both of which contain multiple other components and technologies. Studying how to integrate these with existing, well proven components, provides a major step towards receiver pixels operating at higher frequencies in the future, including for future ALMA Band 4+5 upgrade projects.

As a key initial integration step towards higher sensitivity, broadband, compact receivers, the *TASER* project aimed to develop and integrate LNA and SHIRM technologies. As a technology demonstrator, a state-of-the-art LNA+SHIRM module operating in the 67-116 GHz (ALMA Band 2) frequency range has been designed, built, and tested. In addition, a state-of-the-art SHIRM for the frequency range 125-211 GHz (ALMA Band 4+5) has been designed. Within these developments aspects of the work required for fully integrated MMIC based receivers at higher frequencies have been explored. A feasibility study outlining the next steps towards greater receiver integration at higher frequencies, specifically ALMA Band 4+5. This work was carried out in three work packages:

WP1. Package Integration of a 67 – 116 GHz LNA and SHIRM
Deliverable – Hardware: an integrated LNA and sideband separating mixer unit covering ALMA Band 2 (67-116 GHz) as a proof of concept.

WP2. A SHIRM suitable for use in future ALMA Band 4+5
Deliverable – A sideband separating mixer unit using discrete Schottky diodes suitable for the full frequency range covered by ALMA Bands 4+5 (125-211 GHz).

WP3. A feasibility study of further LNA + mixer integration options
Deliverable – A feasibility study outlining the practicability of an integrated LNA + mixer design onto one MMIC for ALMA Bands 4+5.

The final deliverable is this report, which describes the design, manufacture, and performance achieved throughout the technical development. The following sections introduce the LNA and SHIRM technology that has been developed prior to the *TASER* project, as well as giving an overview of SHIRM operation.

2.1 LNA Technology Context

The LNAs used in this project are part of a suite of LNAs that have been developed by ARIG over the past ten years, initially through ESO funded development projects for the upgrades to the ALMA Band 2 receivers [3] and [5]. These LNAs are based on MMICs that utilise the Northrop Grumman Corporation's (NGC's) 35 nm gate length indium phosphide (InP) High Electron Mobility Transistor (HEMT) semiconductor process [7]. Initially a series of 2-stage MMICs [5] were developed followed later by several 3-stage MMIC designs. The size of the 2 and 3-stage MMICs is the same, and all the transistor stages have independent gate and drain biasing. The packaged LNAs utilise WR10 waveguides for the input and output ports, and custom waveguide to microstrip transitions couple the signals between the waveguides and the MMIC. The LNA blocks include a DC bias PCB and off-chip decoupling capacitors. Photos of the 3-stage MMIC and surrounding LNA can be seen in figure 20. More details about the LNAs can be found in [3, 5]. The noise and gain performance of the LNAs in [3] is shown below in Figure 3.

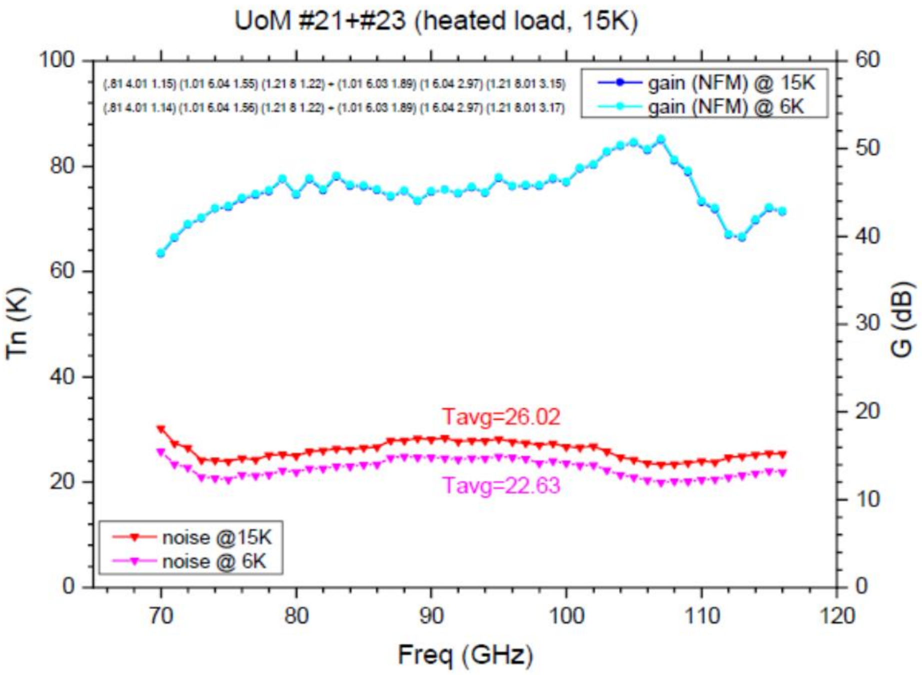

Figure 3 – Performance of a pair of cascaded UoM 3-stage LNAs tested at the Yebes Observatory [3]

Due to the restricted footprint of the closely packed *CARUSO* receiver pixels, the original packages designed for the UoM ALMA Band 2 LNAs in [5] had to be miniaturised to make them suitable for use in the restricted volume of an FPA.

The miniaturise the package has a modified standard UG-387/m waveguide flange on the input and output ports, removing the top and bottom waveguide screw holes from the flange, and utilising a low-profile, custom nano-strip connector. A comparison between these two block designs is shown in Figure 4.

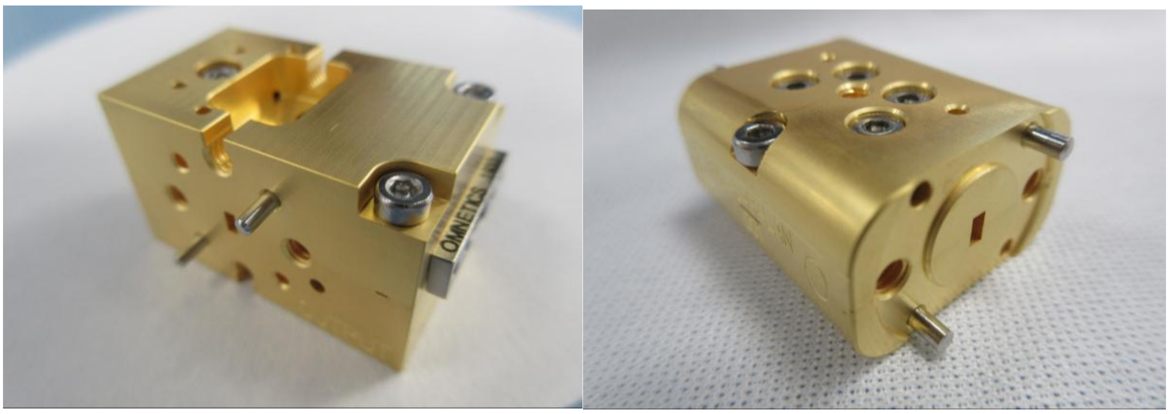

Figure 4 - The original UoM ALMA Band 2 LNA (left) and the miniaturised UoM W-Band LNA (right), featuring a modified UG-387/m waveguide flange

2.2 SHIRM Technology Context

A SHIRM is a type of sideband separating/2SB mixer. The benefit of these types of mixers is that as upper and lower mixer sideband are delivered at separate outputs, both the mixer noise temperature and spectral confusion are reduced. Key components of the SHIRM are the hybrid couplers.

2.2.1 Hybrid Coupler Context

Hybrid couplers are a type of 4-port component that are designed to couple the signal travelling between two of the ports to a third port, such that 50% of the input power will be present on each of the output ports, with a 90° phase difference between them. Figure 5 shows the function of a hybrid coupler and the identification of the four ports. The *CARUSO* SHIRM used the Marki Microwave MMIC 4-18 GHz hybrid coupler, the performance details for which are shown in Table 1 and Figure 6.

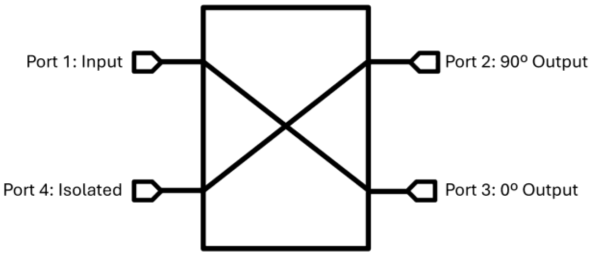

Figure 5 - Diagram of a hybrid coupler showing the layout of the ports

Parameter	Min	Typ	Max	Unit
Amplitude Balance	-	0.4	2	dB
Excess Through Line Insertion Loss	-	1.5	3.2	dB
Impedance	-	50	-	Ω
Isolation	11	16	-	dB
Mean Coupling	-	3	-	dB
Nominal Phase Shift	-	90	-	°
Phase Balance	-	0.5	8	°
VSWR	-	1.1	-	

Table 1 – Room temperature performance of the **Marki Microwave** MMIC **4-18 GHz Hybrid Coupler** [8] used in the *CARUSO* SHIRM.

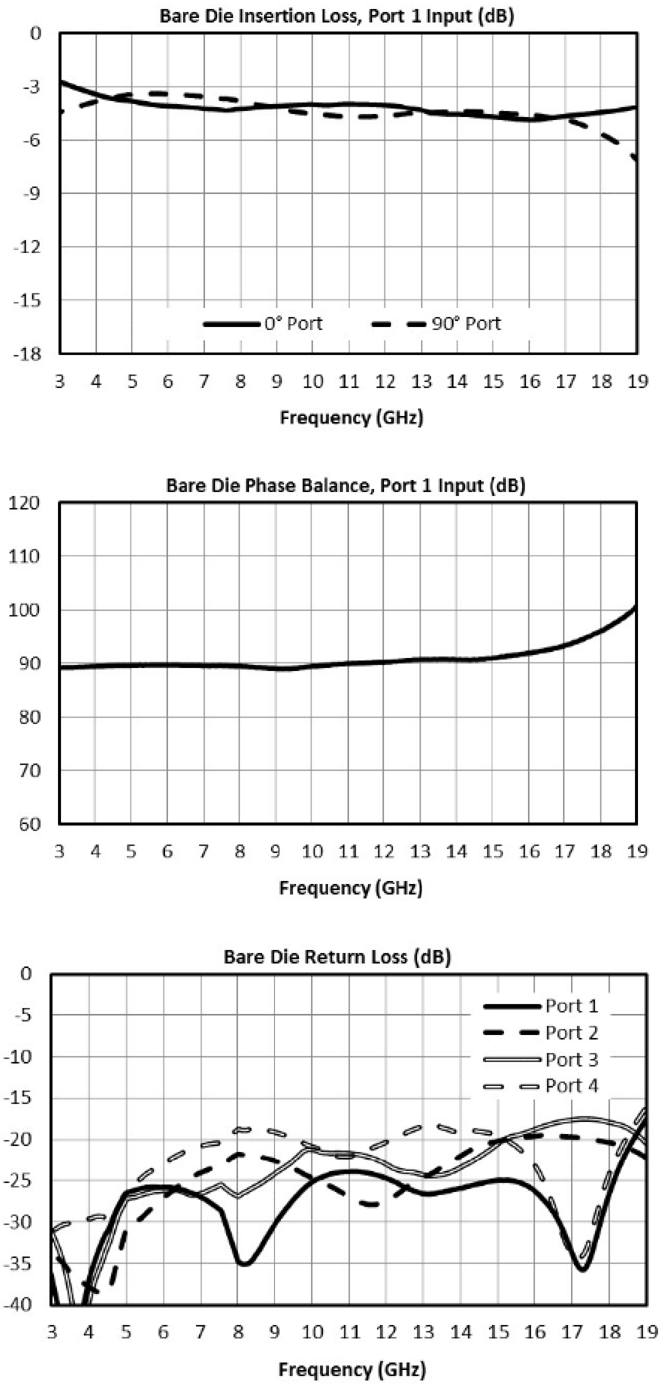

Figure 6 – Room temperature performance of the Marki Microwave MMIC 4-18 GHz Hybrid Coupler [8] used in the *CARUSO* SHIRM. Top shows the insertion loss, middle shows the phase balance, and bottom shows the return loss.

2.2.2 SHIRM Theory

A sideband separating (2SB) mixer is made up of two hybrid couplers, two mixers, an LO signal source, and a power splitter. An RF signal is the input, and the IF products of the upper and lower sidebands are output separately, as in Figure 7.

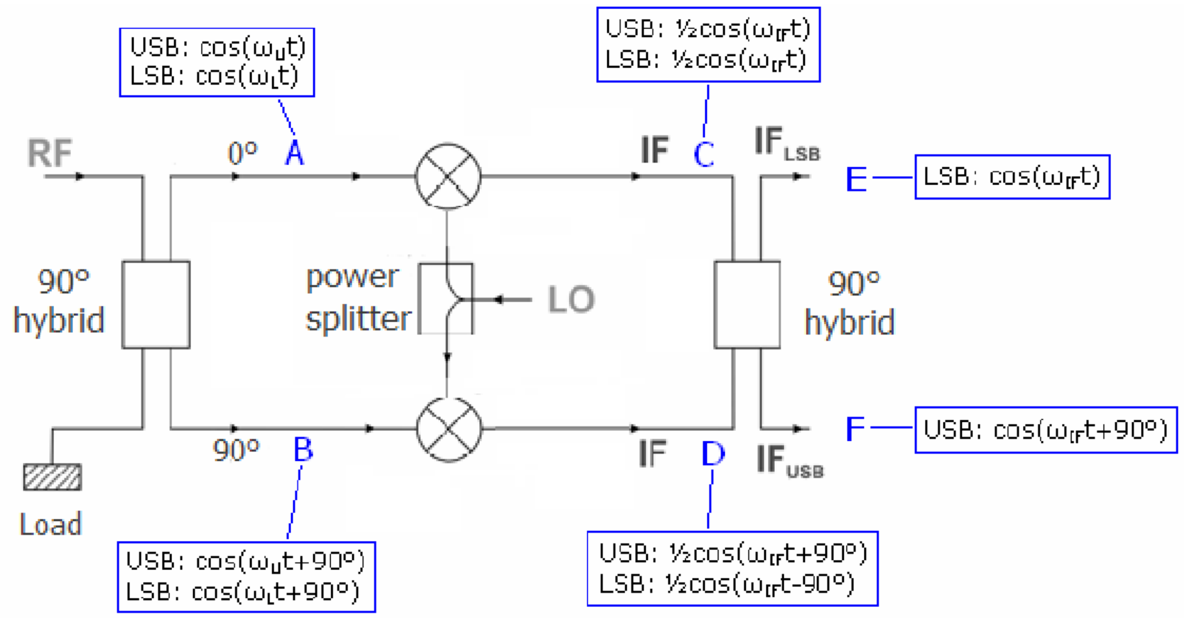

Figure 7 **- Diagram of a 2SB mixer from [8], with labelled points A-F referred to below**

As seen above in Figure 7, an RF signal is input into a hybrid coupler configured as a divider, see Figure 8, the output shows a -90° and -180° phase shift on the output signals. The signal at A and B can have any phase so long as relative to each other they are 90° apart. The time varying signal can be represented at A as:

$$USB_A \propto \cos(\omega_U t)$$

$$LSB_A \propto \cos(\omega_L t)$$

Due to the hybrid coupler, at B there is a 90° phase shift:

$$USB_B \propto \cos(\omega_U t + 90°)$$

$$LSB_B \propto \cos(\omega_L t + 90°)$$

The signals at A and B are then mixed down to an IF by the insertion of an LO signal. This can be described mathematically by multiplication:

$$USB_C \propto \cos(\omega_{LO} t) \cos[(\omega_{LO} + \omega_{IF})t]$$

$$LSB_C \propto \cos(\omega_{LO} t) \cos[(\omega_{LO} - \omega_{IF})t]$$

Then, using the trigonometric identity:

$$\cos(a)\cos(b) \equiv \frac{1}{2}[\cos(a-b) + \cos(a+b)]$$

We get:

$$USB_C \propto \frac{1}{2}\cos(\omega_{IF}t) + \frac{1}{2}\cos[(2\omega_{LO} + \omega_{IF})t]$$

$$LSB_C \propto \frac{1}{2}\cos(\omega_{IF}t) + \frac{1}{2}\cos[(2\omega_{LO} - \omega_{IF})t]$$

Then using the same method for point D:

$$USB_D \propto \cos(\omega_{LO}t)\cos[(\omega_{LO} + \omega_{IF})t] = \frac{1}{2}\cos(\omega_{IF}t + 90°) + \frac{1}{2}\cos[(2\omega_{LO} + \omega_{IF})t + 90°]$$

$$LSB_D \propto \cos(\omega_{LO}t)\cos[(\omega_{LO} - \omega_{IF})t] = \frac{1}{2}\cos(\omega_{IF}t - 90°) + \frac{1}{2}\cos[(2\omega_{LO} - \omega_{IF})t + 90°]$$

From here, we only consider the signals at IF ($\omega_{IF}t$). Each IF signal goes through another hybrid coupler, this time configured as a combiner as in Figure 9. At point E, the upper sideband components arrive out of phase and cancel, leaving only the lower sideband. At point F, the lower sideband components cancel, and only the upper sideband signal remains.

$$\frac{1}{2}\cos(\omega_{IF}t)_{USB} + \frac{1}{2}\cos(\omega_{IF}t)_{LSB} + \frac{1}{2}\cos(\omega_{IF}t + 180°)_{USB} + \frac{1}{2}\cos(\omega_{IF}t)_{LSB} = \cos(\omega_{IF}t)_{LSB}$$

Similarly, at point F:

$$\frac{1}{2}\cos(\omega_{IF}t + 90°)_{USB} + \frac{1}{2}\cos(\omega_{IF}t + 90°)_{LSB} + \frac{1}{2}\cos(\omega_{IF}t + 90°)_{USB} + \frac{1}{2}\cos(\omega_{IF}t - 90°)_{LSB} = \cos(\omega_{IF}t + 90°)_{USB}$$

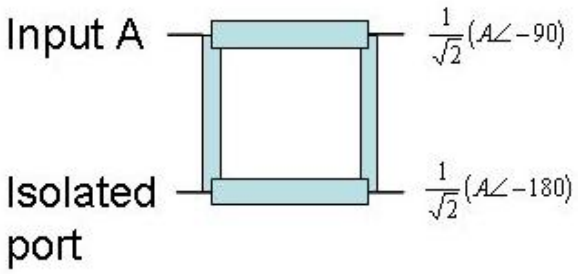

Figure 8 - Branchline coupler as divider from [9]

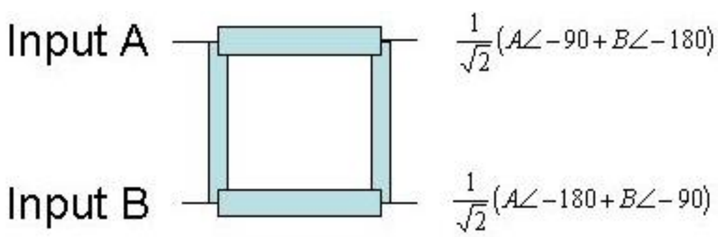

Figure 9 - Branchline coupler as combiner from [9]

2.2.3 The CARUSO SHIRM

A SHIRM was developed by RAL for ALMA Band 2 and then specifically reconfigured to support the *CARUSO* receiver array. All components and structures that form a SHIRM unit, as explained in section 2.2.2, are integrated within a single mechanical package, which provides a very compact solution.

The mixers operate in a sub-harmonic configuration that offers the benefit of increased immunity from Local Oscillator (LO) contamination of the receiver output spectrum. A subharmonic mixer operates using an LO signal at half the RF frequency, which significantly reduces the burden when the RF frequency increases. This is particularly advantageous because achieving sufficient LO power at very high frequencies can be challenging. The configuration implemented in our subharmonic mixer is designed to suppress odd harmonics effectively. Additionally, the waveguide's cut-off frequency provides an extra layer of filtering, further attenuating unwanted lower frequency harmonics that may originate from the LO source. An image of the SHIRM unit is shown in Figure 10.

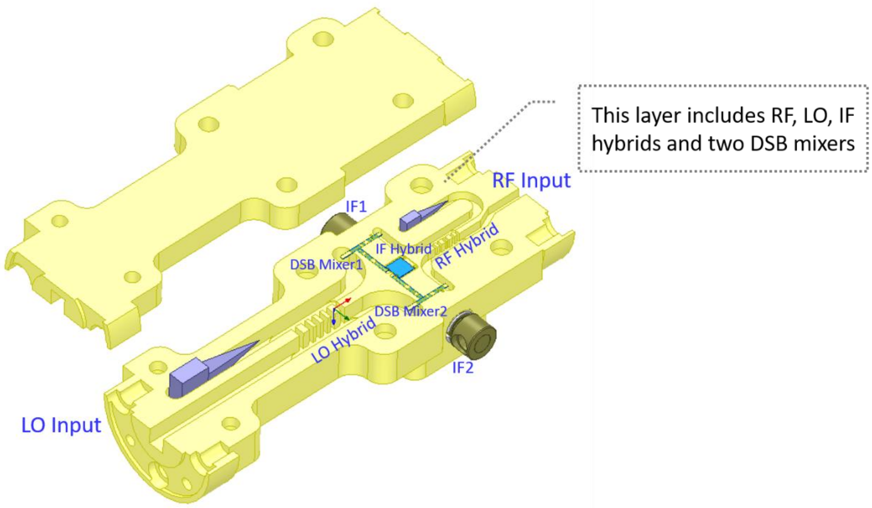

Figure 10 - Mechanical Schematic of SHIRM Internal Structure for *CARUSO* W-Band Receiver

The RAL ALMA Band 2 SHIRM used air-bridged GaAs Schottky diodes as mixers, a technology used in heterodyne receivers for frequencies up to 2.5 THz. The major limitation of these devices is the difficulty in obtaining sufficient LO power as the frequency of operation increases.

Indium Gallium Arsenide (InGaAs) diodes have lower Schottky barrier heights than Gallium Arsenide (GaAs) diodes, providing a drastic reduction in the required LO power. Provided that performance requirements can be met, InGaAs devices offer a viable alternative, with the advantage of lower heat dissipation at cryogenic temperatures, particularly important for multi-pixel arrays.

A comparison of these two types of diode mixers in the context of implementation in a SHIRM is shown below in Figure 11. Figure 12 shows the comparison of DSB mixer performance versus LO power with GaAs and InGaAs diodes operating at room temperature and 20 K. These simulations are based on a previous design of a W-band double sideband subharmonic mixer. Optimum performance of InGaAs diode mixers is achieved at ≈1/10th of the LO power compared to comparable GaAs diode mixers. When operating at room temperature GaAs mixers generally have better performance compared to InGaAs technology; however, InGaAs diode-based mixer conversion loss is improved by 3-4 dB once it is cooled to 20 K. An analysis is also performed to address the mixer linearity with these two different types of diodes, see Figure 13, which presents the simulation mixer conversion gain versus RF input power in dBm. Further detail on the SHIRM can be found in [6].

GaAs	InGaAs
• Subharmonic mixer using planar GaAs Schottky diode • Better performance at room temperature • Require high LO power to achieve best performance ~ 6-8 mW • Existing design for ALMA Band 2+3	• Subharmonic mixer using planar InGaAs Schottky diode • Slightly worse performance but significant improvement when cool down to 20K • Require much lower LO power • CARUSO W-band SHIRM

Figure 11 - Comparison of two types of Schottky diodes used in heterodyne mixers

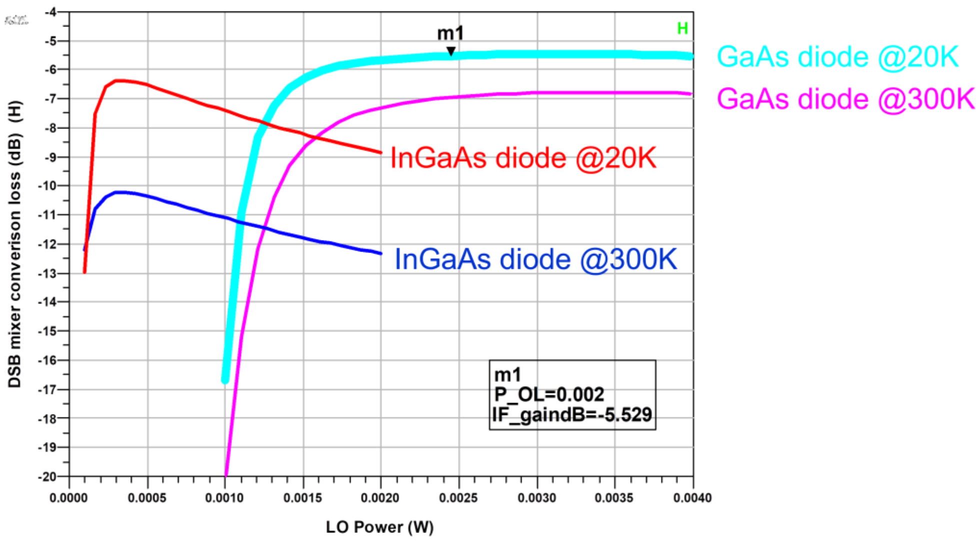

Figure 12 - Comparison of simulated mixer performance with GaAs and InGaAs diodes operating at ambient and cryogenic temperatures

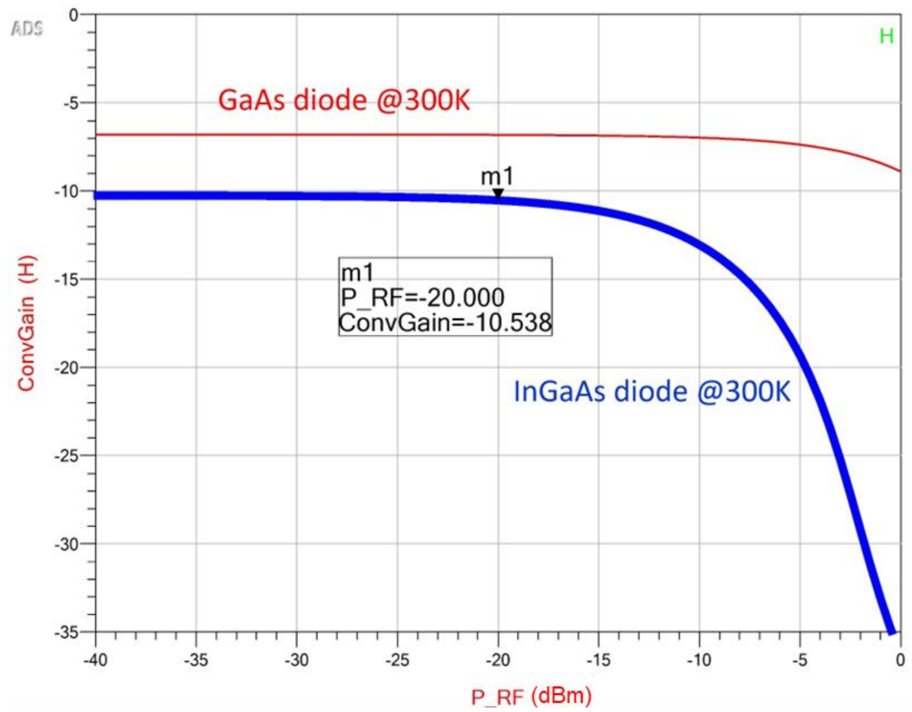

Figure 13 - Comparison of simulated GaAs and InGaAs diode mixer compression points at 300 K.

3. Work Package One: Integrated LNA and SHIRM at ALMA Frequency Band 2

As described in the introduction, WP1 aimed to build on the technology developed by both UoM and RAL in previous projects. In particular, the need for miniaturisation and integration of the receiver pixels to enable the next generation of multi-pixel receivers has been highlighted.

The LNA and the SHIRM components are the most technically complex modules in the receiver, both utilizing multiple different components and technologies. How to integrate these components is one of the major challenges to a fully integrated receiver and forms the basis for this work package in TASER. The aim of this work package was to produce a single proof-of-concept package that contains an RF LNA MMIC (the second stage LNA in Figure 2) and the SHIRM structure. In a receiver this integrated LNA+SHIRM would fill the role of second stage RF LNA and sideband separating mixer. The required interfaces and operating specification for the LNA+SHIRM are shown in Table 2.

Interface	**Frequency Range**	**Type of Interface**
RF Input	67 – 116 GHz	WR10 Waveguide
LO Input	40 – 60 GHz	WR19 Waveguide
IF Output x2	2 – 18 GHz	Coaxial Connector (SMP)
LNA DC Bias	DC	Micro-D Connector
Operating Temperature		
Room Temperature	~293 K	
Cryogenic Temperature	~15 K – 20 K	
Power Dissipation		
Single 3-stage LNA MMIC	Up to ~16 mW per stage	
Sensitivity		
NT: 40 – 50 K (LNA dominated)		
Sideband Rejection Ratio		
> 10 dB		

Table 2 - Specifications and Required Electrical Interfaces for the *TASER* LNA+SHIRM

In this section of the report, we will present our design of an integrated LNA+SHIRM, first discussing the hybrid couplers required for the SHIRM structure. The design will then be explained, and measurements presented. Results will be discussed, and a summary given. Additionally, alternative integration options are presented in WP3, section 5.2.

3.1 Hybrid Couplers

In this section we will present the considerations and design implications of an RF coupler operating at 67 - 116 GHz, an LO coupler at 40-60 GHz, and an IF coupler covering 2 – 18 GHz. The RF and LO couplers were implemented as waveguide couplers, and the IF an on-chip commercial coupler, the Marki Microwaves MQS 0218CH.

3.1.1 The IF Hybrid Coupler

An ultra-broadband IF hybrid covering a 16 GHz bandwidth is required to meet the specifications. A survey of commercially available IF hybrids, including bare die chips and connectorized packaged devices, was conducted. Very few devices are available, and only one bare die chip was identified. A summary of three identified IF hybrids is presented in Table 3. Overall, the MQS-0218 CH bare die chip has worse RF performance than the packaged devices; however, it has the advantage of being suitable for further integration, at the expense of higher loss and lower image rejection ratio.

Part Number	Device type	Freq (GHz)	Amplitude Imbalance (dB)	Phase Imbalance (degrees)	Insertion Loss (dB)
MQS 0218CH	Bare die chip	2-18	± 4	± 3 (max: ± 7)	1.4 (max: 4.2)
KRYTAR 1830	Packaged	2-18	± 0.4	± 7	<1.4
YH90420 1008	Packaged	4-20	± 0.4	± 3	0.35

Table 3 - Summary of the three identified IF hybrid couplers

The commercially available bare die hybrid from Marki was selected for its miniature dimension in the fully integrated SHIRM. The MQS-0218 is an MMIC 2 GHz - 18 GHz 90° splitter/combiner. Wire-bondable 50Ω terminations are available on-chip. The electrical specifications and chip outline are shown below in Table 4 . As discussed in section 2.2.1, a similar hybrid die chip, the MQS-0418CH, was implemented historically and has proven its operation in cryogenic conditions.

Parameter	Frequency (GHz)	Min	Typ.	Max	Units
Coupling	2-18		3		dB
Nominal Phase Shift			90		Degrees
Amplitude Balance	2-3		±2		dB
	3-18		±1	±4	
Phase Balance	2-17		±3	±7	Degrees
	17-18		±5		
Excess Through Line Insertion Loss	2-18		1.4	4.2	dB
Isolation		9	17		dB
VSWR			1.25		
Impedance			50		Ω

Table 4 - Marki MQS-0218CH electrical specification from manufacturer.

3.1.2 The LO Hybrid Coupler

The mixers in the SHIRM require an LO signal in the frequency range of 40 – 60 GHz and at these frequencies a hybrid coupler implemented as a waveguide structure has some advantages, such as the better insertion loss. However, as the hybrid coupler structure is dependent on the wavelength of the signals intended to be coupled, in this frequency range the waveguide coupler structure is comparatively physically large compared to the rest of the SHIRM and the LNA components. This can be seen from the image of the *TASER* LNA+SHIRM in Figure 16. Switching to an on-chip hybrid coupler for the LO would result in a much smaller structure then the waveguide implementation, offering significant miniaturisation, albeit with worse insertion loss.

After an extensive review of commercially available hybrid couplers, none were identified that were suitable for use as the LO coupler as commercial hybrids are not available at high enough frequencies. A custom on-chip LO coupler has been designed and is presented in section 5.1 although it was not feasible to fabricate it during this project. We are continuing to investigate the methods to fabricate these on-chip couplers in preparation for future projects.

3.1.3 The RF Hybrid Coupler

The RF input of the SHIRM is designed for signals in the 67 – 116 GHz frequency range therefore, similarly to the LO coupler, the RF hybrid coupler is implemented as a waveguide structure. At these higher frequencies, the wavelength and therefore the size of the hybrid is smaller than the LO coupler by roughly a factor of two, but the structure is still large enough that there would be significant miniaturisation potential in switching to an on-chip RF coupler. At these higher frequencies the reduced size of an on-chip coupler also opens the potential for on-MMIC integration along with the LNAs, which will be explored in more detail in section 5.1 and 5.2.

3.2 Final Design

Several integration options have been investigated during this project with the intention to provide several approaches to the challenge of integration of the second stage LNA, the SHIRM and ultimately the complete receiver. These were presented in the *TASER* mid-term review as possible paths to take through the rest of the project. The outcome of the review led to us to focus primarily on the integration option seen in Figure 14, specifically with a focus towards then pushing this integrated technology towards higher RF frequencies. The other options are discussed further in section 5.2, and offer potential benefits towards further integration and miniaturisation of receivers, including for future FPA applications.

The chosen approach to integrating the second stage LNA and SHIRM was to maintain the waveguide interfaces of both components (the output of the LNA and input of the SHIRM), see Figure 14. This integration would allow for the removal of the two waveguide flanges, associated screw and dowel holes, and importantly a length of waveguide between the output of the LNA and the input of the SHIRM. All the components in the LNA and SHIRM offer very high performance and have been extensively modelled in the HFSS 3D EM simulator as well as manufactured in larger numbers as part of previous projects, allowing us to focus on the task of integration.

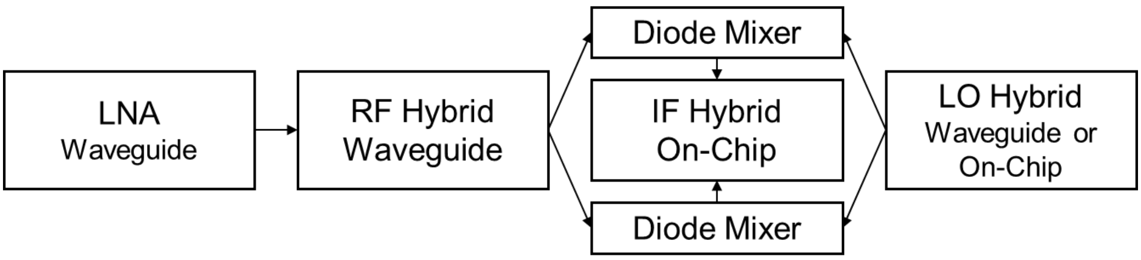

Figure 14 - Block Diagram of the Chosen Integration Topology

This integration option required the least changes to the pre-existing LNA and SHIRM designs but also offered the least benefits of integrating the components (due to the waveguide coupler) and the least potential for future developments towards on-chip integration. However, the development of the integrated second stage LNA+SHIRM with a waveguide RF coupler provides a technology platform for further developments in future projects, particularly with a view towards prototyping devices for higher frequencies and FPAs.

The design of the *CARUSO* LNA and SHIRM components include several elements that enabled the receiver pixel to fit within the footprint of the feedhorn, including removing two of the screws from the waveguide flange and using a low-profile nano-strip connector. The LNA+SHIRM manufactured for *TASER* is not required to conform to the same restrictions, so several design choices have been made to ease the manufacture and characterisation process. More specifically:

- A micro-D connector was chosen to provide the LNA bias instead of the custom nano-strip connector due to reduced costs and shorter lead times.
- A full UG-237 waveguide flange was used on the RF and LO inputs to provide connections between the LNA+SHIRM and other components.
- In order to simplify and shorten the manufacturing process the external rounding and chamfering on the block was not used.

In addition, a 3-stage version of the UoM LNA MMIC was used to provided improved performance (see figure 3 for the performance of cascaded 3-stage LNAs), the extra gain provided from the third stage (~5 dB) helps to reduce the noise contribution of the mixers in the SHIRM. Using the 3-stage LNA required redesign of the biasing PCB and modification of the block in this area, Figure 15 shows the new PCB and a comparison of the micro-D and nano-strip DC connectors. The design of the LNA+SHIRM is easily modified in future projects to make use low profile connectors such as the nano-strip or nano-D connector, or to included rounded edges or reduced size waveguide flanges when required.

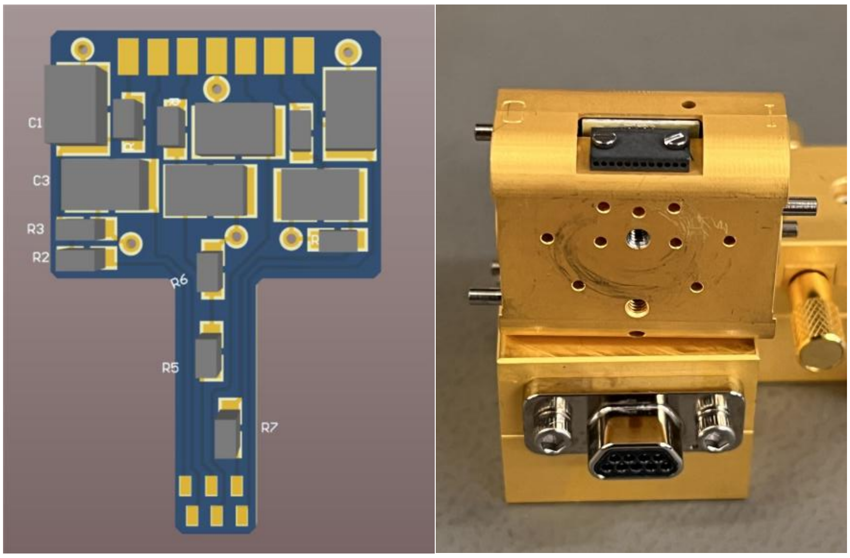

Figure 15 - Left shows the bias PCB for the three stage MMIC, right is a comparison of the custom nanostrip (top) and the micro D connectors (bottom)

The completed design of the LNA+SHIRM is shown in Figure 16, including the various components positioned and labelled for reference. This integration allowed for the removal of the intervening waveguide flange interface, the space required in the block for two sets of screw and dowel pin holes, and the short length (~11 mm) of waveguide between the output of the LNA and the input of the hybrid coupler that had been necessary to accommodate these. The overall length of this integrated LNA+SHIRM design is 73 mm.

In addition, an early version of the design was developed that used the design choices that would make the LNA+SHIRM suitable for use in FPAs to provide a reference as to what a future, low-profile LNA+SHIRM could be like. Images of this CAD model are shown in Figure

17. Further work would be needed on this 'FPA Style' device to make it suitable for manufacture and it is shown here for reference only. Photos of the manufactured and assembled second stage LNA+SHIRM are shown in Figure 18, Figure 19 and Figure 20.

A)

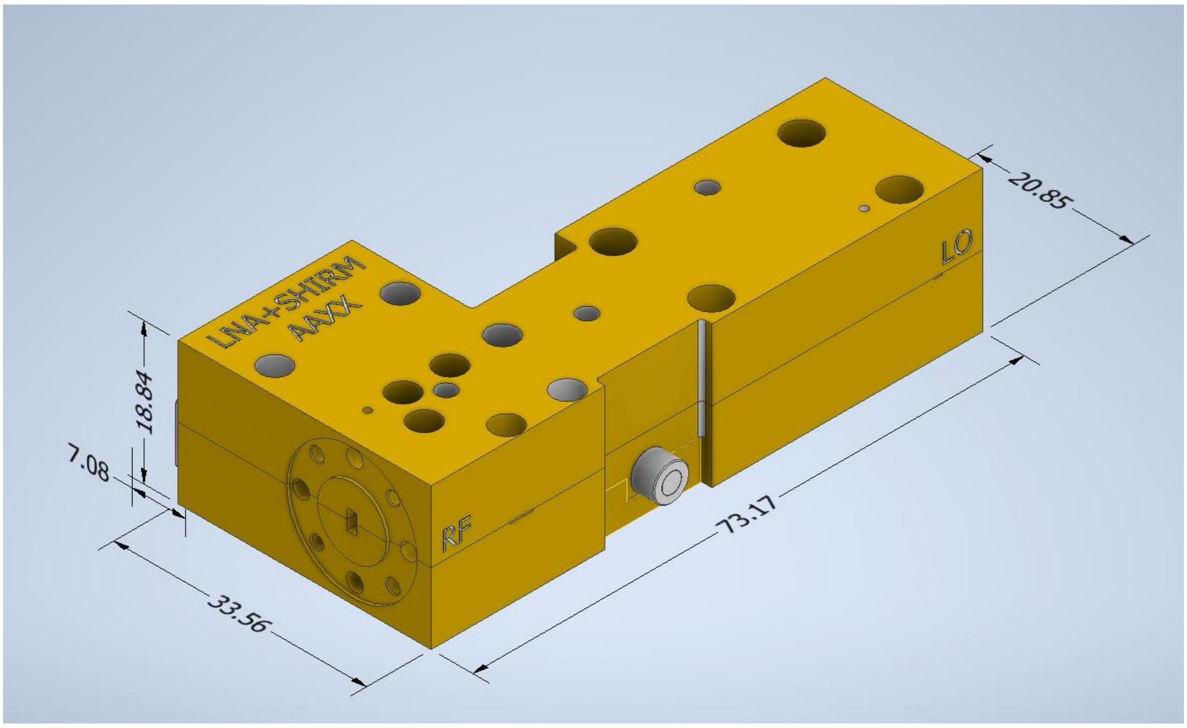

B)

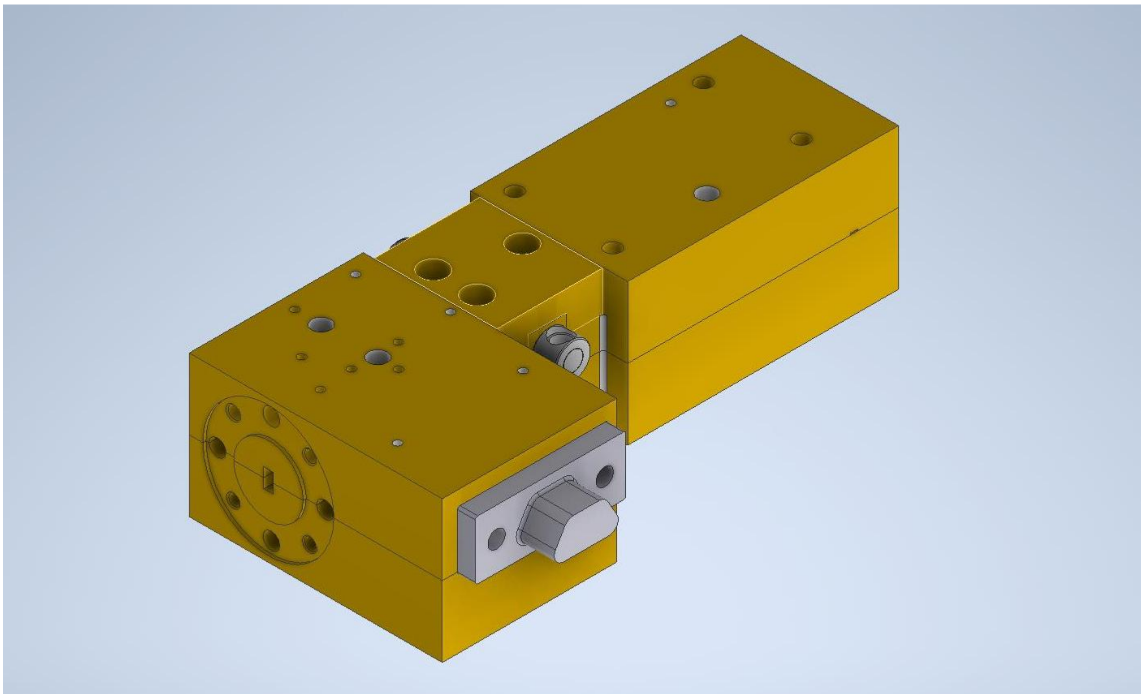

C)

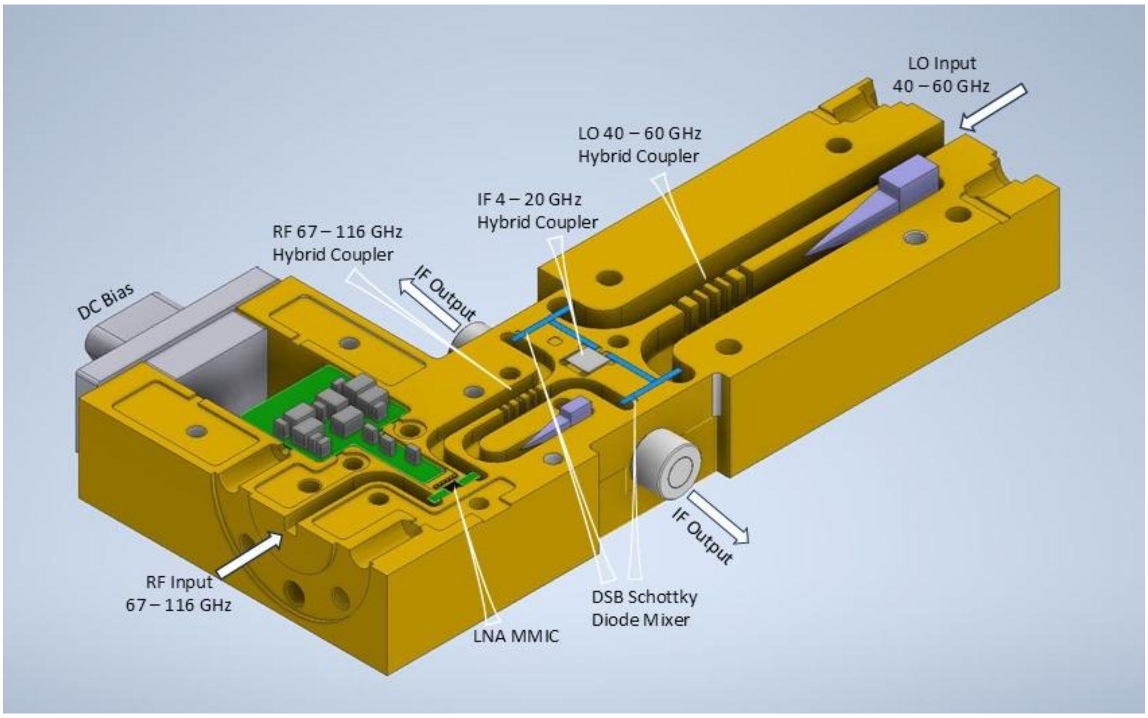

Figure 16 - CAD images of the *TASER* LNA + SHIRM, A) exterior of the block showing dimensions, B) Underside of the exterior of the block, C) Inside the block with the components labelled.

A)

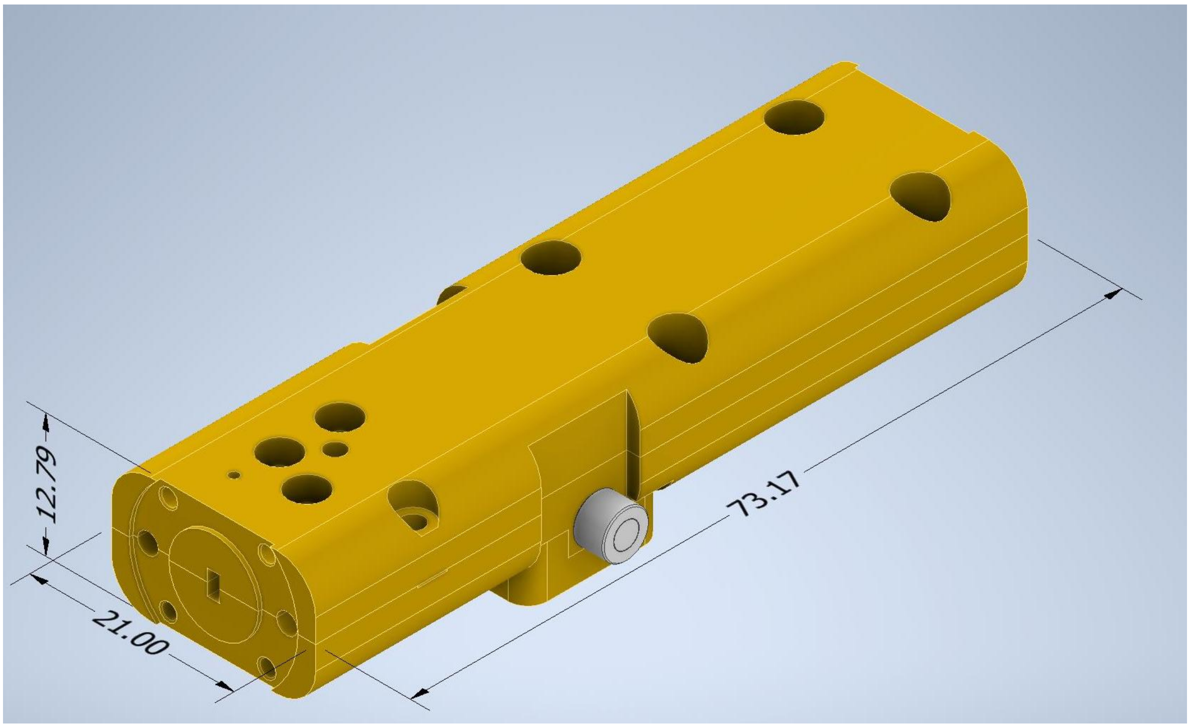

B)

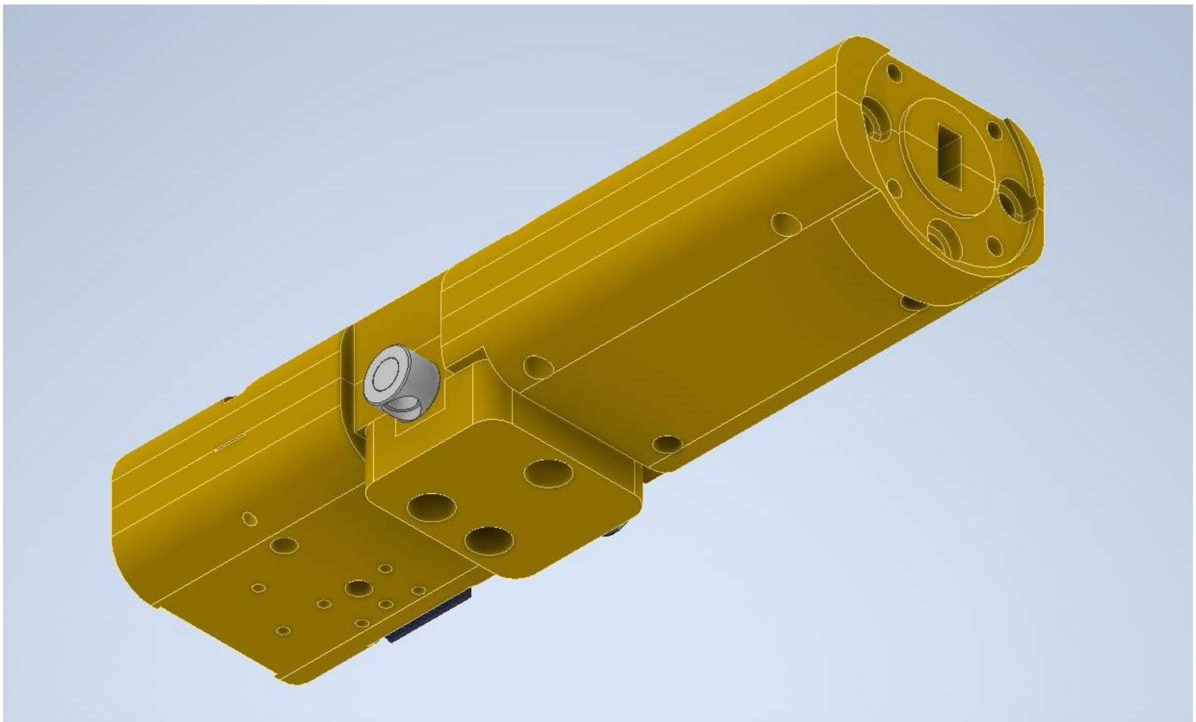

C)

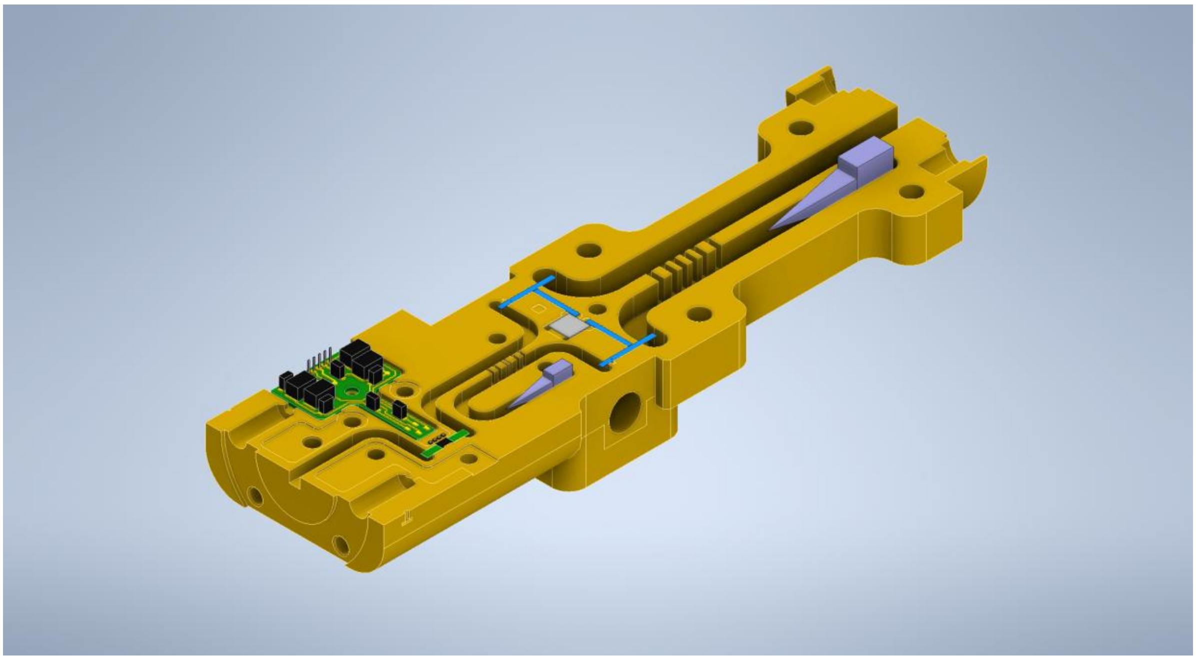

Figure 17 - CAD images of the 'FPA Style' LNA+SHIRM, A) Exterior of the block with dimensions and B) Underside of the block, C) Inside of the block

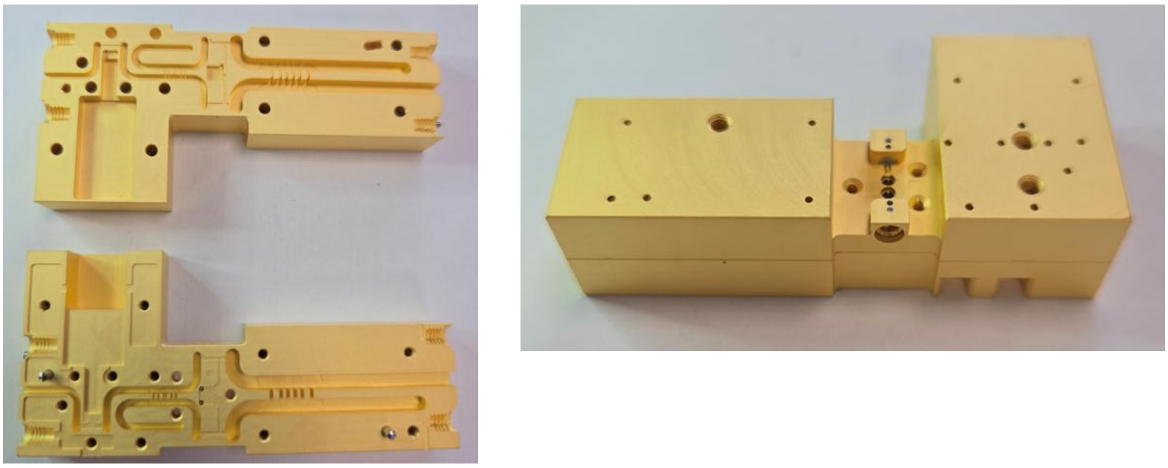

Figure 18 - LNA+SHIRM block prior to assembly, manufactured by RAL

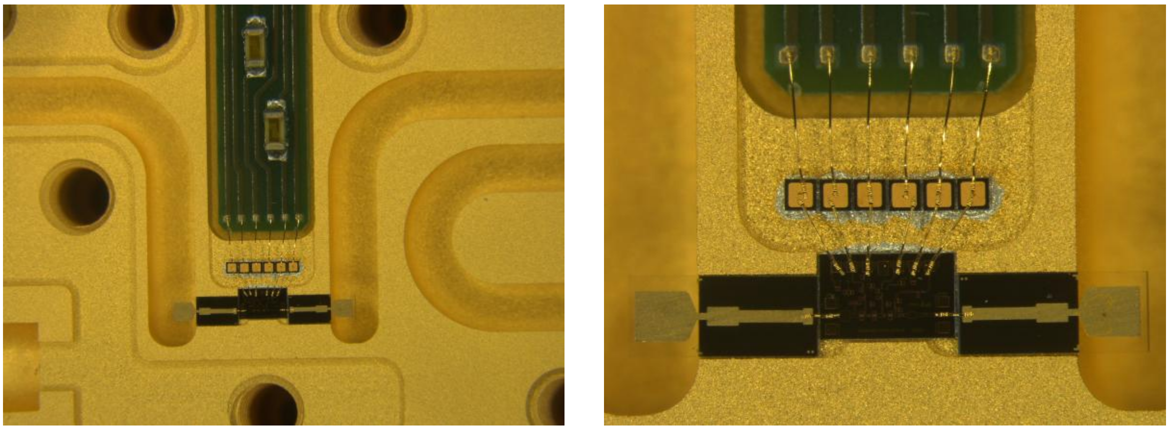

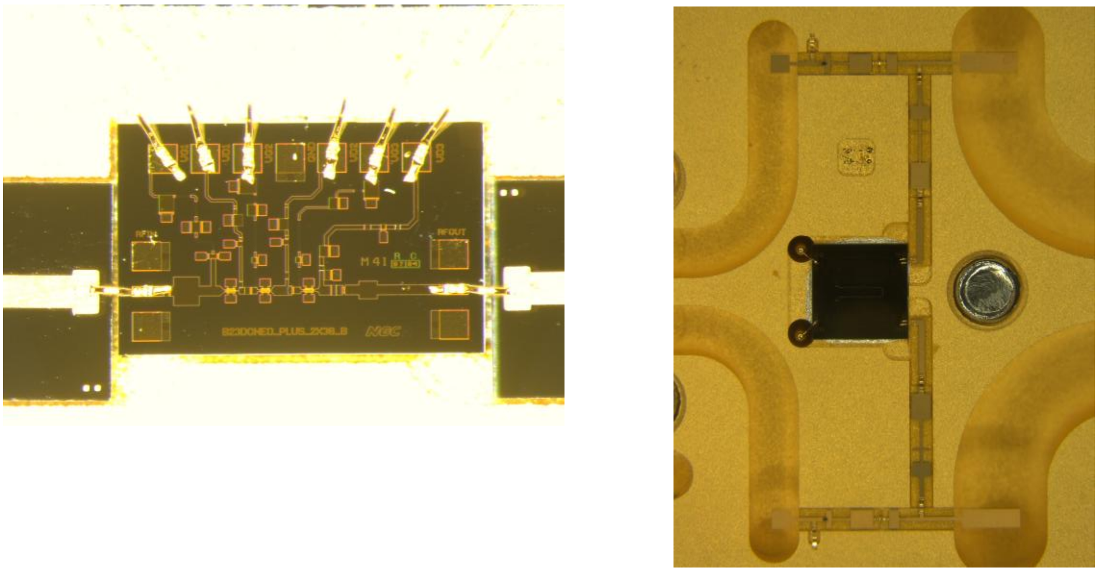

Figure 19 - Photographs showing the components inside the assembled LNA+SHIRM, Top row: The MMIC area; Bottom row: Left: The MMIC; Right: The IF hybrid coupler. Assembly done by RAL.

A) B)

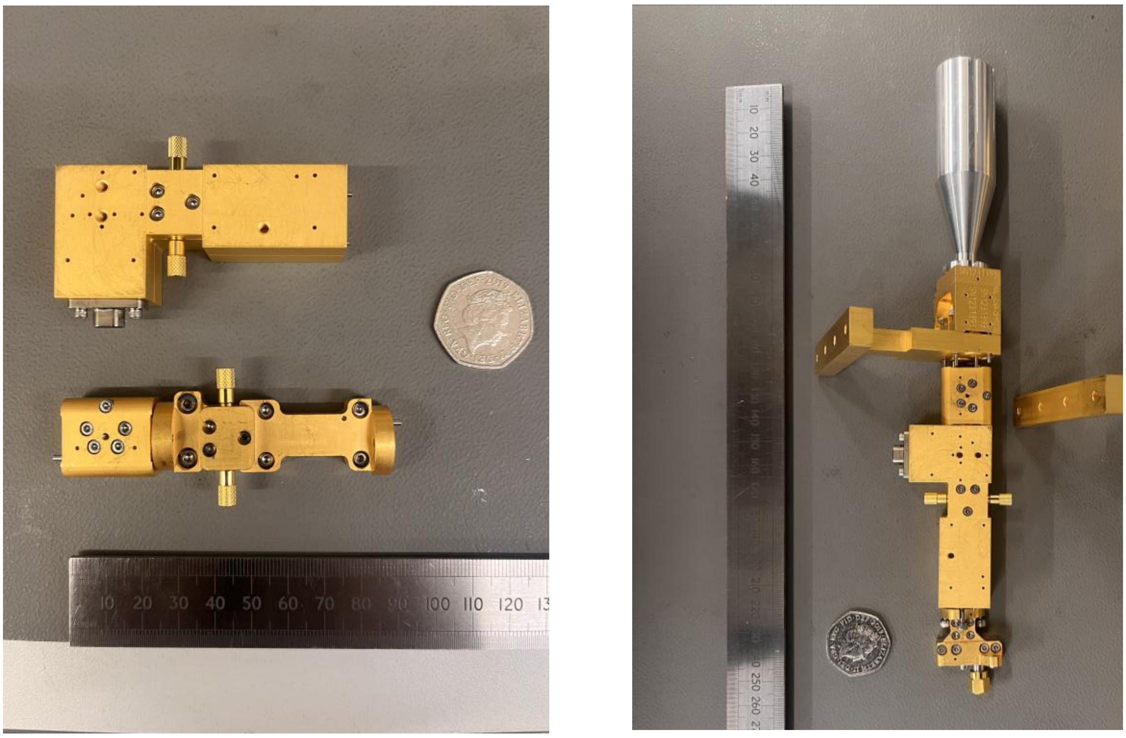

Figure 20 - Size comparison of the manufactured *TASER* LNA+SHIRM and A) the *CARUSO* LNA and SHIRM, and B) a full *CARUSO* pixel incorporating the integrated *TASER* LNA+SHIRM (left).

3.3 Measurement Process

Two identical LNA+SHIRM blocks (referred to as block A and block B) were manufactured, assembled and tested at RAL. The LNA+SHIRM blocks were tested using the *CARUSO* receiver test setup in the lab at RAL. The gain and noise temperature were tested using the Y-factor method [11]and image rejection was tested using the procedure described in [12] [11]. The performance of the LNA+SHIRM was optimised using RAL owned software, this allowed an automated sweep of the LNA bias and the LO power to identify the optimum performance. Due to configuration of the software for the testing system it is only currently possible to bias 2-stage LNAs. The UoM 3-stage LNAs work very well with the second and third stages biased together, a small amount of performance tuning is lost but we know from previous experience that excellent performance can be attained. For these tests the devices were cooled to 20 K inside the test cryostat, see Figure 21 and Figure 22. The instrumentation setup outside of the cryostat can be seen in Figure 23.

The test setup is described in section 3.3. The noise temperature, gain, and image rejection results are given in section 3.4. Section 3.5 will present a discussion of these results, finally drawing conclusions in 3.6.

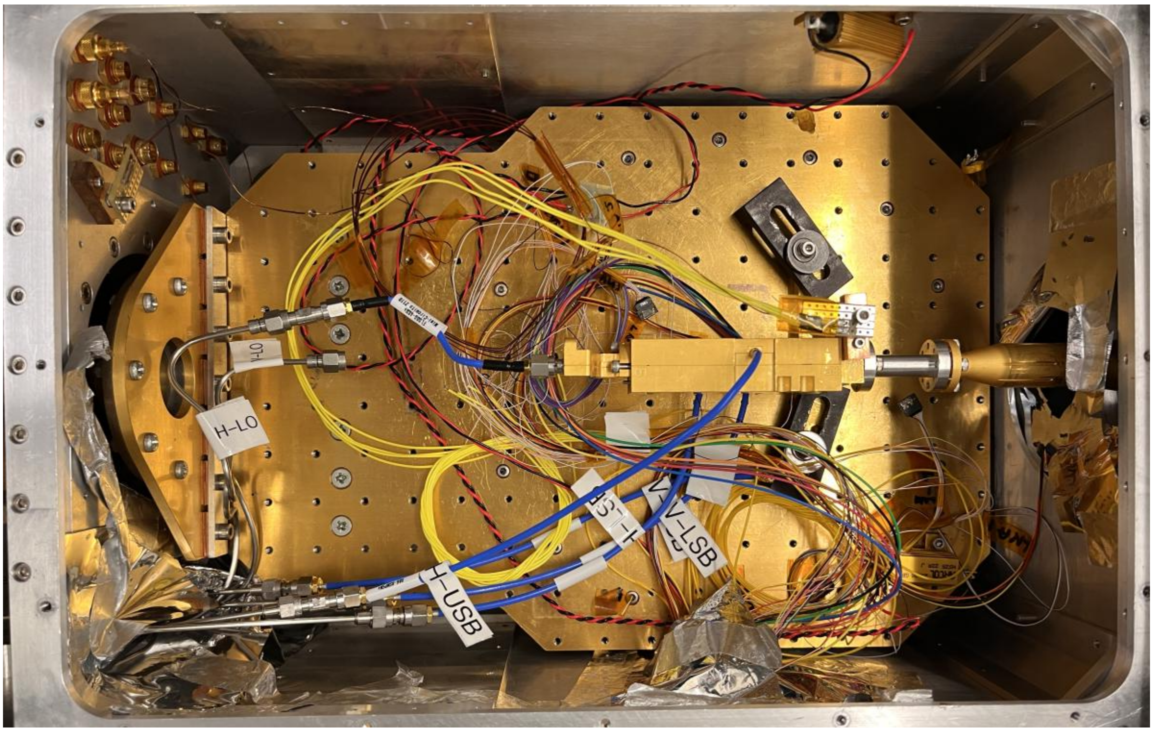

Figure 21 – Cryostat internal at RAL containing *TASER* LNA+SHIRM for measurement

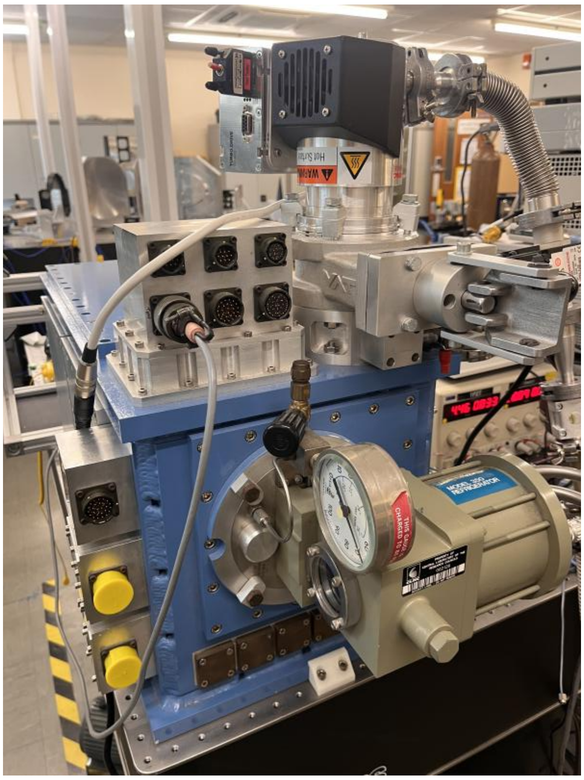

Figure 22 - External view of Cryostat at RAL

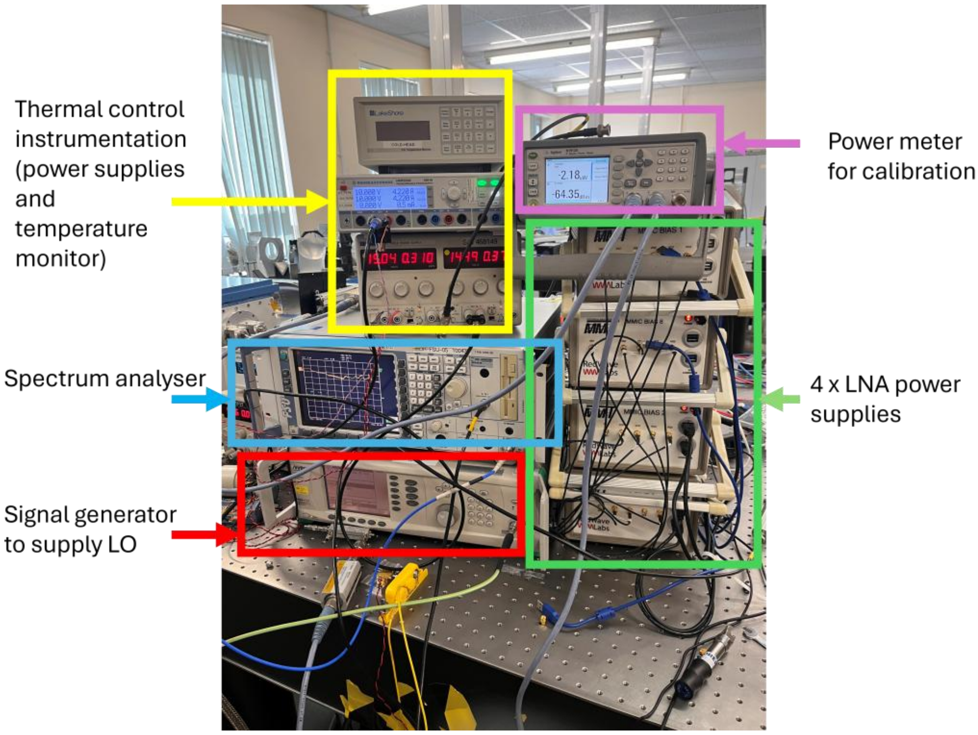

Figure 23 – RAL's cryogenic setup's measurement equipment

3.3.1 Noise Temperature and Gain Test Setup

Figure 24 shows the setup used for measuring the double side band (DSB) noise temperature and gain of the LNA+SHIRM blocks. The single side band (SSB) noise temperature is also given, although this is a mathematical function of the DSB noise temperature and the image rejection (detailed in section 3.3.2). The upper and lower sidebands are measured alternately, with 50-ohm terminations attached on the port not being measured. The 41-52 GHz LO source comprises a baseband signal which is upconverted by a Schottky tripler developed by RAL-Space. For the Y-factor measurements the hot and cold loads were presented to the LNA+SHIRM via a window in the cryostat, with an automated mirror controlled by the measurement system able to switch between them (see Figure 25). The hot load was an absorber panel at room temperature (295 K) and the cold load was held in a pot of liquid nitrogen at 80 K. The feedhorns which are attached in front of the LNA+SHIRM for this measurement are shown in Figure 26 and Figure 27. The IF amplifiers were calibrated separately and kept at room temperature: their performance was de-embedded from the measurements. Several different IF amplifiers were tried. Four different LO frequencies were swept, 41 GHz, 45 GHz, 49 GHz, and 52 GHz, using 0.2, 0.3, 0.4, and 0.5 mW LO powers, with optimums reported.

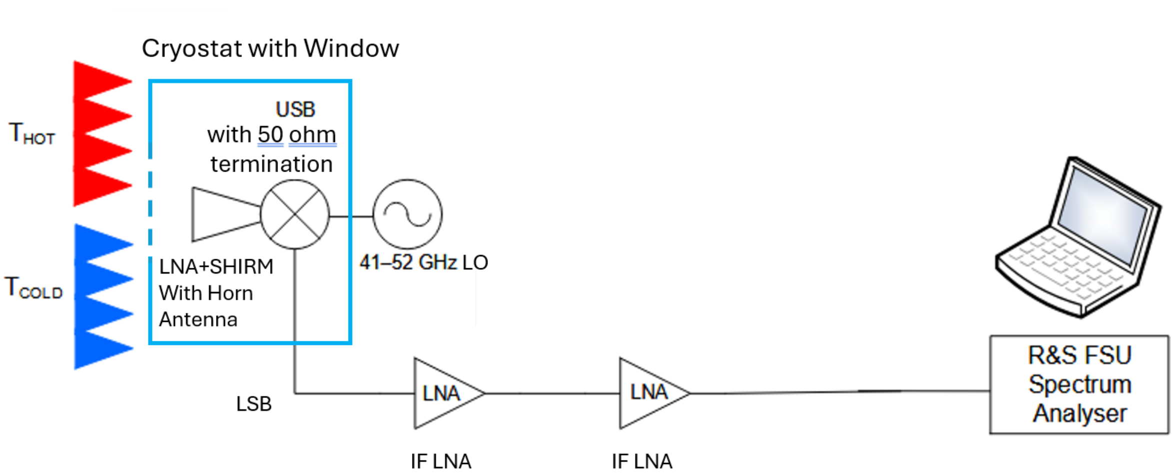

Figure 24 - Y Factor measurement setup.

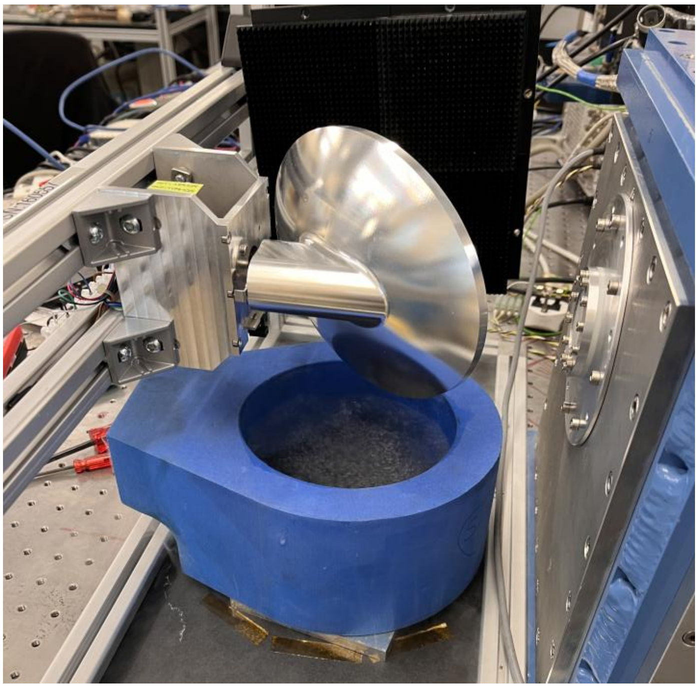

Figure 25 - Cryostat automated reflector temperature setup

Figure 26 - Feedhorns used for TASER

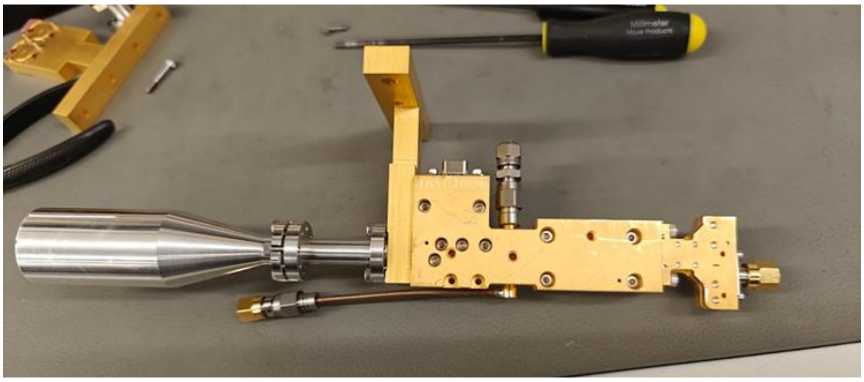

Figure 27 - A *TASER* LNA+SHIRM ready for testing in the cryostat

3.3.2 *Image Rejection*

Sideband separating mixers, such as SHIRMs, have a figure of merit called image rejection, which refers to a mixer's ability to eliminate one sideband from converting to the IF. A good image rejection is important as it allows for a better noise temperature to be achieved. The image rejection is measured by injecting continuous wave (CW) signals of known relative amplitudes into the upper and lower sidebands, then measuring the output of the IF ports, see Figure 28. More detail is given in [12]. Figure 29 shows a simplified test setup, a WR10 VNA frequency extender head is used for the CW signal injection.

By taking the conversion gains from RF input to each IF output, denoted by $G_{i,j}$, we can get image rejection R_1 at IF port 1, and R_2 at IF port 2:

$$R_1 = \frac{G_{1U}}{G_{1L}} \ and \ R_2 = \frac{G_{2U}}{G_{2L}}$$

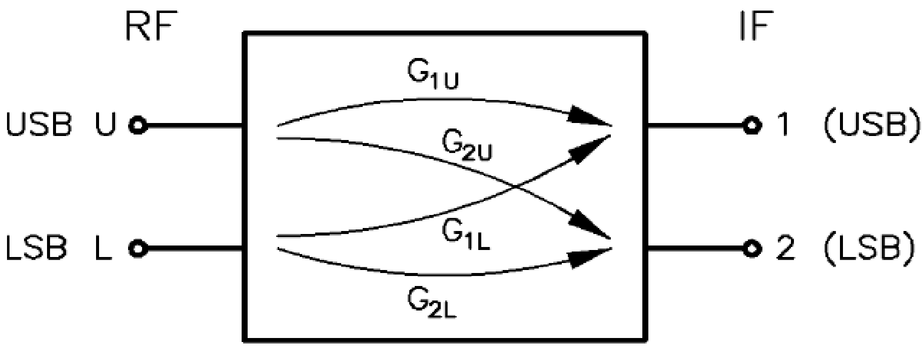

Figure 28 - Power gains of a sideband separating mixer [12]

To get these ratios, first we use a CW test signal in the upper sideband, which results in IF signals at IF ports 1 and 2, which are measured. The ratio of these powers is:

$$M_U = \frac{G_{1U}}{G_{2U}}$$

Doing the same, but with the CW test signal in the lower sideband:

$$M_L = \frac{G_{2L}}{G_{1L}}$$

Measuring the changes in output power at IF ports 1 and 2 when a cold load is replaced by a hot load, the change being ΔT, at the receiver input:

$$\Delta P_1 = k_B\, \Delta T(G_{1U} + G_{1L})$$

$$\Delta P_2 = k_B\, \Delta T(G_{2U} + G_{2L})$$

We can then define the ratio of these as M_{DSB}:

$$M_{\mathrm{DSB}} \triangleq \frac{\Delta P_1}{\Delta P_2} = \frac{G_{1U} + G_{1L}}{G_{2U} + G_{2L}}$$

From these, we can calculate R_1 and R_2 as follows, with the derivation found in [12]:

$$R_1 = M_U \cdot \frac{M_L M_{\mathrm{DSB}} - 1}{M_U - M_{\mathrm{DSB}}}$$

$$R_2 = M_L \cdot \frac{M_U - M_{\mathrm{DSB}}}{M_L M_{\mathrm{DSB}} - 1}$$

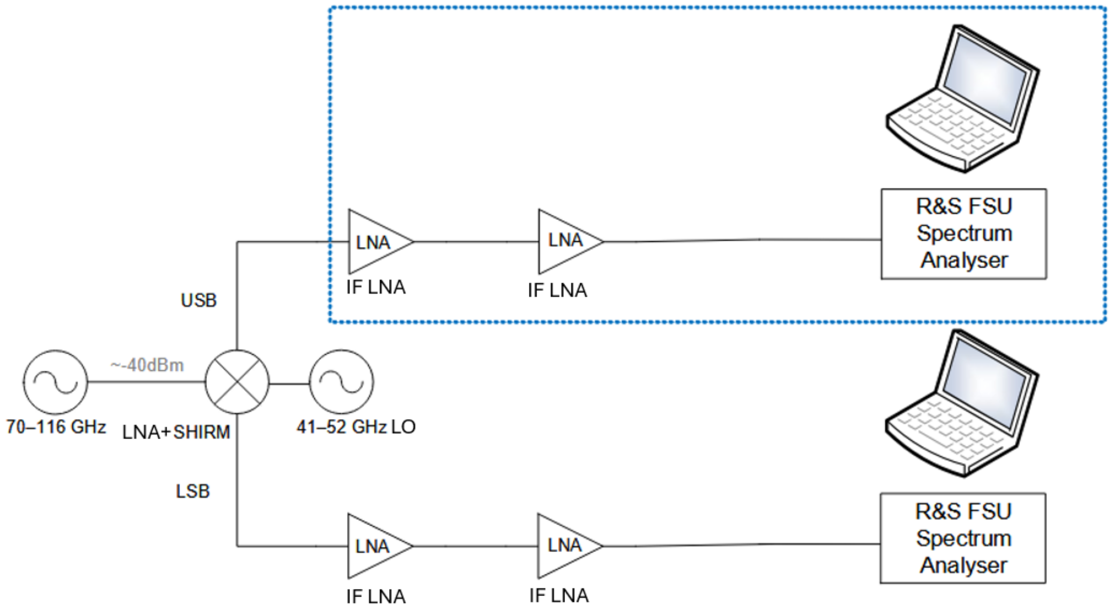

Figure 29 - The image rejection measurement setup, during the measurement of each side band, the other port was terminated with a 50 ohm load through a switch, this switching was automated.

3.4 Results

This section details the results of the measurements taken for the cryogenic DSB noise temperature and gain, as well as the SSB noise temperature and image rejection. Block A and Block B were both tested using the test setup at RAL described in section . All measurements were taken at 20 K ambient temperature. RAL's bias optimisation method takes iterative measurements of receiver noise and gain over the specified frequency bandwidth, varying the LNA bias within a set range of values. From an initial drain voltage and drain current provided to the system, the measured results being fed back into an algorithm developed at RAL that calculates iterative steps in LNA bias. The algorithm can be chosen to optimise for a range of parameters, typically when optimising LNA bias this is either the receiver noise temperature or gain. For these TASER blocks noise temperature was optimised for to try and achieve the best performance possible. The gain optimisation is often used for optimising the bias of second stage LNAs, where the effect of changing LNA bias should no longer have an influence on the noise performance under typical operating conditions.

After bias optimisation using the RAL software, the bias values reported in Table 5 were used to perform a final measurement.

The IF chains used for measuring Block A and Block B differed due to practical constraints, the measurements were taken on different dates, and the same IF LNAs were not available. However, in all cases, the IF chain was calibrated out of the final measurement. For the IF chain used to measure Block A two cascaded Miteq 0.1 to 16 GHz AFS4-00101600-23-10P LNAs were used, for Block B two cascaded Miteq 2-18 GHz LNA AFS4-02001800-45-0P-JS-R LNAs were used.

Section 3.4.1 shows the DSB noise temperature and gain results, and section 3.4.2 shows the image rejection and SSB noise temperature results. The noise measurement setup was shown in section 3.3.1, and image rejection in section 3.3.2. Results will be discussed in section 3.5 including considering the effect of adding a first stage LNA in front of these LNA+SHIRM units.

	Block/Amplifier Stage			
	A/1	**A/2+3**	**B/1**	**B/2+3**
Gate Bias (V)	0.39	0.29	0.12	0.21
Drain Bias (V)	1.08	1.36	0.93	1.34
Drain Current (mA)	6.06	17.53	3.61	16.45

Table 5 - Bias values post-optimisation.

3.4.1 Cryogenic Noise Temperature and Gain Measurements

Figure 30 shows the upper and lower sideband noise temperatures with approximately 70 K average for Block A, and 50 K for Block B, using optimal LO pump powers for each LO frequency. There is a high frequency ripple which stems from the IF chain. The abrupt peaks are from the LO leaking through to the IF signal, this is because the IF bandwidth is larger than it was for *CARUSO*, and therefore it would be better to use a different multiplication factor in the LO chain to move the LO fundamental frequency outside of the IF bandwidth. Figure 31 shows the USB and LSB gain curves, with gain in the order of 14 dB. These display a low frequency ripple, which is potentially due to an internal mismatch within the LNA+SHIRM block, this would require more intensive design work in future iterations to understand and minimise. Further analysis of all of these observations will be conducted in the discussion in section 3.5.

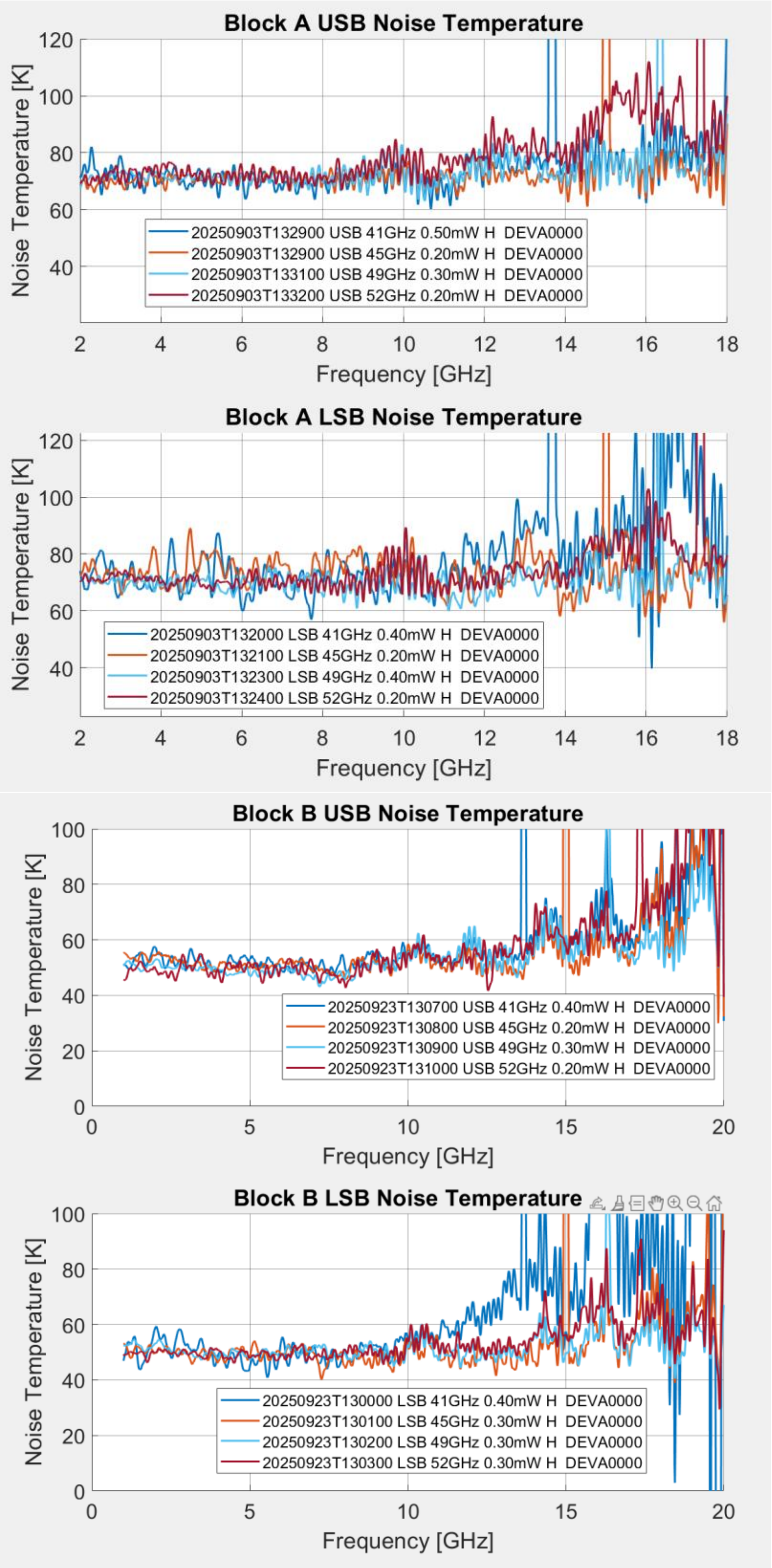

Figure 30 - DSB noise temperature results at 20 K

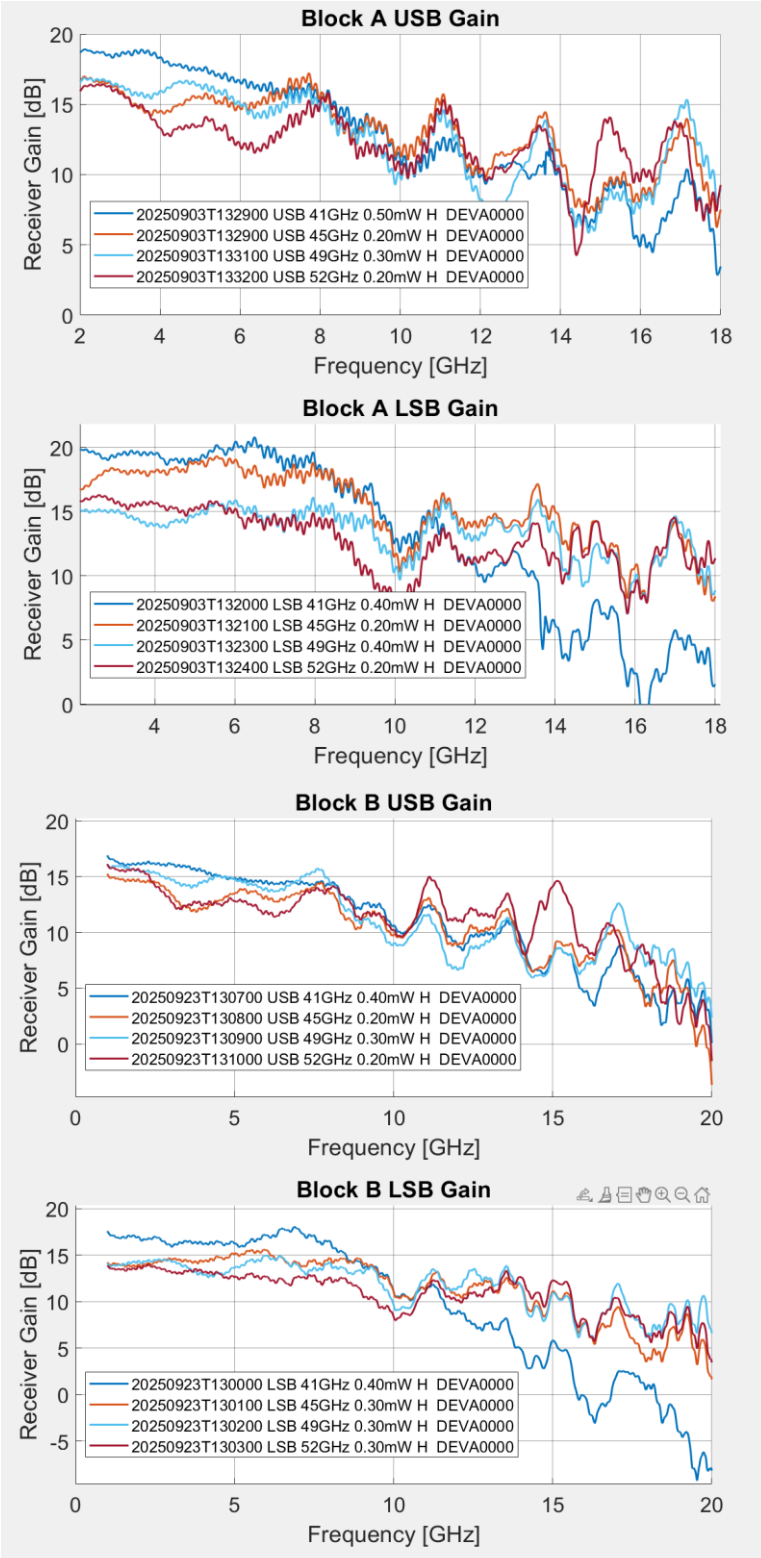

Figure 31 - DSB Gain Results at 20 K

3.4.2 Cryogenic Image Rejection Measurements

Figure **32** shows the optimised image rejection and SSB noise temperature. For Block A only 0.5 mW LO pump power was measured, whereas for Block B, 0.2, 0.3, 0.4, and 0.5 mW LO pump power was measured, with the optimum being chosen for each LO frequency. Additionally, where the upper and lower side bands overlap, the better result was taken. The limit lines are those set for the *CARUSO* project, and act as a guide for the performance of the LNA+SHIRM measurements. These results will be discussed in more detail is section 3.5, including a comparison with the performance requirements for ALMA. A dip in the image rejection ratio is observed around 101 GHz for both devices. This could potentially be attributed to the RF LNA and SHIRM, possibly due to a high reflection point at this RF frequency, although the exact cause is not clear at this stage. Further investigation could involve shifting to a different LO frequency to cover the same RF frequency range, as the image rejection ratio is LO frequency dependent.

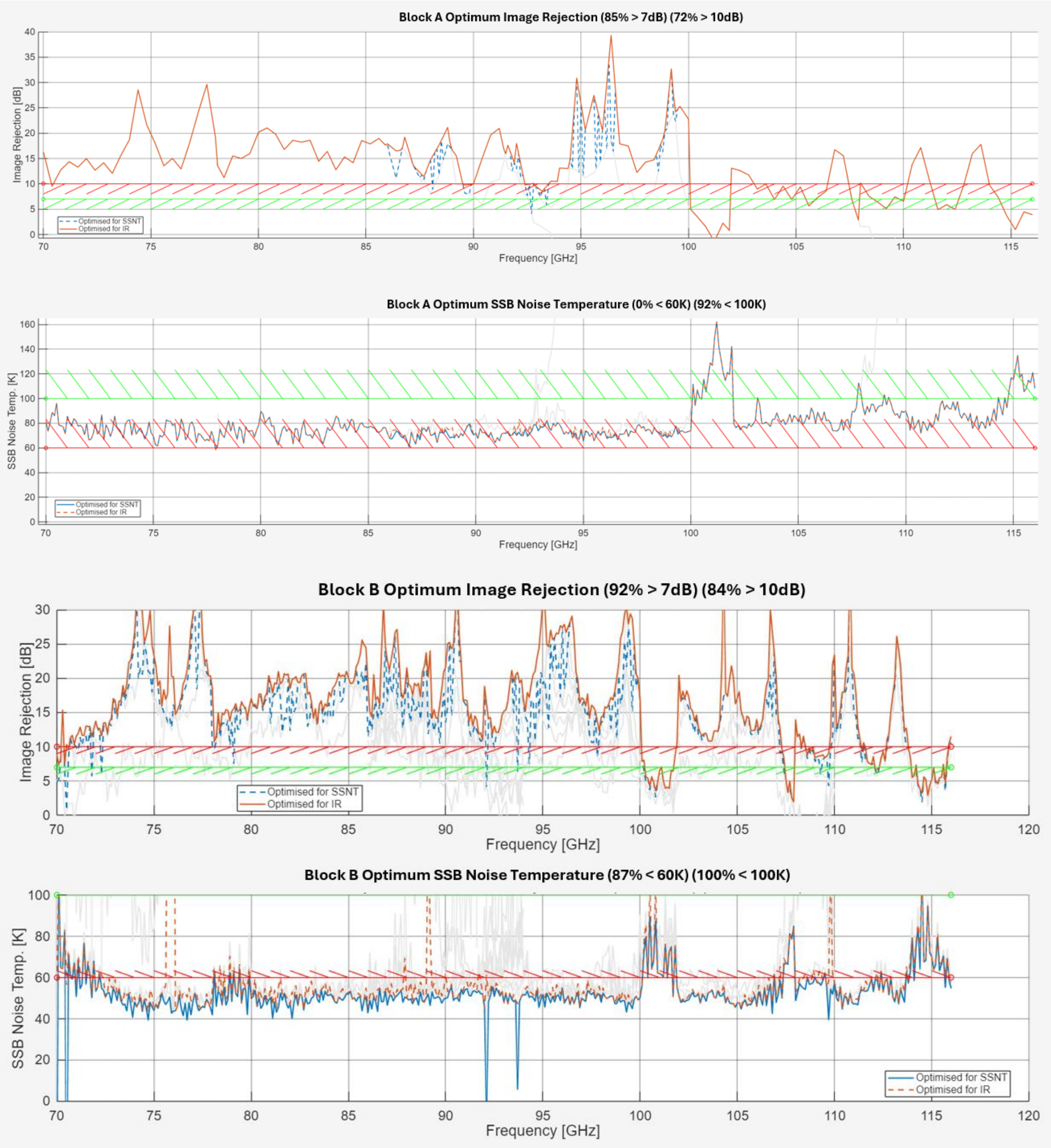

Figure 32 - Block A image rejection and SSB noise temperature results, faint grey lines show measurements at other LO frequencies

3.5 Results Discussion

The performance of both LNA+SHIRM units are very promising. There is clearly a difference in performance between the two units, with block B showing better performance than block A. Table 6 shows the specification table originally shown in Table 2, with the performance of the two blocks added. This section will present a discussion on these results.

Interface	**Frequency Range**	**Type of Interface**	**Achieved**
RF Input	67 – 116 GHz	WR10 Waveguide	Yes
LO Input	40 – 60 GHz	WR19 Waveguide	Yes
IF Output x2	2 – 18 GHz	Coaxial Connector (SMP)	Yes
LNA DC Bias	DC	Micro-D Connector	Yes
Operating Temperature			
Room Temperature	~293 K		Yes
Cryogenic Temperature	~15 K – 20 K		Tested at 20K
Power Dissipation			
Single 3-stage LNA MMIC	Up to ~16 mW per stage		Block A: 30.4 mW Block B: 25.4 mW
Sensitivity			
Based on *ALMA Band 2*	NT: 80% < 30 K, 100% < 47 K NT: 80% < 37 K, 100% < 60 K		Block A: 80 K (92% < 100 K) Block B: 50 K (87% < 60 K)

Sideband Ratio		
Based on *ALMA Band 2*	100% > 10 dB	Block A: 72% >10dB Block B: 84% >10dB

Table 6 - Comparison of the Specification to Achieved Performance

For block A the results show for SSB noise Tn ≈ 80 K, where 92% of the bandwidth is less than 100 K, and for block B Tn ≈ 50 K, where 87% is less than 60 K (Figure **32**). Although these values are higher than the specification there could be several factors leading to this, the main unknown being the performance of the two LNA MMICs that have been used in these LNA+SHIRM units. The difference in noise performance between the two blocks could be attributed to the difference in noise performance of the two MMICs, a 30 K difference is just about within the range of performance that we have seen with the 2-stage version of the MMICs. This means that pre-selection of the LNA MMICs to use in integrated devices is very important from a performance perspective, especially if the first stage of amplification is ever integrated. Pre-selection of LNA MMICs could not be performed within the time scale and budget of this project, although methods of pre-selection are a priority for future research, this is discussed more in section 6.

Typically, in a complete receiver two stages of LNA would be used to improve the noise and gain. The Friis's formula for receiver noise can be used to assess how adding a first stage LNA in front of the LNA+SHIRM block would change the performance. Assuming such a first stage LNA has a gain of 17 dB and noise temperature of 26 K (typical performance for a moderately good 3-stage UoM LNA, using noise temperature from Figure 3), for Block A, taking a noise temperature of the LNA and SHIRM of 80K (see Figure **32**) the noise temperature can be given by:

$$T_{sys} = T_{LNA} + \frac{T_{LNA+SHIRM}}{G_{LNA}}$$

$$T_{sysA} = 26 + \frac{80}{50.12} = 27.6\ K$$

And for Block B, taking a noise temperature of 50K (see):

$$T_{sysB} = 26 + \frac{50}{50.12} = 27\ K$$

This is a promising result for an initial attempt for meeting the ALMA specification should pre-selection of the MMICs be good enough, with reference to the ALMA specification for noise temperature and sideband rejection as seen in Table 6. The. Both results are within the expected range for a *CARUSO* receiver for noise temperature, with a higher gain from the three stage amplifiers instead of the original two stage, which shows that the integration of an LNA and SHIRM has not have a negative effect on the overall receiver performance. Additionally, it shows low variance in the overall receiver noise temperature, despite the 30 K difference in noise temperature between block A and block B, due to the overall importance of a high gain and low noise first stage LNA.

From [13], the practical noise limit for HEMT devices is four times the quantum limit, which in the middle of ALMA Band 2 (91.5 GHz) is 17.6 K. In Table 7 the noise temperature results presented in work package 1 are shown as multiples of the quantum noise limit. For the TASER blocks on their own, we are at 11 and 18 times the quantum limit, when paired with a first stage LNA as discussed above, however, this goes down to ~6 times. Figure 33 shows noise temperatures for the ALMA receiver for comparison. Above band 2, receivers utilise SIS mixers rather than pre-mixer LNAs. A big advantage for the use of HEMT technology over SIS is that it requires less cooling, approximately 4 K for SIS and 15 to 20 K for HEMT and therefore saves on power consumption and cryostat complexity.

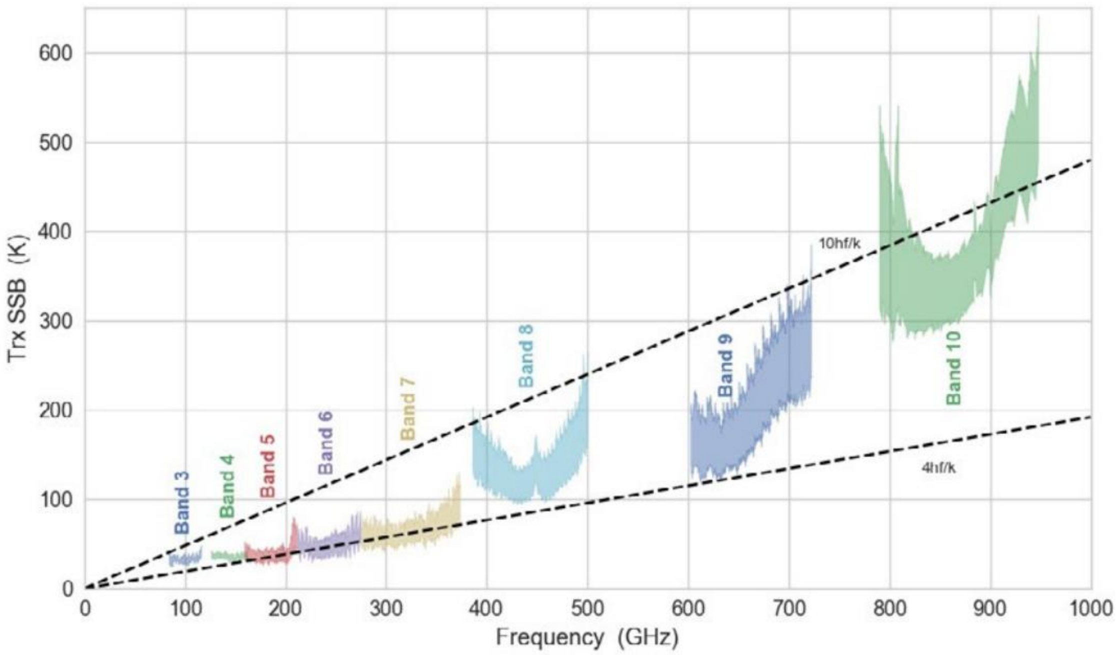

Figure 33 – From [14], 'Receiver noise temperature for the ALMA receiver, where the shaded region encompasses 75% of the receivers about the median receiver temperature'

Configuration	Configuration Noise / K	Multiples of Quantum Limit (hf/k)
Cascaded LNAs at 15 K*	26	5.9
Block A	80	18.2
Block B	50	11.4
Block A + 1st Stage**	27.6	6.3
Block B + 1st Stage**	27	6.1

*As seen in Figure 3

**As described above

Table 7 - Noise temperature results as multiples of the quantum noise limit (hf/k) at mid ALMA Band 2 (91.5 GHz) (4.4 K)

Finally, the image rejection is specified at >10 dB, which for block A is true for 72% of the band, and block B 84%. This is a promising result for the first iteration of these complex devices, further investigation into the factors affecting this aspect of performance can be undertaken in future projects to inform subsequent design iterations and help to improve the performance.

Power dissipation is given at ~16 mW per stage, or 48 mW for a three stage device, for block A the total dissipation was 30.4 mW, and for block B 25.4 mW, which is well within specification. A figure of 16 mW per stage is typically at the high end of what could be needed to bias an LNA and is often seen when the gain of the LNA needs to be pushed to higher levels (typically with second stage LNAs). Measuring lower power dissipation could therefore be a sign that the LNA is operating closer to the optimum noise performance bias, but further analysis through the UoM LNA measurement system that can produce heat maps of device performance over a range of bias points would be needed to confirm this. Adding a first stage LNA in front of the LNA+SHIRM would increase the overall level of gain and could therefore lower the LNA bias further. Lower power dissipation is also beneficial for receiver operation, particularly in FPAs with higher numbers of LNAs.

There are a few ways which the results presented could be improved. The measurement system in Manchester was not available during *TASER*. Originally, sweeps of LNA gate and drain voltage were performed at UoM on each amplifier to give bias performance heat maps of optimum gain and noise bias for each stage of the LNA. The heat maps were used to identify the optimum bias point for a final LNA measurement. At RAL, this optimum bias for each LNA was used to give a starting point for the LNA bias optimisation performed as part of the receiver measurements. We have found that the optimisation software at RAL performs much better when given a bias close the LNA optimum as a starting point rather than a nominal value as was used for the *TASER* measurements.

In the DSB plots for noise temperature, Figure 30, we can see a high frequency ripple that is due to the way in which the IF chain is de-embedded from the receiver noise temperature measurements. To remove this better matching between the two IF LNAs, and the SHIRM output and initial IF LNA (see Figure 24) is necessary, an isolator would also fix this issue. It would be better to specify an IF LNA with larger bandwidth, higher return loss, and better noise performance to minimise this effect.

In the DSB gain plots, Figure **31**, there is a low frequency ripple which is likely due to a component mismatch within the LNA+SHIRM. Further analysis of the design can be undertaken to identify and try to solve this mismatch before the next design iteration of these designs. In addition, it will highlight the area of concern as we move towards LNA+SHIRM design at higher frequencies.

Additionally, it can be seen from the spikes in performance in Figure 30 that the LO is leaking through to the IF. This means that either more LO-IF isolation is needed, this could be achieved with further development of the design, or a different source and factor of multiplier in the LO chain is required to move the LO out of the IF range of interest.

Finally, the variation in components is an important consideration with integrated devices. Because individual parts can't be packaged, tested and paired together in optimum pairs, it is important to either have a production process with a high level of repeatability, or to have a good MMIC probing setup that allows for pre-assembly measurement of the LNA MMICs. Being able to probe MMICs prior to packaging, would re-enable the ability to select component to achieve a more consistent average receiver performance. However, probing MMICs and other on-chip components causes unavoidable damage to the pads where the probes land. Typically, the amount of damage is minor and does not cause further problems, although excessive vibrations from the cold head in a cryogenic probe station and long measurement times often needed for noise measurements will exacerbate this, increasing the amount of damage and potentially preventing bond wires being attached to the pads during assembly or causing further reliability concerns. More work would be needed to develop a suitable cryogenic on-wafer probe station setup suitable for characterising on-chip components prior to assembly and to understand and prevent the risks posed by the damage to probe pads that is caused by probing.

3.6 Summary

Two proof-of-concept LNA+SHIRM units operating with an RF input frequency of 67 – 116 GHz (ALMA Band 2) have been developed. The IF band was chosen to be 2-18 GHz (to give 16 GHz IF bandwidth), the Marki MQS 0218CH was chosen as the IF coupler to provide this bandwidth. Significant space saving has been achieved, as can be seen in Figure 20. Testing was performed at RAL with the LNA+SHIRM cooled to 20 K. The results show promising performance, with Block A achieving Tn ≈ 80 K, and 72% IR >10 dB, and Block B achieving Tn ≈ 50 K, and 84% IR >10 dB.

The intention is that this LNA+SHIRM would provide the second stage LNA and SHIRM devices in the receiver, and typically this would need to be combined with a first stage LNA to boost the signal gain and drive down the noise performance. A typical UoM 3-stage LNA with gain of 17 dB and noise temperature of 26 K, such as those shown in Figure 3. The effect of combining one of these LNAs with the LNA+SHIRM can be calculated, giving noise temperatures of 27.6 for block A and 27 K for block B.

This shows that the integration of the LNA and SHIRM has not negatively affected performance of the receiver chain, and has been successful, offering a promising approach to further integration and miniaturisation of receivers.

4. Work Package Two: ALMA Band 4+5 SHIRM

An InGaAs Schottky diode based SHIRM has been developed by RAL for a possible future ALMA Band 4+5 (125-211 GHz) receiver. Further challenges for this specific study include:

- Wideband IF requirement, from 2-18 GHz or 4-20 GHz, for any future ALMA wideband upgrade
- Broadband waveguide hybrids, requiring high-precision CNC machining at higher frequency
- Overall smaller and compact mechanical housing

This section will present the design process towards a fully integrated SHIRM with its individual simulation results prior to the complete SHIRM predicted performance, with specifications given in Table 8.

Parameter	Specification	Comment
RF Input Centre Frequency (GHz)	125-211	
LO frequency (GHz)	72.5-95.5	
IF Bandwidth (GHz)	4-20	
Conversion Loss (dB)	TBC	LNA as 1st stage
Image rejection ratio (dB)	>10	
RF waveguide	WR-05 or customized	
LO interface	WR-10	
Overall dimension	-	Compact

Table 8 - Target SHIRM Specification

4.1 Double Sideband (DSB) mixer with predicted performance

The DSB subharmonic mixer is the most critical component in the integrated SHIRM unit. This mixer uses discrete diodes on a 20 µm thick InP, as shown in Figure 34. The diodes are mounted on a 75 µm thick quartz substrate with associated matching and filtering circuitry. The mixer block is split in the E-plane of the RF and LO waveguides with fixed RF and LO back-shorts. This configuration simplifies the assembly of the mixer and reduces waveguide losses. The microstrip channel is perpendicular to the RF and LO waveguides. Two-sided waveguide-to-microstrip transitions are used to couple both the RF and LO signals into the channel. The detailed design and optimization methodology combines 3D electromagnetic modelling using HFSS (Ansys) with harmonic balance simulation using ADS (Keysight). Note that the diode electrical parameters are also adjusted for physical effects via the bespoke modelling tools and for cryogenic operation.

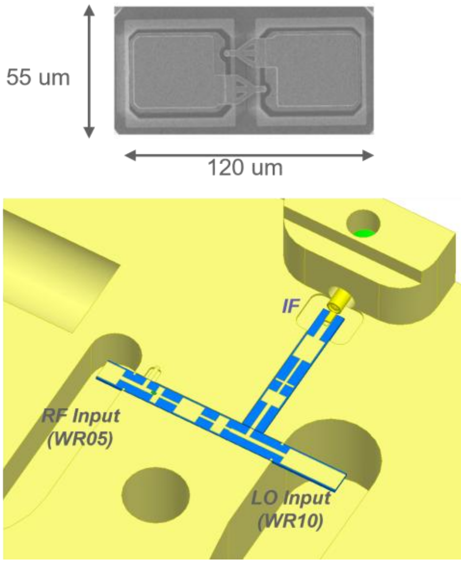

Figure 34 - Schematic of the broadband DSB subharmonic mixer circuit and waveguide matching elements in a split block, a photograph of an anti-parallel pair of RAL's InGaAs diodes is shown above.

The mixer is optimised for IF from 1-20 GHz and RF from 125 to 211 GHz. The simulation predicts a conversion loss of ~10 dB with LO at 85 GHz operating at room temperature and ~6 dB at 20 K, with 0.3 mW of LO power. Significant mixer performance improvement, both for conversion loss and noise temperature, is achieved when the mixer is cooled to 20 K (Figure 35). Figure 36 shows the mixer conversion gain over the IF range when operating at 20 K. There is potential performance improvement when the mixer is cooled further to 4 K. However the ALMA's current cryostat 4 K stage can only handle 16 mW power dissipation, which is exceeded by the RF LNA in this receiver configuration.

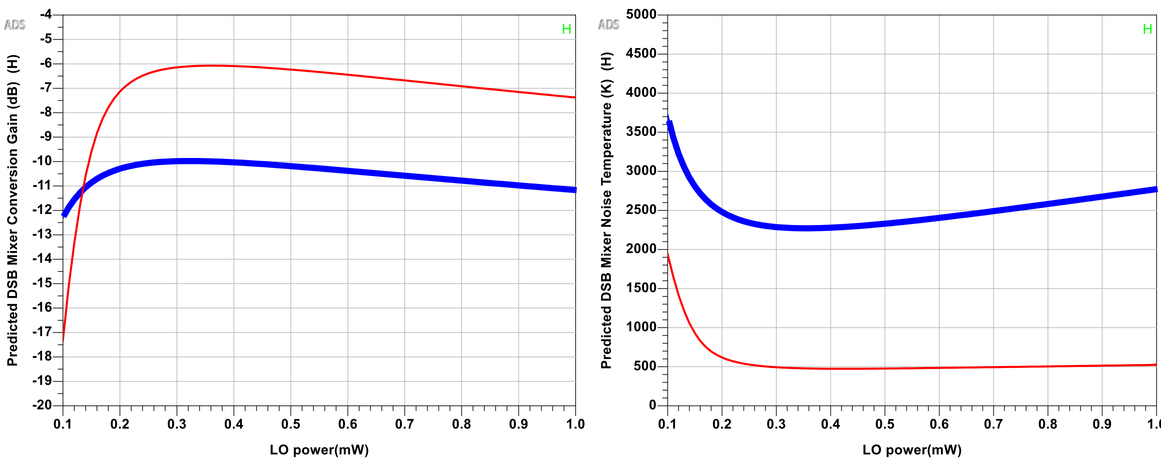

Figure 35 - Predicted DSB mixer conversion loss and noise temperature vs LO power at room temperature 300 K (blue curves) and cryogenic temperature 20 K (red curves).

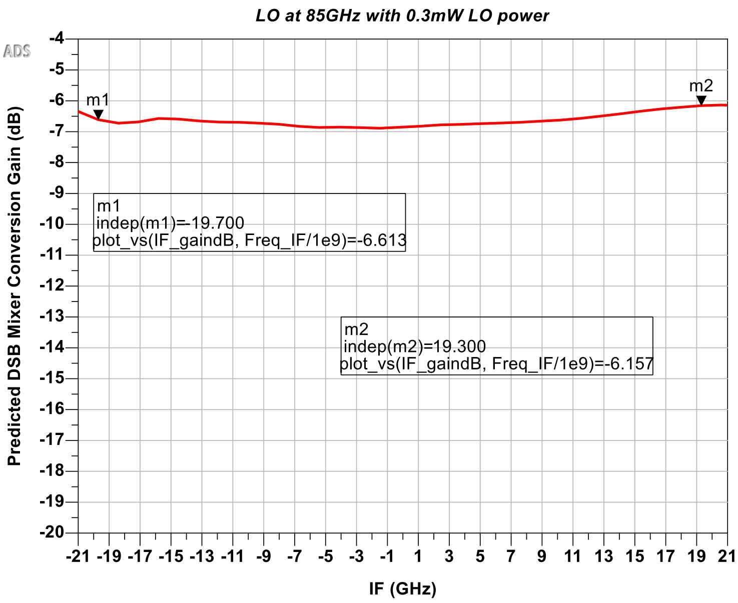

Figure 36 - Predicted DSB mixer conversion gain vs IF at a temperature of 20 K.

4.2 RF, LO, and IF Hybrids

Three 3 dB 90° hybrids are required for our proposed SHIRM configuration, which includes two waveguide-based RF and LO hybrids, and a semiconductor-based IF hybrid. Amplitude and phase imbalance in the RF and IF quadrature hybrids reduces the sideband separation ratio of a sideband-separating mixer, as indicated in Figure 37.

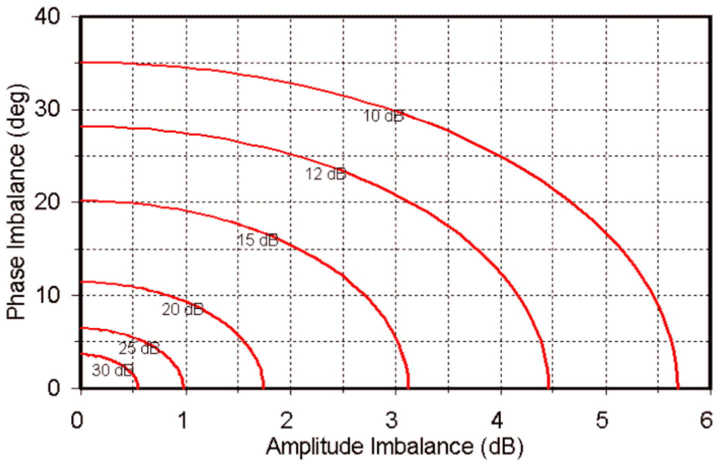

Figure 37 - Effect of amplitude and phase imbalance in sideband-separating and balanced mixers. Contours of constant sideband rejection ratio or LO noise rejection are plotted against amplitude and phase imbalance.

We have chosen to use the branch-line waveguide coupler because of its compatibility with the split-block type of construction and its simplicity of fabrication. To optimize the design r, we used a commercial 3D electromagnetic simulation software HFSS from Ansys. We have adopted a quadrature hybrid with six branch lines: Figure 38. The simulated results of the RF and LO coupler are shown in Figure 39 and Figure 40. We have optimized the bandwidth, coupling, amplitude and phase imbalance while retaining ease of manufacture. The main challenge is to minimize the amplitude and phase imbalance over the 52% bandwidth of the RF hybrid. The selection of the final RF and LO hybrid designs are trade-offs between of the amplitude imbalance and the frequency bandwidth.

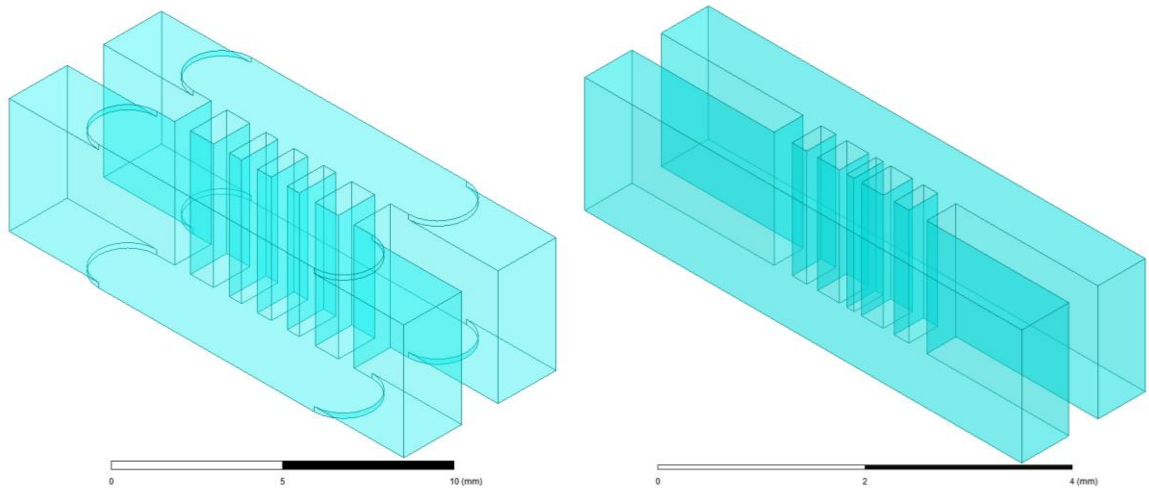

Figure 38 - Designs of the RF (Left) and LO (Right) waveguide quadrature hybrids.

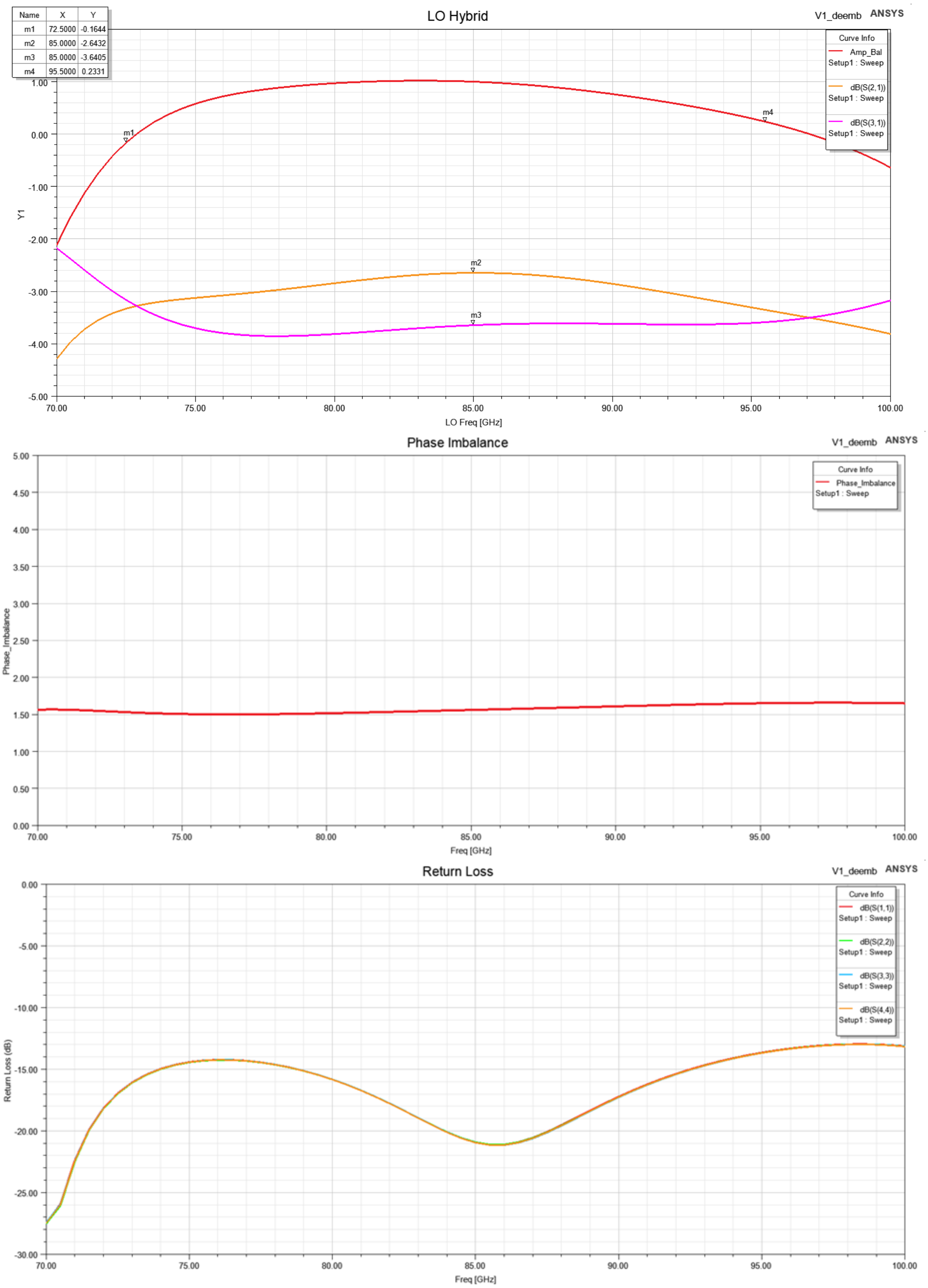

Figure 39 - Simulated results of LO quadrature hybrid's amplitude imbalance, phase imbalance and return loss.

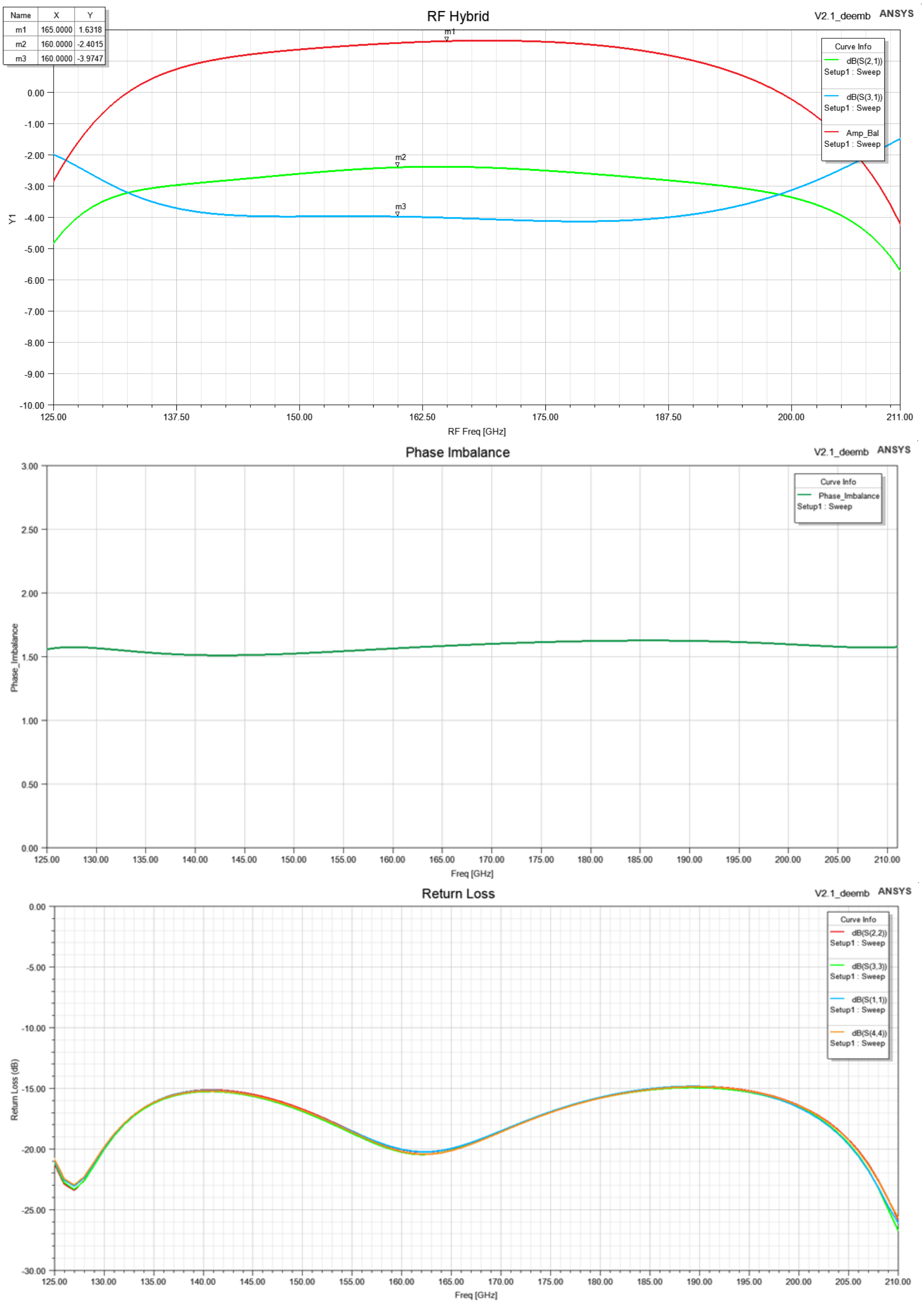

Figure 40 - Simulated results of RF quadrature hybrid - amplitude and phase imbalance and return loss.

An ultra-broadband IF hybrid covering a 16 GHz bandwidth is required to meet the specifications, see section 3.1.1. The impact of the RF, LO and IF hybrid on the SHIRM performance has been analysed: Table 9 gives a summary of different performance aspects. The design and selection of the hybrids is based on this to meet the overall SHIRM requirement.

	Conversion Loss or NT	Image Rejection	USB/LSB Imbalance
RF Hybrid			
Insertion Loss	Yes		
Amplitude Imbalance		Yes	
Phase Imbalance		Yes	Yes
Return Loss		Yes	
LO Hybrid			
Insertion Loss	Small impact		
Amplitude Imbalance		Small impact	
Phase Imbalance		Yes	Yes
IF Hybrid			
Insertion Loss	Yes		
Amplitude Imbalance		Yes	Yes
Phase Imbalance		Yes	Yes
Return Loss		Yes	

Table 9 - Effect of amplitude and phase imbalance in sideband-separating mixer

4.3 Predicted SHIRM Performance

The optimization of the overall SHIRM is performed with the harmonic balance simulation using ADS from Keysight. The simulation results as example are shown below with the LO frequency at 84 GHz and power of 0.4 mW, while IF ranges from 2-18 GHz. This represents the upper sideband (USB) from 170 GHz to 188 GHz and the lower sideband (LSB) from 148 GHz to 166 GHz.

All simulations below use the same DSB subharmonic mixer design as shown above. First, a SHIRM with ideal hybrids for RF, LO, and IF was used to predict the ideal case, where all hybrids have uniform insertion loss (0.1 dB), amplitude imbalance (1 dB), and phase imbalance (1°) over the respective frequency ranges. The USB mixer performance and rejection ratio are shown in Figure 41. However, actual hybrids do not have uniform performance over such a wide frequency range. For example, Figure 42 shows the S-parameters from the Marki 2-18 GHz IF hybrid data sheet, where the insertion loss is greater than 1 dB, and the amplitude imbalance is approximately 3 dB, both of which significantly impact the integrated SHIRM's performance.

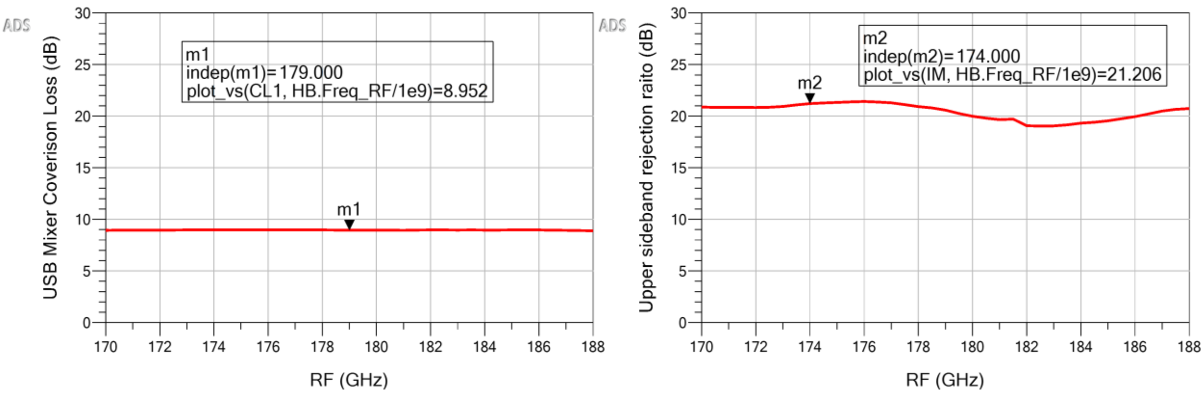

Figure 41 - Predicted USB mixer conversion loss and rejection ratio vs RF at 20 K.

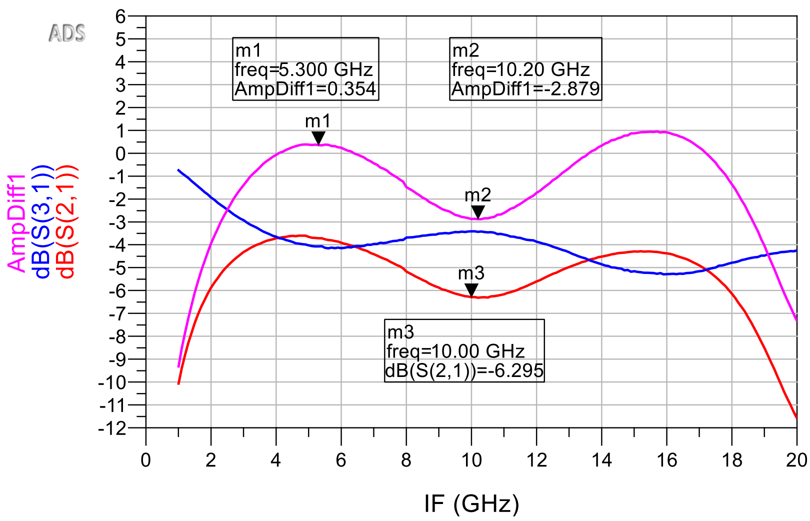

Figure 42 - Marki IF hybrid performance retrieved from supplier datasheet.

Figure 43 shows the USB mixer conversion loss performance and rejection ratio, comparing an ideal IF hybrid and the Marki 2-18 GHz hybrid, as shown earlier in Figure 42. The SHIRM is composed of an actual RF and LO waveguide hybrid, designed specifically for this study. In the case of the ideal IF hybrid, an insertion loss of 1 dB, an amplitude imbalance of 1 dB, and a phase imbalance of 1° were used in the simulation. It was demonstrated that the actual IF hybrid has degraded both the conversion loss and rejection ratio.

Finally, predicted SHIRM performance with actual RF, LO and IF hybrid with respected USB and LSB mixer performance and rejection ratio are shown below in Figure 44 and Figure 45.

The plots shown were based on the Marki IF hybrid, which is the only commercially available bare-die chip. While it can be integrated, it offers the worst overall performance. Alternatively, we could sacrifice full integration for better performance by using the connectorized IF hybrid from either Krytar or Yebes, which would result in significantly better performance.

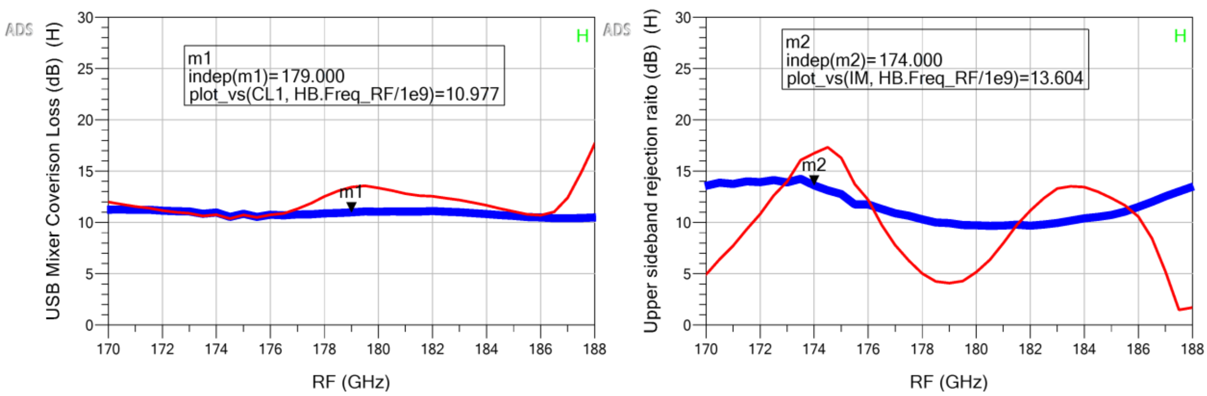

Figure 43 - Predicted SHIRM USB conversion loss and image rejection ratio vs RF with ideal IF hybrid (blue curves) and the selected Marki 2-18 GHz IF hybrid (red curves)

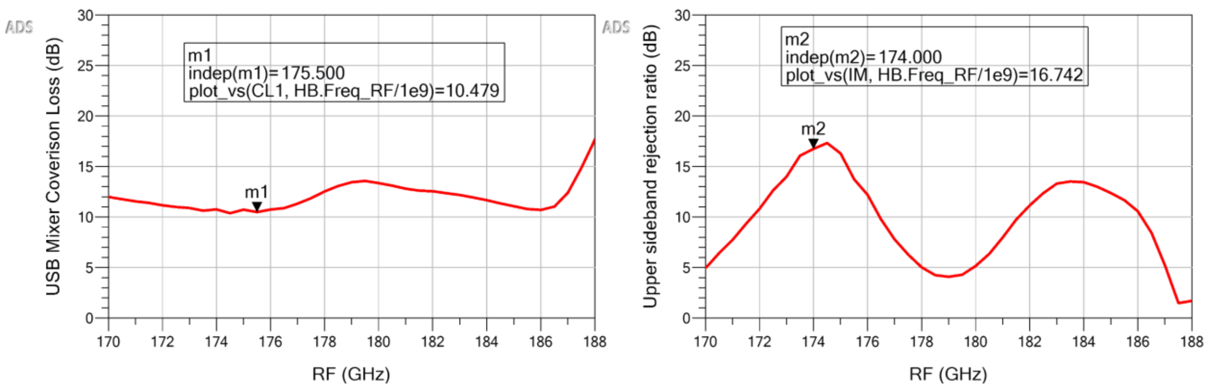

Figure 44 - Predicted USB conversion loss and image rejection ratio vs RF at 20 K.

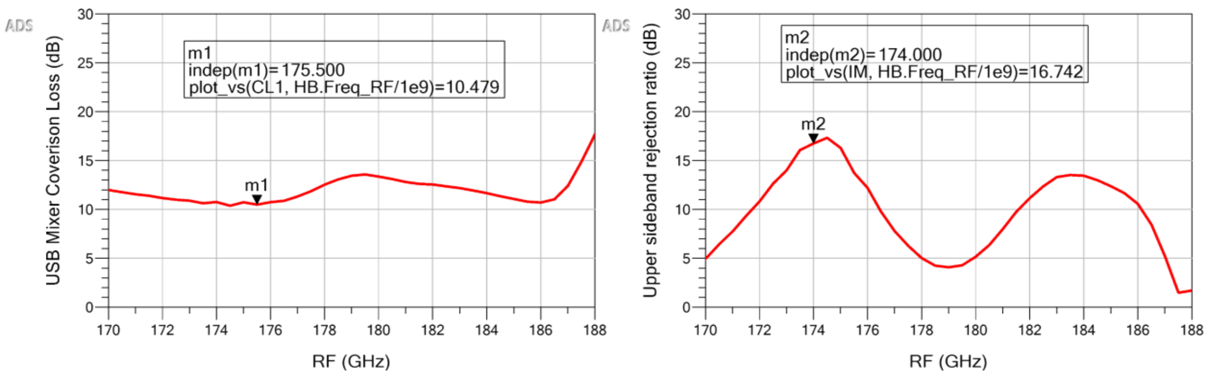

Figure 45 - Predicted USB conversion loss and image rejection ratio vs RF at 20 K.

4.4 Measured RF results

The DSB mixer and SHIRM for ALMA Band 4+5 have been manufactured, assembled and tested at RAL. All RF measurements are performed at room temperature. Based on measurement heritage and physical modelling on Schottky diode devices, their performance at cryogenic temperatures can be evaluated using the 300 K measurement data. A summary of the devices is shown in Table 10; RF performance is presented in the following subsections.

Device Identification	Quantity	Serial Numbers
RAL_DSB168	4	SN250025 SN250026 SN250027 SN250028
RAL_SHIRM168	2	SN250037 SN250038

Table 10 - Summary of devices with serial numbers

4.4.1 DSB mixer performance at room temperature

The internal view of the lower half mixer block is shown in Figure 46. The Y-factor technique was used to test the mixer using ambient and liquid nitrogen-cooled loads as blackbody references. The equivalent noise temperature of the receiver was measured by presenting alternatively the blackbodies in front of the mixer feed horn via an automated motor driven mirror.

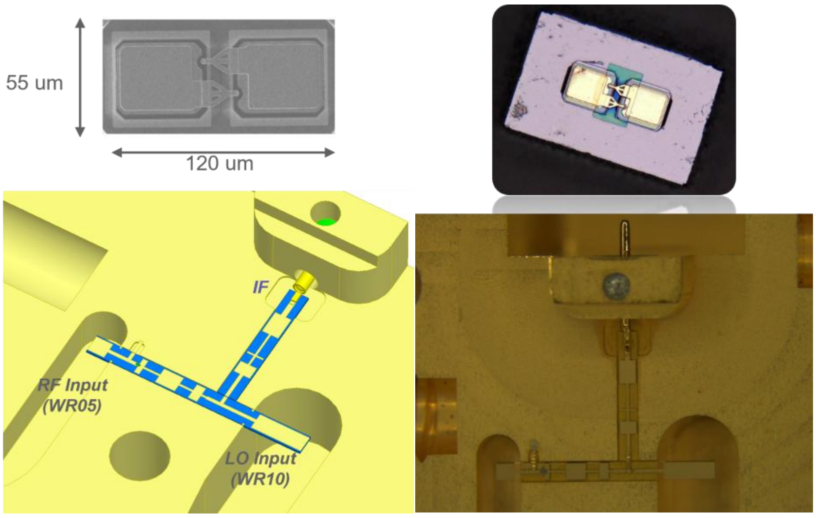

Figure 46 - Internal 3D view (left) and assembled picture (right) of the DSB mixer in the lower half mixer block. Top pictures show the GaAs (left) and InGaAs (right) Schottky diodes used.

The measurement was performed at three different LO frequencies 72.5 GHz, 84 GHz and 95.5 GHz. The LO source is composed of a commercial AMC unit; it is driven by a signal synthesiser. The LO power at each LO frequency has been calibrated from 0.2 mW to 0.5 mW per 0.1 mW step. A 1-18 GHz IF LNA was used for the measurement; the equivalent noise temperature of the IF chain is 250-300 K when measured using a noise tube. The mixer performance was de-embedded from the measured receiver performance using this IF calibration. A picture of the mixer measurement setup is shown in Figure 47.

All the measurements were performed at room temperature, and a total of four devices were tested. The DSB mixer noise temperature and conversion loss as a function of IF at three LO frequencies are presented in Figure 48 to Figure 50. The optimum pump power shows very good agreement with the simulation results, as does the measured conversion loss. The mixer exhibits a DSB equivalent noise temperature of ~ 2000 K and a conversion loss of around 10 dB over the 1-20 GHz IF band, with around 0.4 mW of LO power. All four devices demonstrated repeatable performance. There is no sharp degradation in mixer performance at 20 GHz, indicating that the mixer should operate beyond this frequency. Some spurious signals are observed across the IF range when the LO was set to 72.5 GHz: Figure 49. A commercial x6 source has been used as the LO source; however, its coverage is specified as 75–110 GHz. Since 72.5 GHz is outside this range, the x6 LO signal may have unwanted harmonics or spurious tones. Measurements have been performed at different LO frequencies in the 75-110 GHz band, and no spurious signals were observed for other LO frequencies. The tone peaking at 12.08 GHz is the fundamental LO signal leaking into the IF output.

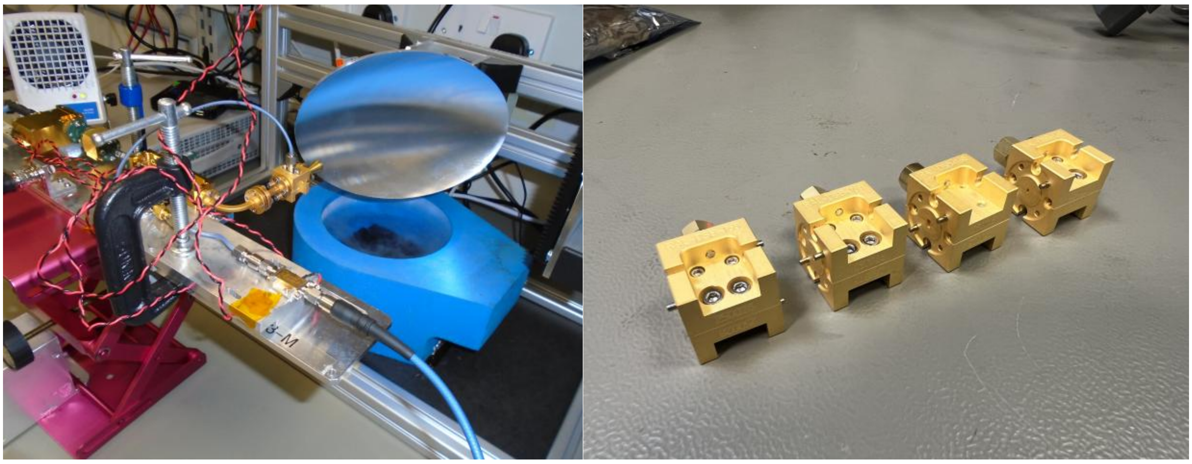

Figure 47 - Picture of the DSB mixer measurement setup (left) and the four DSB mixer blocks.

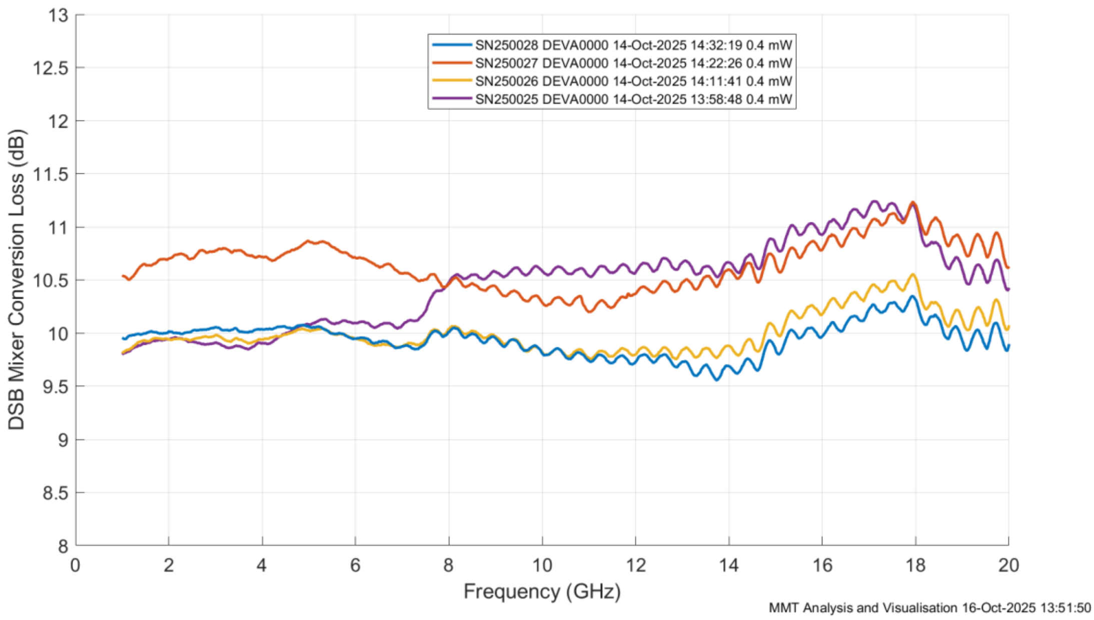

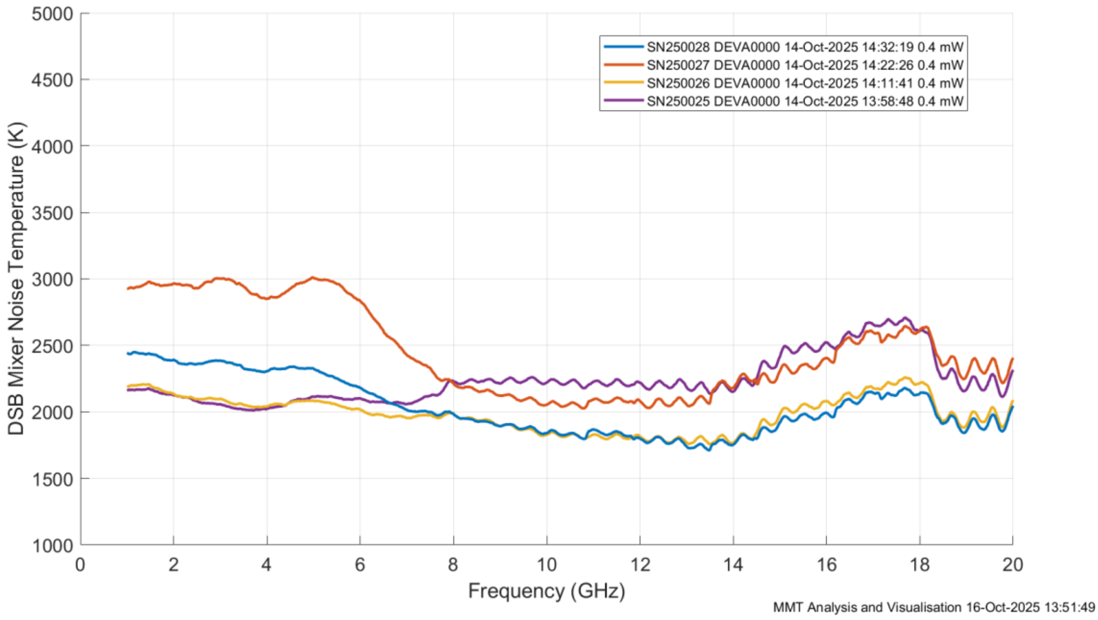

Figure 48 - Measured DSB mixer conversion loss and noise temperature at room temperature with LO at 84 GHz over the 1-20 GHz IF range.

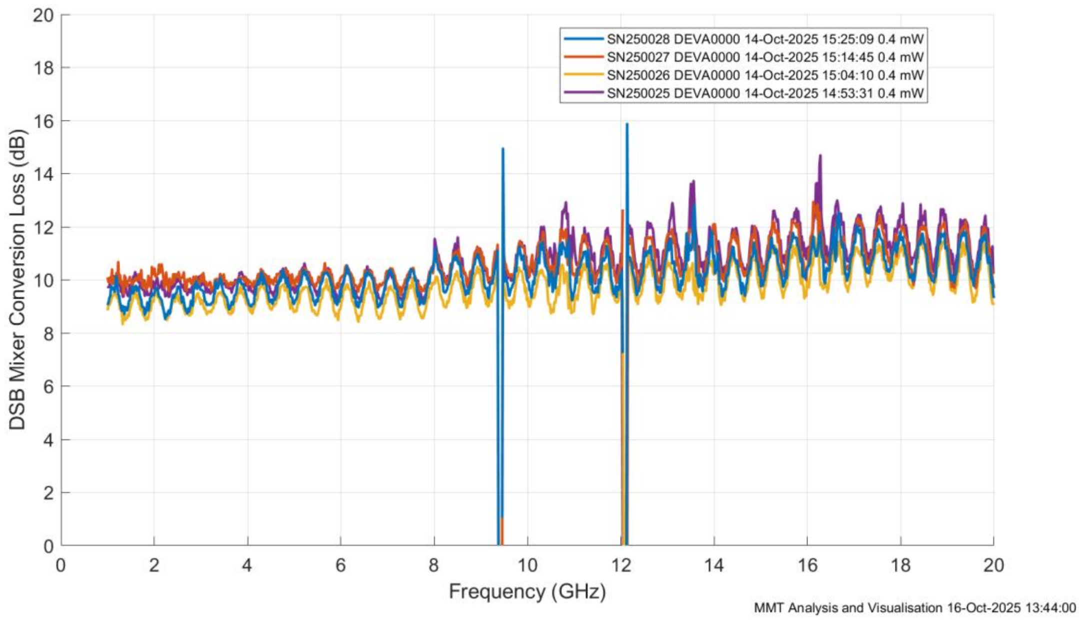

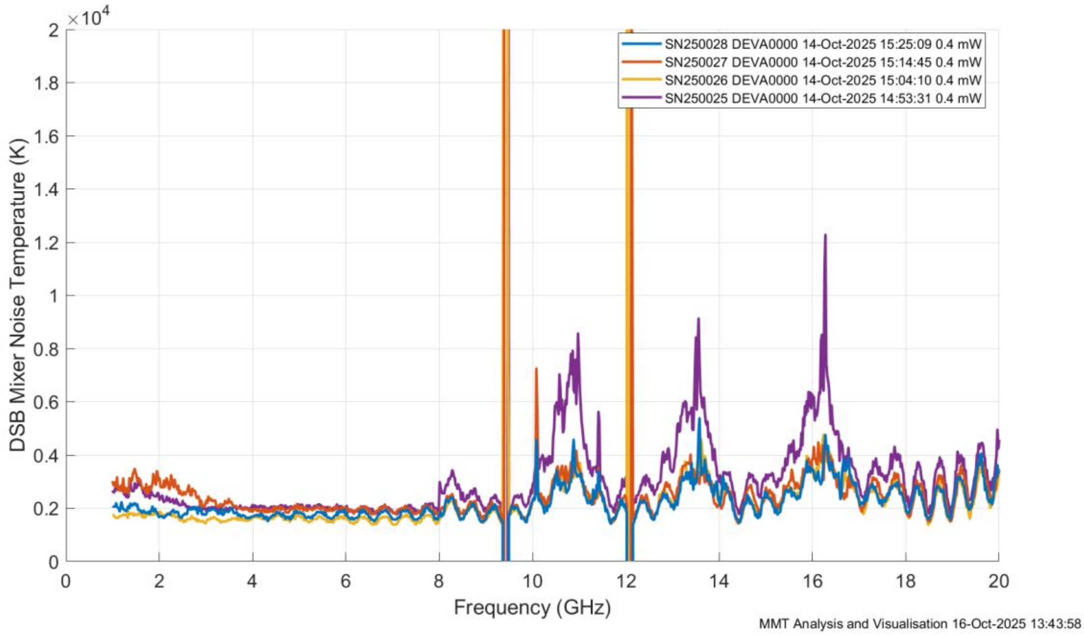

Figure 49 - Measured DSB mixer conversion loss and noise temperature at room temperature with LO at 72.5 GHz over the 1-20 GHz IF range. Spikes at 12.08 GHz are from LO leakage. Please note this measurement was made outside of the nominal LO source tuning range, hence some spurious features appeared making this measurement unreliable.

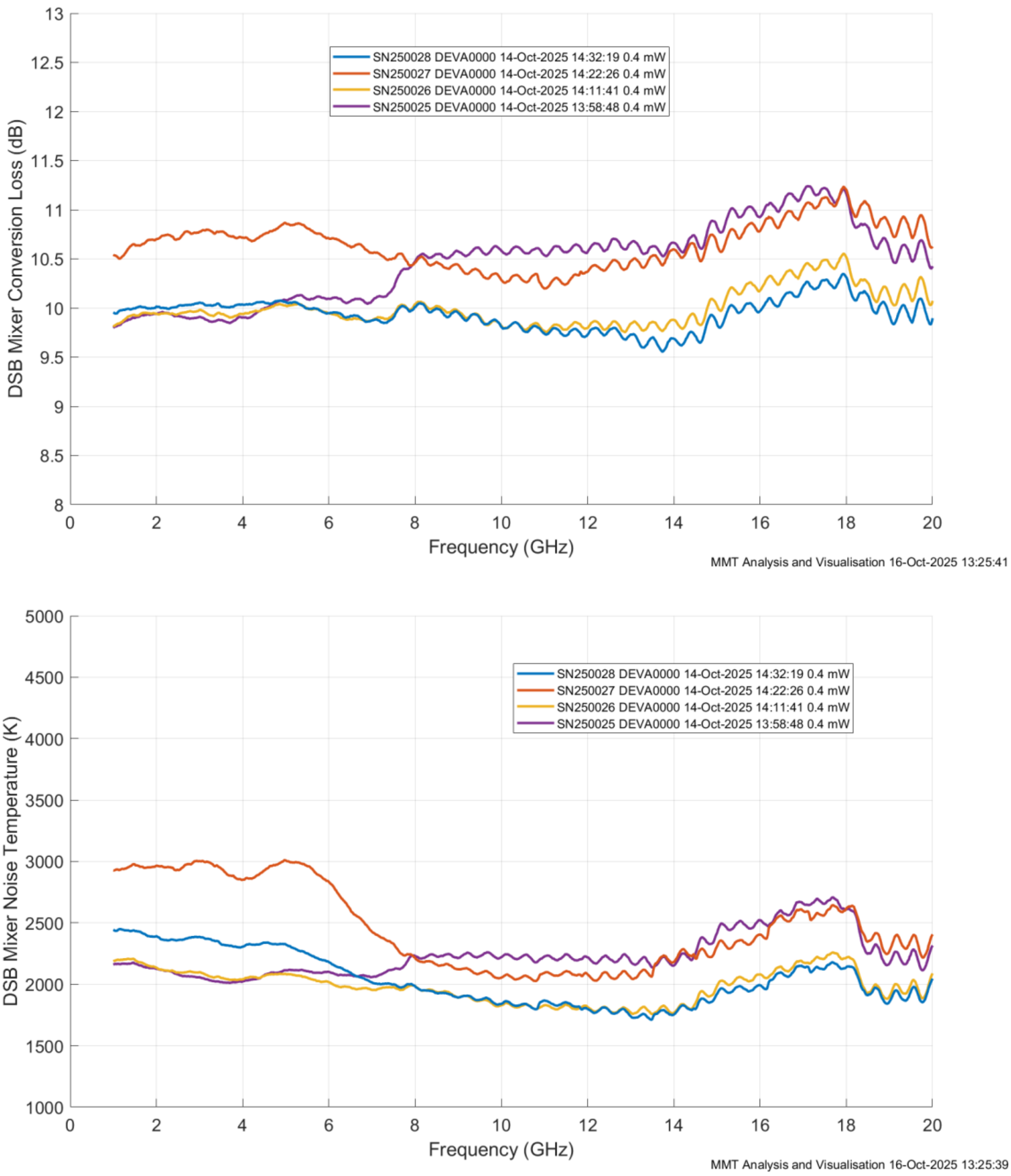

Figure 50 - Measured DSB mixer conversion loss and noise temperature at room temperature with LO at 95.5 GHz over the 1-20 GHz IF range.

4.4.2 SHIRM performance at room temperature

The SHIRM block is E-plan split into two halves, CNC machined in brass and gold plated. The block includes two waveguide branch line hybrids, see Figure 51. The quartz matching circuits are mounted into the metal block, and the discrete diode chip was soldered in place. The mixer

RF grounding is through the bonded gold ribbon connected directly to the metal block. Thermocompression bonding are used to make connection to matching circuits and SSMA connectors at various places. Figure 52 show the assembly image of SHIRM with internal view.

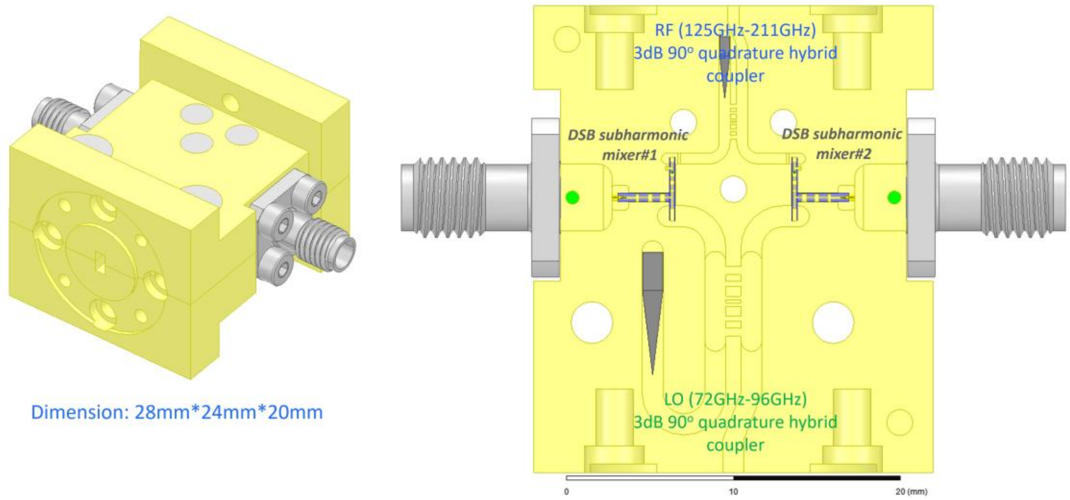

Figure 51 - 3D model of the SHIRM mechanical block (left), internal view of the SHIRM (right), exclude the IF hybrid.

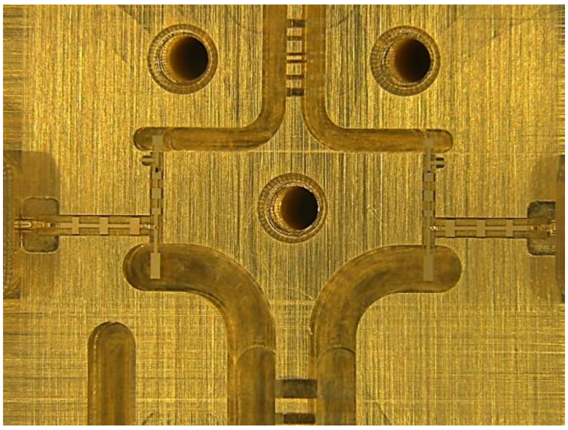

Figure 52 - Image of CNC machined SHIRM blocks with fully assembled circuit in one-half block.

The same measurement method and setup described above were used to test the SHIRM noise performance. A picture of the SHIRM noise temperature measurement setup is shown in Figure 53. Measurement was performed at four different LO frequencies: 80 GHz, 84 GHz, 88 GHz and 95.5 GHz. These LO frequencies were selected to ensure that the RF range fully covers the WR-05 band 140-220 GHz, in conjunction with a 4 - 20 GHz IF range. The LO power at each LO frequency was calibrated from 0.3 mW to 0.8 mW in 0.1 mW steps. Block SN250037 was measured using three different IF hybrids, as summarised in . The *TASER* SHIRM is designed for use with an external IF hybrid, allowing us to assess the impact of the IF hybrid on SHIRM performance. Figure 54 shows the *TASER* SHIRM with three IF hybrids, compared to the *CARUSO* SHIRM on the right, which features a fully integrated IF hybrid, highlighting its ultra-impact design.

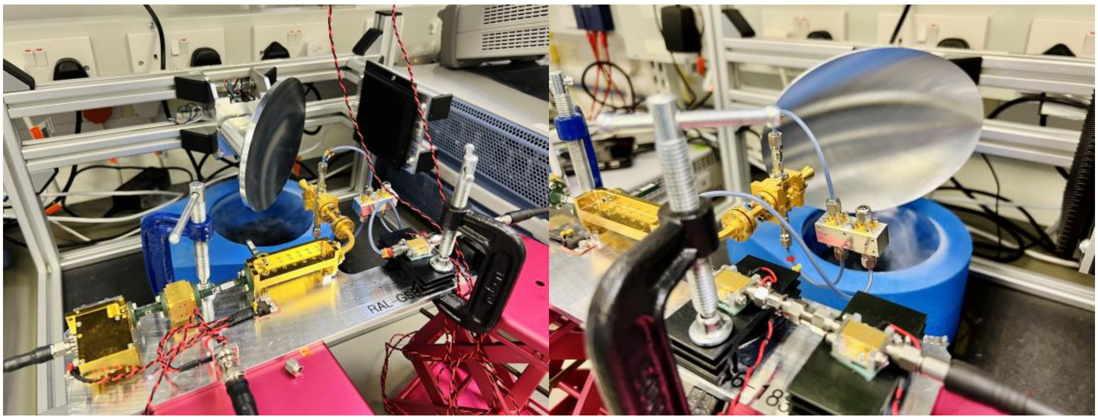

Figure 53 - Picture of the SHIRM NT measurement setup.

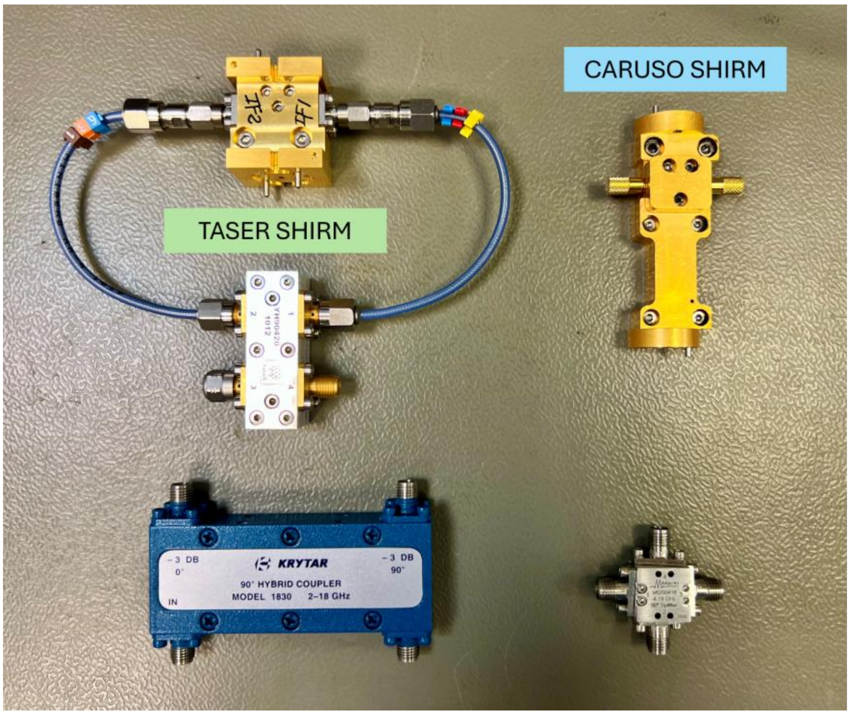

Figure 54 - Picture of the TASER SHIRM along with three IF hybrids used for the measurement, the CARUSO SHIRM is on the right corner.

All measurements were performed at room temperature. The SHIRM conversion loss as a function of IF with the LO at 88 GHz and LO power ranging from 0.3 to 0.8 mW, is shown in Figure 55. Under the same conditions, the corresponding noise temperature is shown in Figure 56. The two side bands demonstrate balance and comparable performance.

Additionally, two SHIRM blocks were assembled and tested using the Krytar IF hybrid. The performance compassion of the two SHIRM units at 88 GHz with an LO power of 0.6 mW is shown in Figure 57 and Figure 58, the results exhibit highly repeatable performance, confirming the robustness and reliability of the SHIRM design and build.

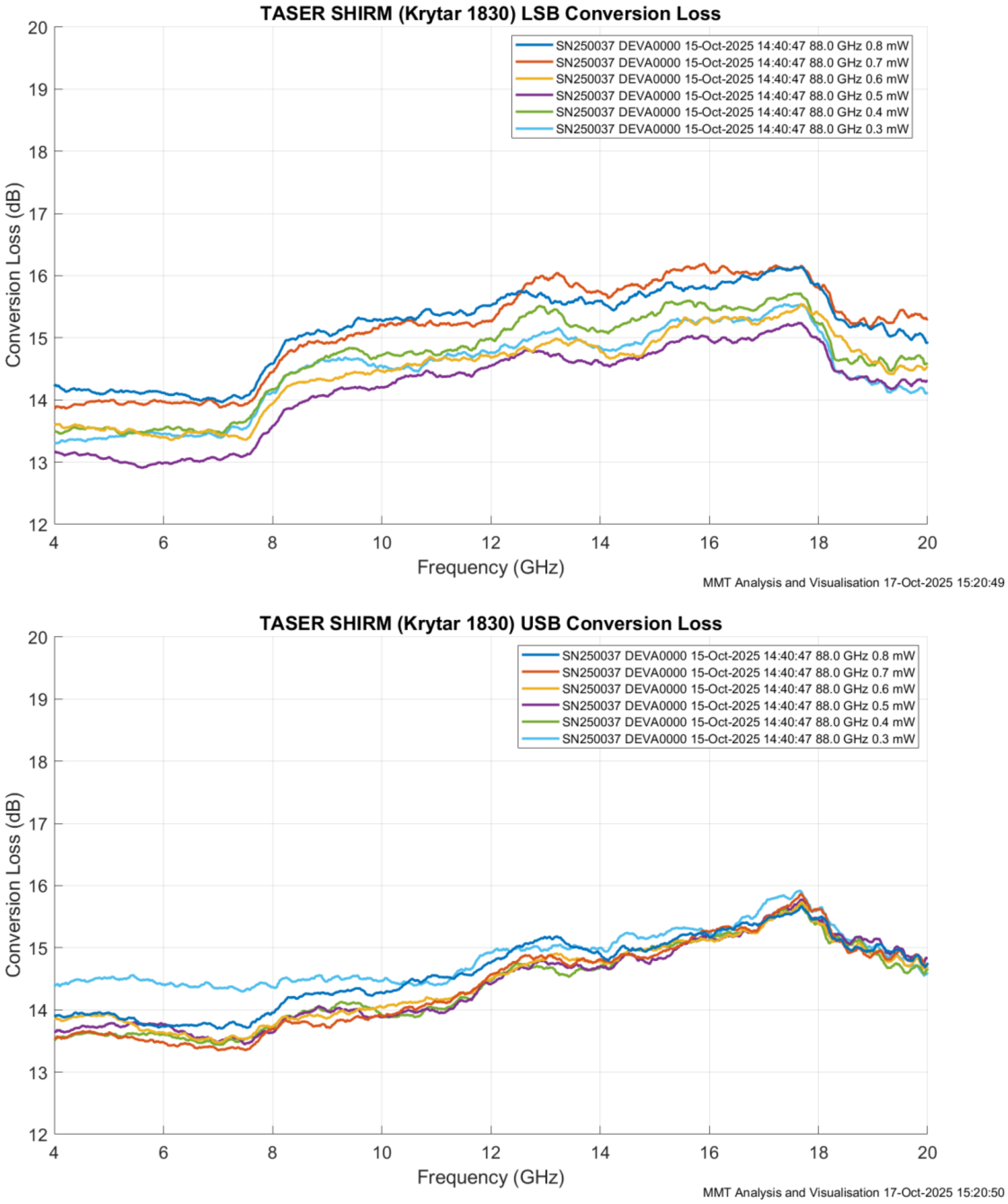

Figure 55 - Measured SHIRM SN250037 LSB (above) and USB (lower) conversion loss at room temperature versus IF with Krytar IF hybrid.

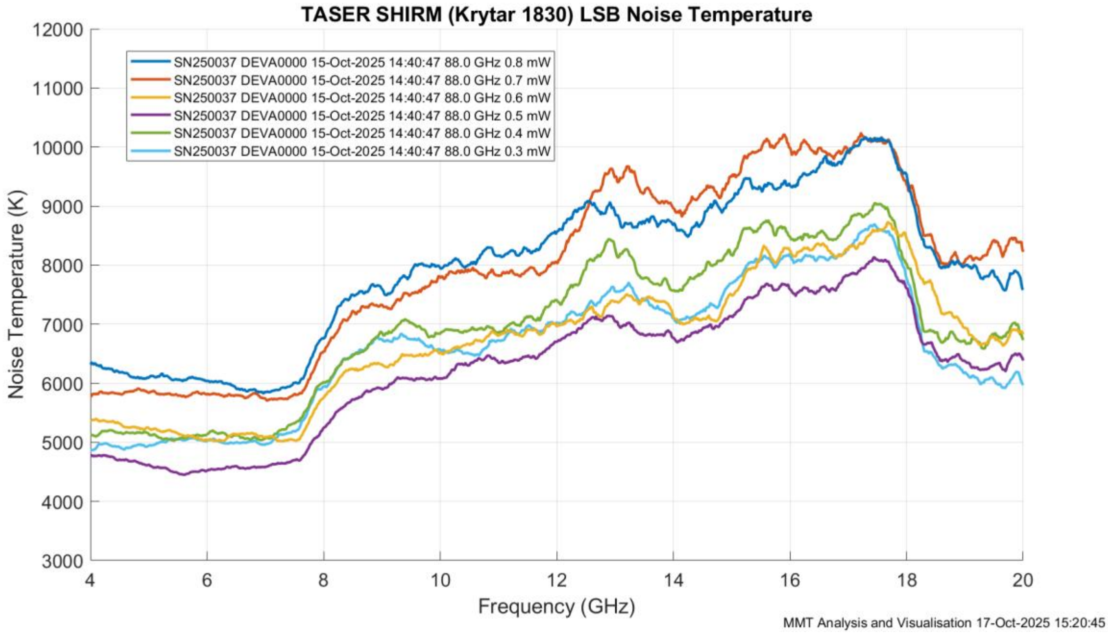

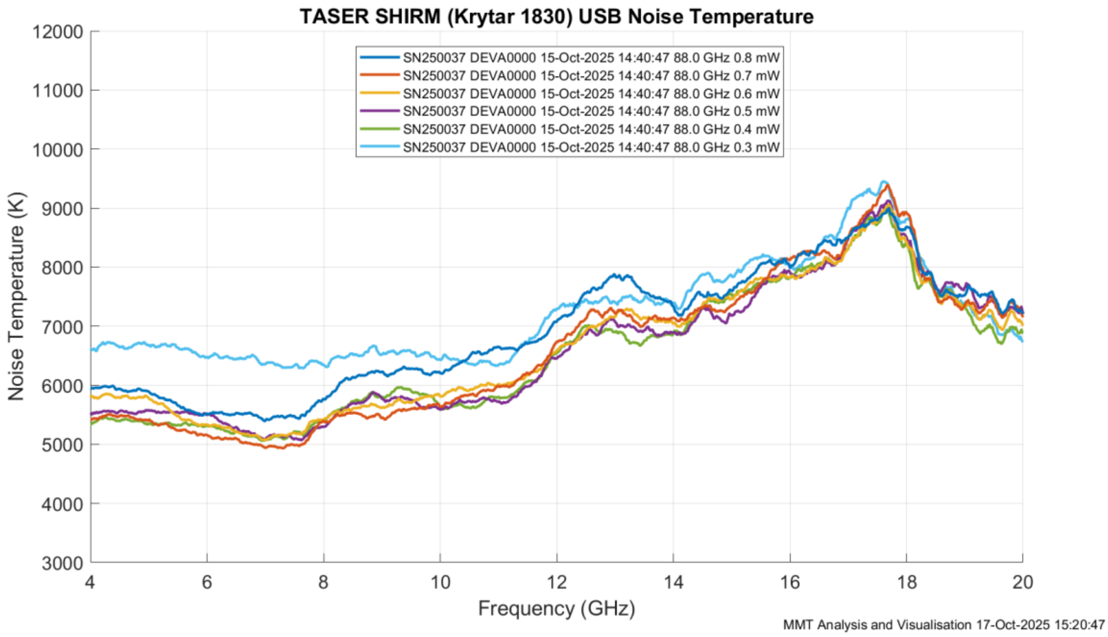

Figure 56 - Measured SHIRM SN250037 LSB (above) and USB (lower) noise temperature at room temperature versus IF with Krytar IF hybrid.

Figure 57 - Measured SHIRM SN250037 and SN250038 LSB (above) and USB (lower) conversion loss at room temperature versus IF with Krytar IF hybrid.

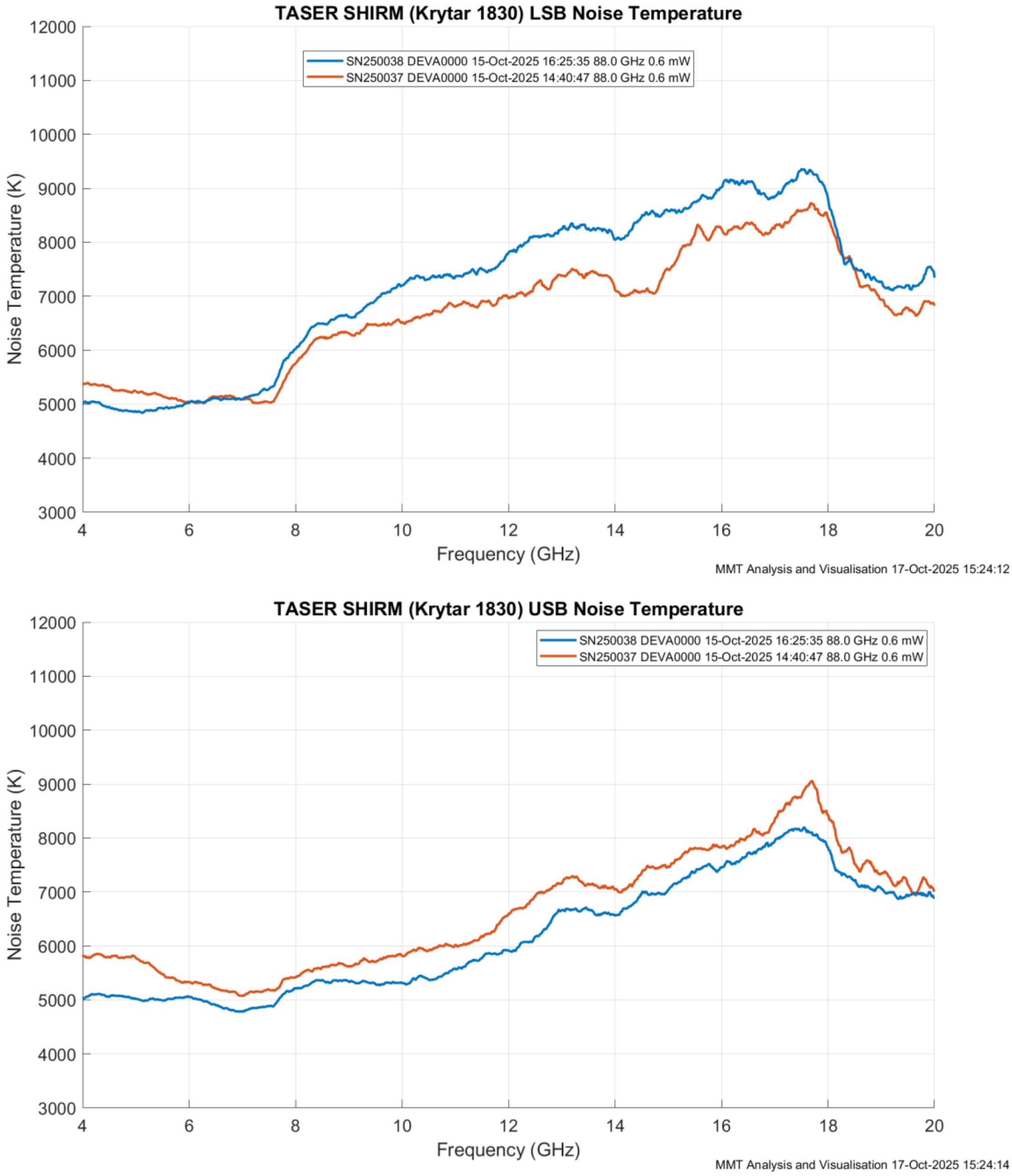

Figure 58 - Measured SHIRM SN250037 and SN250038 LSB (above) and USB (lower) noise temperature at room temperature versus IF with Krytar IF hybrid.

To access the impact of different IF hybrids on SHIRM performance, measurements were performance on SN250037 using three distinct IF hybrids (as shown in Figure 54), Figure 59 presents a representative dataset showing the SHIRM conversion loss associated with each IF hybrid. However, the Yebes IF hybrid is a cryogenic device, and its loss contribution doesn't accurately reflect its true impact under typical operating conditions. Nevertheless, the data clearly indicate that the insertion loss and amplitude balance of the IF hybrids significantly influence the SHIRM conversion loss and the balance performance between the upper and lower sidebands. These findings underscore the importance of selecting an IF hybrid with optimal characteristics to ensure balanced and efficient SHIRM performance.

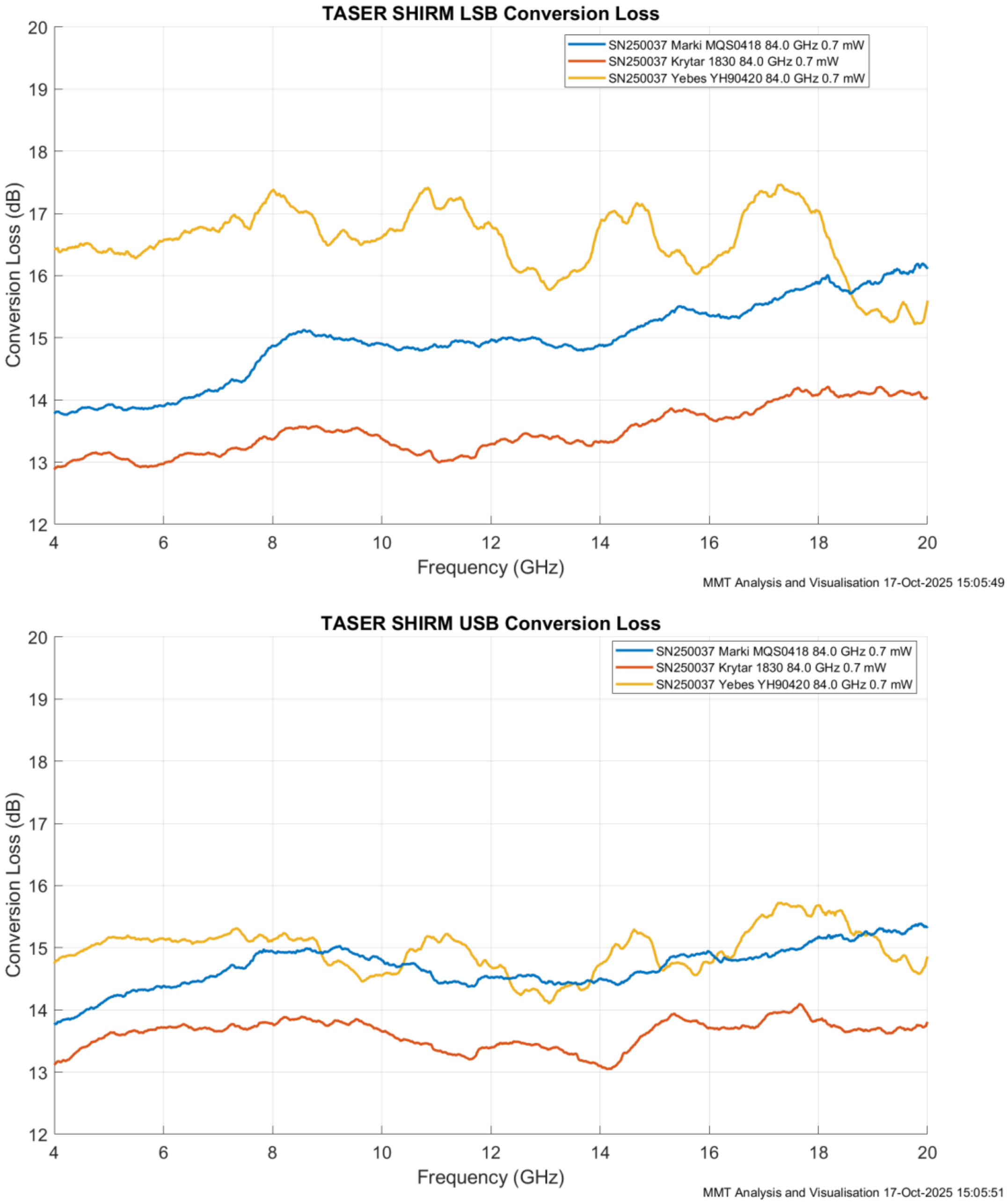

Figure 59 - Measured SHIRM SN250037 LSB (above) and USB (lower) conversion loss at room temperature versus IF with three different IF hybrids.

The image rejection ratio of the SHIRM SN250037 with two IF hybrids was tested using the setup shown in Figure 60. The injected RF power was calibrated to -40 dBm from 140-220 GHz. The sideband rejection ratio is then measured using a spectrum analyser. Figure 61 show the SHIRM image rejection ratio using two different IF hybrid.

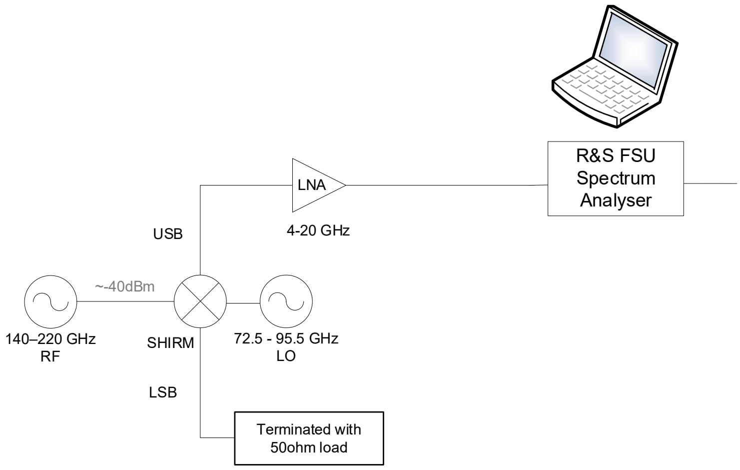

Figure 60 – Schematic of test setup for SHIRM image rejection ratio measurement.

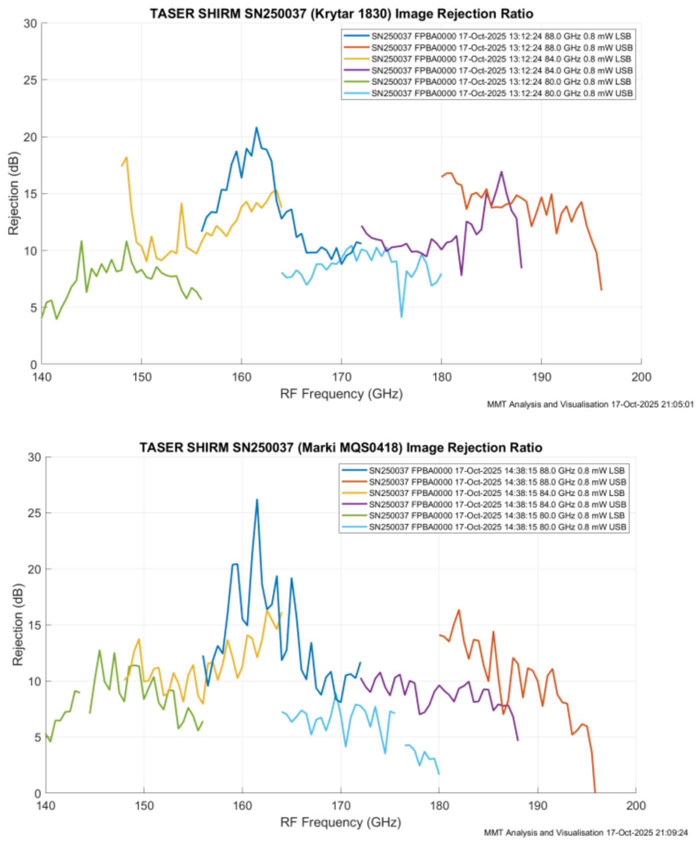

Figure 61 - Measured SHIRM SN250037 image rejection ratio at room temperature versus RF with two different IF hybrids.

4.5 Conclusions

The development of the ALMA Band 4+5 SHIRM has successfully built upon the *CARUSO* SHIRM heritage, demonstrating the feasibility of compact, high-frequency subharmonic mixers using InGaAs Schottky diodes. The design addressed key challenges including wideband IF requirements, precision waveguide hybrid fabrication, and miniaturised mechanical integration.

Measured room temperature performance of both DSB mixers and SHIRM units confirmed the robustness of the design, with consistent results across multiple devices and LO frequencies. The SHIRM blocks exhibited balanced performance between upper and lower sidebands, and the impact of IF hybrid selection was clearly demonstrated, highlighting the trade-off between integration and performance.

The SHIRM exhibits an average noise temperature of approximately 6000 K across the IF range of 4-20 GHz when operating at room temperature. Due to resource constraints and the limited timeframe of this study, no cryogenic measurements have been performed on these devices. However, similar devices have been tested previously, showing significant performance improvements at an operating temperature of 20 K, including a reduction in conversion loss by 3-4 dB and a decrease in noise temperature by a factor of 5-6. Consequently, SHIRM is expected to achieve a noise temperature of around 1000 K at 20 K, while requiring a very low LO power of only 0.6 mW. This represents the first demonstration within the frequency range of 125–211 GHz, offering superior performance and bandwidth. For comparison, the ALMA Band 2 specification for a WCA SHIRM is approximately 10000 K.

Overall, the Band 4+5 SHIRM development has delivered a compact, high-performance mixer unit potentially suitable for future ALMA upgrades. The low LO power requirement is also a key advantage for future array receivers. The work lays a strong foundation for further integration efforts, including cryogenic testing and potential on-chip hybrid implementation, and supports the broader TASER goal of advancing receiver miniaturisation and integration for next generation radio astronomy instrumentation.

Table 11 - Summary of the Band 4+5 SHIRM performance

<table>
<tr><td colspan="2">RF (GHz) 125-211; LO frequency (GHz) 72.5-95.5; IF Bandwidth (GHz) 4-20
Dimension: 28mm*24mm*20mm (exclude IF hybrid)</td></tr>
<tr><td colspan="2">Noise temperature (K)</td></tr>
<tr><td>Measured at 300K: ~ 6500K</td><td>Predicted at 20K: ~ 1300K</td></tr>
<tr><td colspan="2">Conversion loss (dB)</td></tr>
<tr><td>Measured at 300K: ~ 14.5 dB (LSB and USB)</td><td>Predicted at 20K: ~ 11.5 dB (LSB and USB)</td></tr>
<tr><td colspan="2">LO power: ~ 0.6 mW</td></tr>
<tr><td colspan="2">Image rejection ratio: 5-20 dB</td></tr>
</table>

5. Work Package Three: Feasibility Study of Future Amplifier and Mixer Integration Methods

WP3 aims to provide an overview of the potential future directions which could be taken for the LNA+Mixer, as well as further receiver, integration. First, a discussion on the potential of on-chip hybrid couplers, including UoM simulations of a 30-50 GHz, and 40-60 GHz Lange coupler, are presented in section 5.1. After this, options for alternative LNA+SHIRM integrations which were investigated during work on WP1 are introduced. One option utilises on-chip hybrid couplers and this is discussed in section 5.2.1. Another option introduces the idea of a SHIRM topology which utilises a balanced amplifier, this is outlined in section 5.2.2. A summary of each option is given in section 5.2.3. From here integration of the tripler, IF amplifier, and initial LNA stage are all discussed separately in sections 5.3, 5.4, and 5.5 respectively. Finally, the triple cascode mixer is introduced in section 5.6, as a step toward integrating both a mixer and LNA on the same MMIC.

5.1 On-Chip Hybrid Couplers

Replacing waveguide hybrid coupler structures with on-chip hybrid couplers is a promising route towards further receiver integration and package space saving. There are some drawbacks to using on-chip couplers, they generally have higher insertion loss than waveguide structures and require packaging considerations to avoid cavity resonances [15], but they offer many advantages for receiver integration. For example, as the dimensions of the coupler are in some manner dependant on the wavelength of the signals in their operating band, at lower frequencies on-chip couplers save significant package space. For an example of this see Figure 16, the 40-60 GHz LO coupler takes up almost half of the packaging space. For an idea of the space saving possible in Figure 16, if the LO coupler is also implemented as an on-chip component then it would be of an equivalent size or smaller than the on-chip IF hybrid coupler shown here.

As frequency increases, the amount of package space saved using an on-chip hybrid coupler compared to a waveguide implementation reduces. However, as the footprint of the hybrid coupler reduces implementing them on a MMIC chip becomes more feasible and cost effective, this opens the potential to integrate couplers onto other MMICs in the receiver. Doing this would remove the need for bond wires, which become bigger sources of loss as frequency increases, even if they are kept small.

An additional benefit of using on-chip couplers instead of waveguide-based structures is the requirements in mechanical precision for the packaging. Waveguide hybrid coupler structures rely on very precise gaps in the waveguide, in the order of micrometres, which can be a challenge to machine, adding expense. Looking at the gaps in the RF and LO coupler structures in Figure 16, it can be seen that as the operational frequency of the coupler increases, the gaps get smaller, so the precision required by the packaging manufacturer increases. Use of on-chip couplers would alleviate this problem, although these chips get smaller as frequency increases and can be harder to manufacture, packaging them is typically straight forward.

Depending on the chosen topology for the on-chip hybrid coupler different challenges present themselves. Various coupler topologies were considered as part of this project, including

Branchline couplers, Lange couplers and Wilkinson splitters. Lange couplers were chosen over Wilkinson splitters and Branchline couplers for simulation despite their increased fabrication complexity due to Wilkinson and Branchline splitters having generally smaller bandwidths [16] [17] [18], and combined ALMA bands requiring high bandwidth. Additionally, [19] shows they are possible to implement at millimeter wavelengths.

Lange couplers, such as in Figure 62, are a very common topology due to their bandwidth capabilities, low losses, and small area layouts, making them ideal for inclusion on MMIC chips. However, at higher frequencies they require air bridges, adding complexity, especially as tracks get thinner, and limiting their ease of fabrication. They are also susceptible to process variation and tolerance issues, so finding a reliable lithographic process is important.

It can be difficult to produce on-chip Lange couplers at millimetre wave frequencies due to the conflicting requirements of thin substrates and the width/spacing of the transmission lines [20]- the thin substrates required for high frequency operation require narrower transmission line widths and finger spacings. The limitation becomes what is possible with the fabrication process. However, Northrup Grumman have recently demonstrated on-chip Lange hybrid couplers with a centre frequency of 165 GHz [19]. While performance of their coupler is not directly shown, successful operation of a "Switched 180º Phase Shifter Receiver Macrocell", which incorporates their 165 GHz hybrid couplers, is shown. This highlights the feasibility of on-chip couplers for frequencies >100 GHz. For on-chip couplers at ALMA Band 4+5 the choice of substrate and manufacturing methods will be crucial, as the demonstrated coupler in [19] uses Northrup Grumman's 35 nm Indium Phosphide (InP) HEMT process, which is state-of-the-art.

We have simulations of two Lange coupler designs working at 30-50 GHz, and 40-60 GHz, these are shown in section 5.1.3 with results discussed in 5.1.4. Upon successful manufacture of these, we will be aiming for the 67-116 GHz band utilising the design and manufacturing experience from the lower frequency devices. Above this frequency, it will be preferable to integrate the couplers on-MMIC, as the physical coupler structure is so small, and bond wires introduce more loss with higher frequencies.

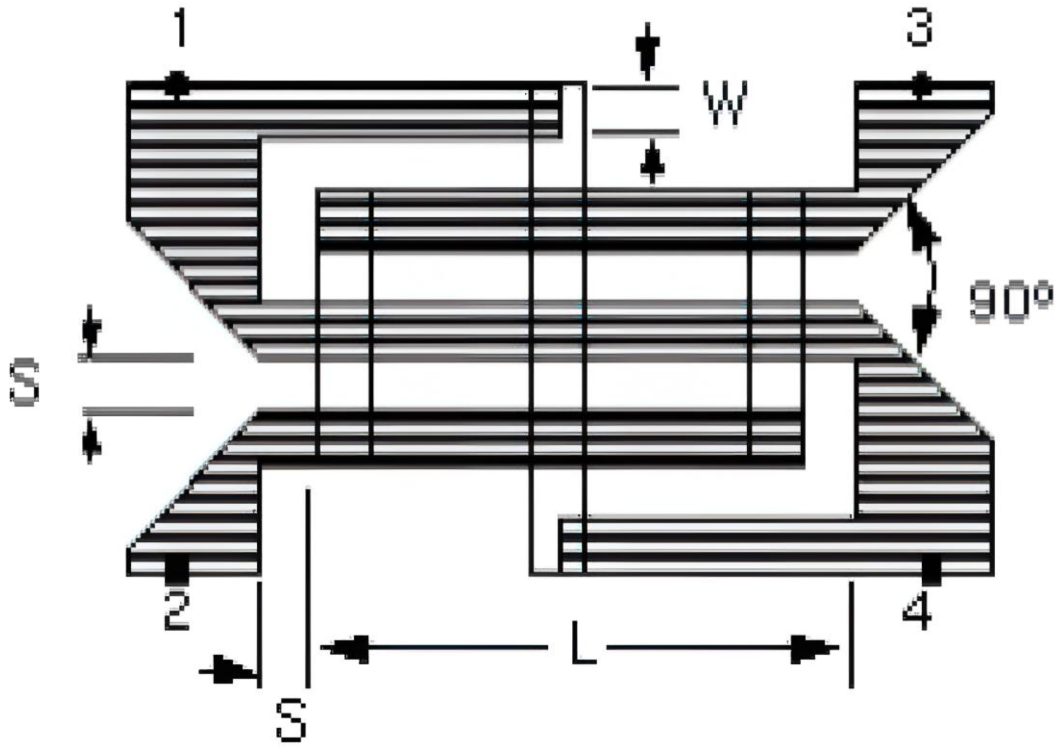

Figure 62 – Example Lange coupler diagram from [21] showing the parameters S, L, and W, which set the performance of the coupler.

5.1.1 Design Considerations

Two Lange hybrid couplers have been designed for operation at 30-50 GHz and 40-60 GHz. Initially, we started with a 40-60 GHz design, as this would cover the LNA+SHIRM LO frequencies. The 30-50 GHz variant was made as it is quite simple to tweak the frequency of Lange couplers that far, and it is easy to test in the UoM with a 50 GHz VNA. The chosen dielectric was quartz, this is because of its low dielectric constant (3.78), low loss tangent (0.0001), it is the same material used for the waveguide to microstrip transitions and the circuitry of the mixers in the LNA+SHIRM devices making further integration feasible and allows these circuits to be fabricated at both RAL and UoM.

Typically, high frequency electronic circuits will be matched at their input and output to a characteristic impedance of 50 ohms. 50 ohms on quartz requires a track width of 213.7 µm on 100 µm thick quartz substrate, which is large compared to the rest of the Lange coupler. For a Lange coupler the thin transmission line fingers have a very high impedance which will need to be matched down to 50 ohms. A large track width in this situation can result in sizeable parasitic elements being introduced to a circuit, which can increase insertion loss and undesirable effect on circuit performance, and additionally require a lot of chip space. Additionally, the larger the difference in impedance that has to be matched, the more complicated, narrower band and higher loss the circuit becomes. Instead, it is common to pick an intermediate characteristic impedance such as 75 or 100 ohms, design the Lange coupler to match to this and then add additional matching networks to convert down to 50 ohms. These additional matching networks can take up a lot of space on the chip, potentially as much as double or triple the initial area of the Lange coupler.

As we can control the design of the elements within a future SHIRM, it gives some freedom to choose the characteristic impedance of these components. With a 100-ohm characteristic impedance, the impedance is closer to the impedance of the Lange ports, and requires a track width of 52.4 µm on 100 µm thick quartz substrate, which is substantially easier to work with, and will allow for better insertion loss. Because of this, the designs for both the 30-50 GHz and the 40-60 GHz couplers have taken a characteristic impedance of 100 ohms.

For use in the SHIRM the couplers for the RF and LO require a matched load on the isolation port in order to cancel reflections which re-enter from the output ports. There are several options for the load, in this case 100 ohms, on the isolated port. It would be easiest if a resistive material, such as Nichrome (NiCr), could be used. This would allow for an on-chip resistor, which would simplify packaging substantially. An alternative option would be to have an off-chip resistor, this would have the benefit of simplifying the chip production. UoM is investigating the on-chip resistor options, and for this design it has been taken that a 50-ohm square resistive material could be used, such that two squares in series would give a 100-ohm resistor.

5.1.2 Hybrid Coupler Designs

The on-chip Lange hybrid couplers for the frequency bands 30 – 50 GHz and 40 – 60 GHz were designed in ADS, see Table 12 and Figure 63, and simulated using Momentum Microwave. 100um thick quartz was used as a substrate, with 1 µm thick gold as the conductor. Bond wires have been accounted for in the simulations for these devices, specifically the EBOND ADS model for two 12.5 µm radius 100 µm long connected in parallel to each port. Designs were simulated for room temperature operation and would ultimately need to be altered for cryogenic temperatures, although this is beyond the scope of this short study.

	40-60 GHz	**30-50 GHz**
Variable	**Size (µm)**	**Size (µm)**
Length (L)	885	1110
Width (W)	3.6	5.0
Spacing (S)	4.95	4.7

Table 12 - Hybrid coupler design dimensions with reference to Figure 62

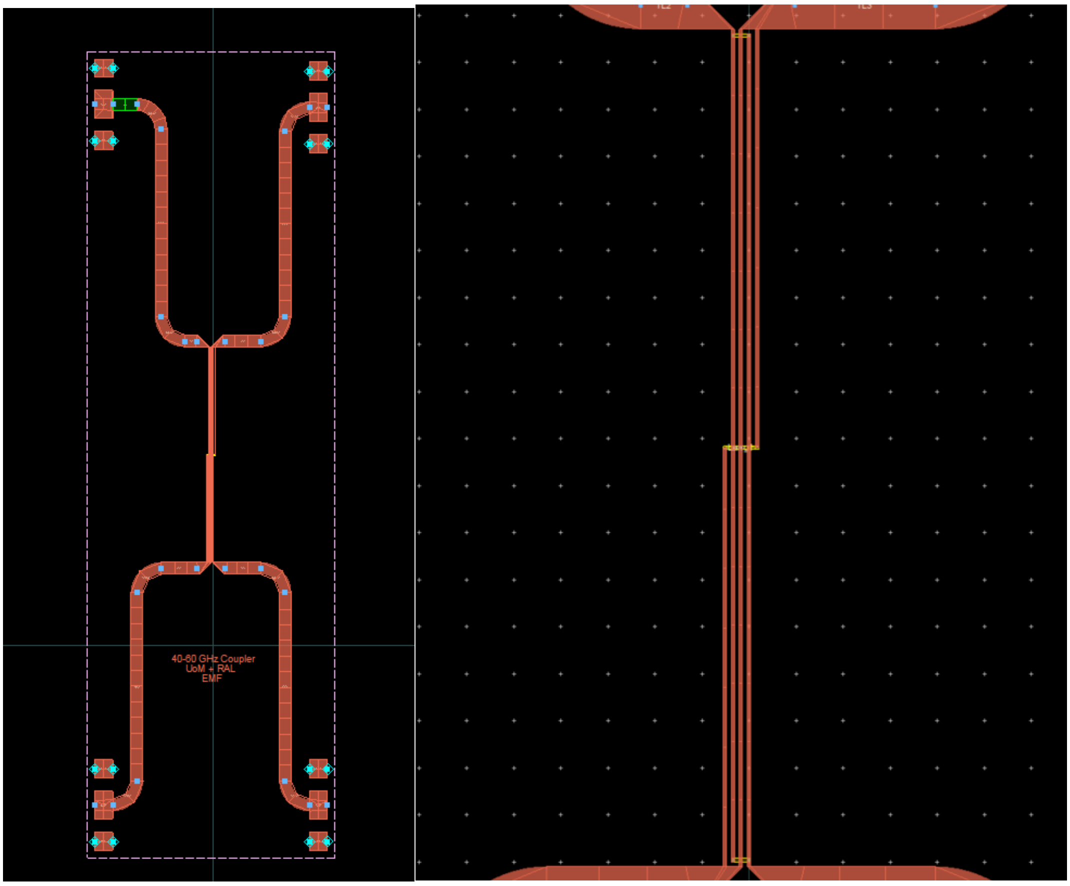

Figure 63 - Hybrid coupler layout. Left shows full layout, right shows a zoom in of the Lange coupler

5.1.3 Simulations

Simulations for both the 30-50 GHz and 40-50 GHz Lange hybrid coupler are given below in 5.1.3.1 and 5.1.3.2. The insertion loss, amplitude balance, phase response, isolation, and return loss are show for each. These results are discussed in 5.1.4.

5.1.3.1 40-60 GHz Hybrid Coupler Simulations

Figure 64 shows insertion loss and amplitude balance. In a hybrid coupler, as it functions as a power splitter, an insertion loss of -3dB to each port is ideal, as this shows a perfect power split. In this case, we have an additional loss of approximately 0.5 dB. The amplitude balance could perhaps be tweaked slightly further for a lower maximum but is ultimately showing around 0.4 dB maximum within the band. Figure 65 shows the phase response and isolation. The phase response is within 0.5° of 90° over the whole band. The isolation between the two output ports is seen to be approximately -19 dB at the end of the band, with the majority being <-20 dB. Figure 66 shows the return loss, which is particularly important to hybrid couplers in a sideband separating receiver scheme, as mentioned in [22] image rejection is more tolerant of phase/amplitude imbalance than it is of standing waves, which a good return loss helps prevent. In these designs, the return loss is below -20 dB across the entire band. These results will be discussed further in section 5.1.4.

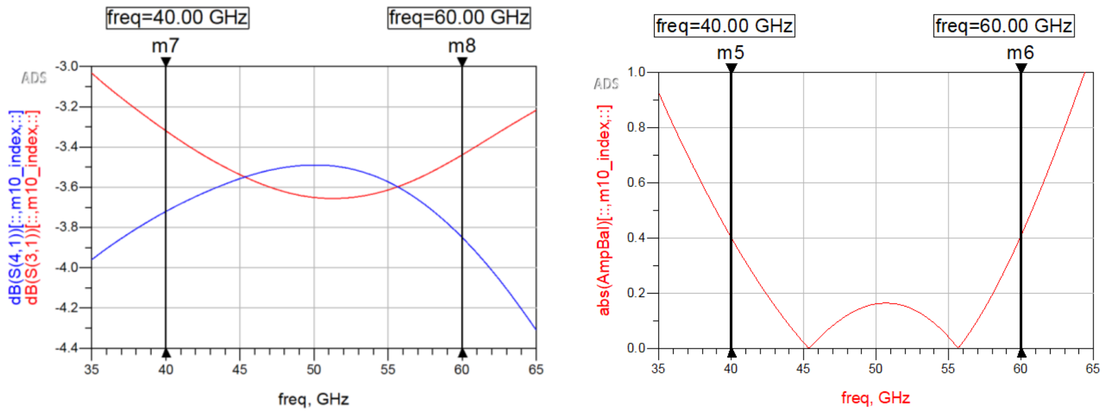

Figure 64 - 40-60 GHz Simulations - Left: Insertion Loss - Right: Amplitude Balance

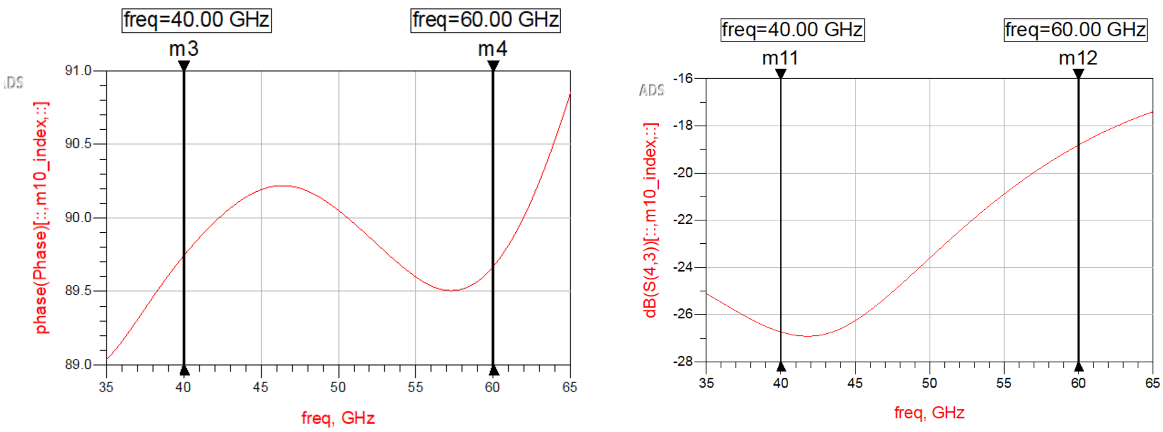

Figure 65 – 40-60 GHz Simulations - Left: Phase Response - Right: Isolation

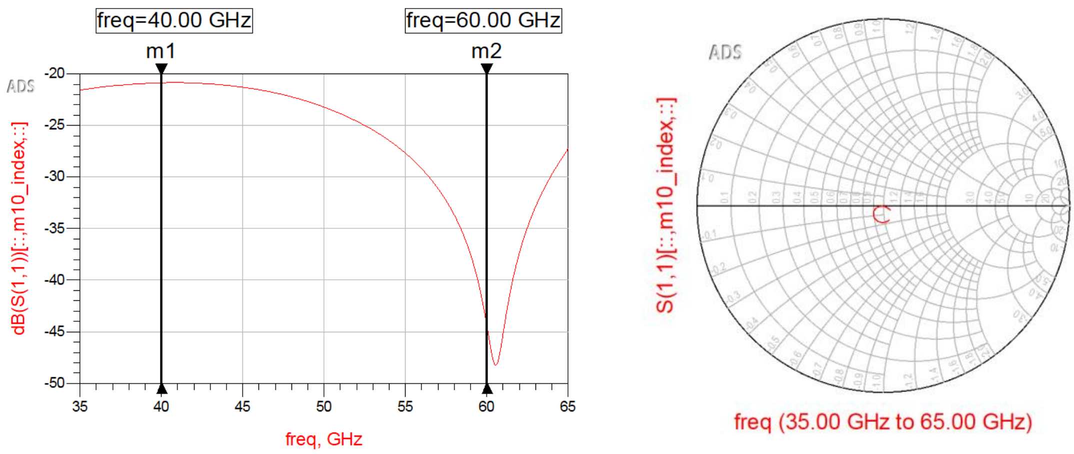

Figure 66 - 40-60 GHz Simulations - Left: Return Loss Graph - Right: Return Loss Smith Chart

5.1.3.2 30-50 GHz Hybrid Coupler Simulations

Figure 67 shows insertion loss and amplitude balance. There is an additional loss of approximately 0.6 dB. The amplitude balance could perhaps be tweaked slightly further for a lower maximum but is ultimately showing around 0.4 dB maximum within the band, which is acceptable. Figure 68 shows the phase response and isolation. The phase response is within 1.5° of 90° over the whole band, and within 0.5° for around 75% of it. The isolation between the two output ports is less than -21 dB across the whole band. Figure 69 shows the return loss, this is below -20 dB across the entire band, the importance of which mentioned in section 5.1.3.1. These results will be discussed further in section 5.1.4.

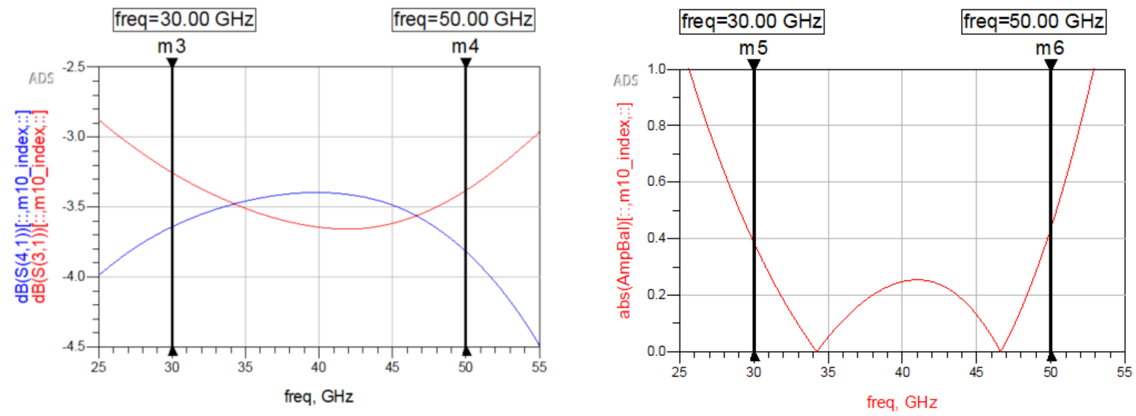

Figure 67 - 30-50 GHz Simulations - Left: Insertion Loss - Right: Amplitude Balance

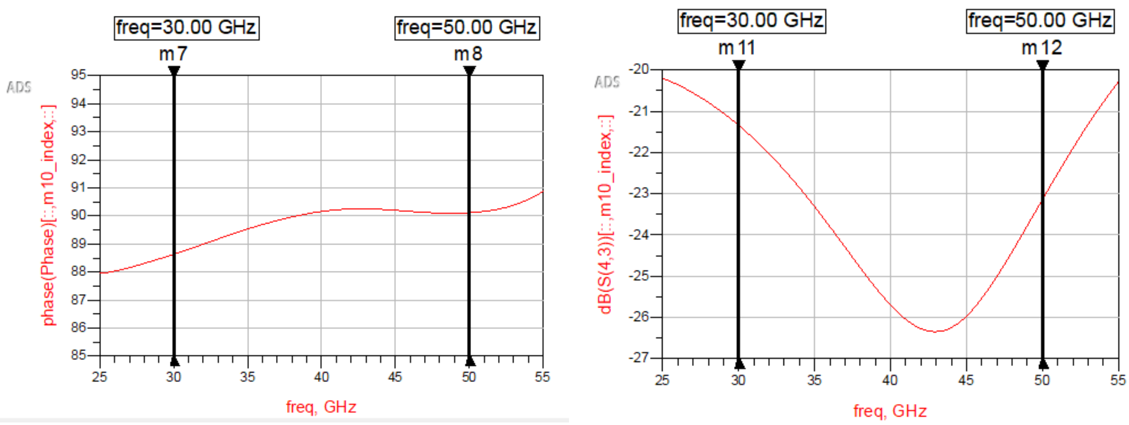

Figure 68 - 30-50 GHz Simulations - Left: Phase Response - Right: Isolation

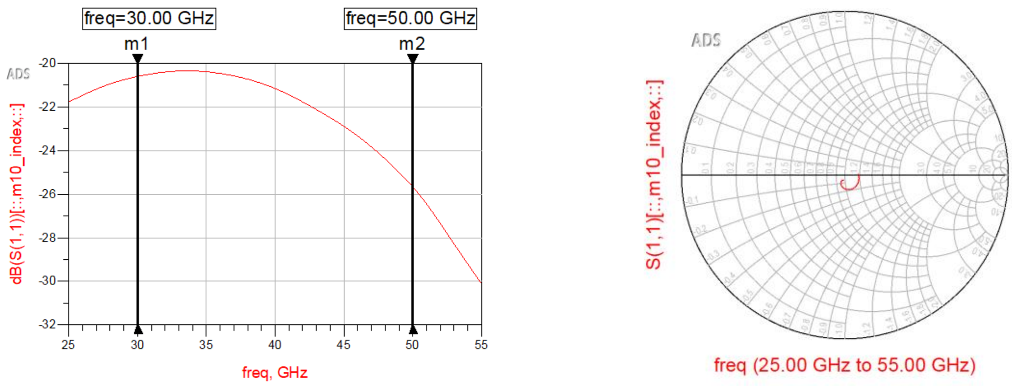

Figure 69 - 30-50 GHz Simulations - Left: Return Loss Graph - Right: Return Loss Smith Chart

5.1.4 Discussion

Both couplers simulate very well, within the region of 3.5 to 3.6 dB insertion loss across the band on average, where 3 dB is ideal for a hybrid coupler. Phase response for the 40-60 GHz coupler is very strong, with 0.5 degree maximum variation over the band, for the 30-50 GHz, the start of the band is about 1.5° away from 90°, which is as far away as it goes. Return loss is better than -20 dB for both coupler variants. Isolation is better than -20 dB across the band for the 30-50 GHz variant, and better than -18 dB for the 40-60 GHz variant. Something to consider; however, is the performance of the on-chip IF coupler from Marki successfully used in Work Package 1 and Work Package 2. The MQS 0218 (see Table 4) has quite significant additional insertion loss, typically 1.4 dB.

As expected, the manufacture of these devices has proved to be a challenge and not within the budget/time constraints of this project; however, simulations show insertion loss and phase response over the 30-50 GHz and 40-60 GHz bands which is potentially in line with ALMA specifications. While electron beam lithography, which is available at UoM, can achieve the required track widths and spacings, the thickness of the track being deposited is critical, and at UoM this is 50-100 nm at standard, although thicker is being investigated. In Figure 70 we can see how thickness changing influences the insertion loss. It seems that below 300nm, the losses start to grow quite noticeably.

The simulation results are very sensitive to the trace thickness. The insertion losses for 100 nm, 400 nm, and 1000 nm trace thicknesses are shown in Figure 70. It seems that from 100 nm to 400 nm quite drastic change of approximately 1.4 dB occurs, whereas from 400 nm to 1 µm substantially less changes, approximately 0.1 dB. Other fabrication methods besides electron beam lithography are also being investigated that will allow traces of around 1 µm to be used.

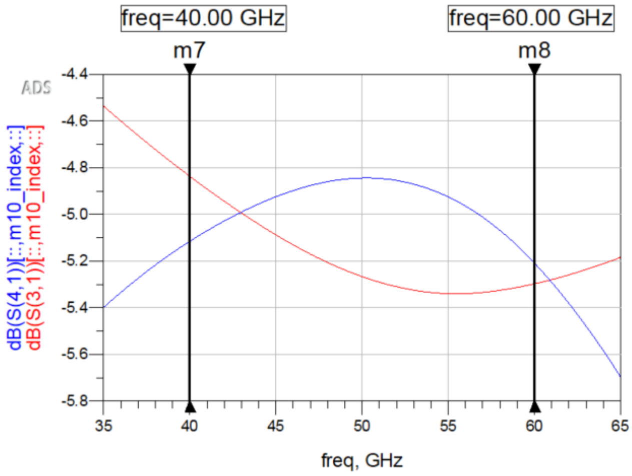

freq=40.00 GHz
freq=60.00 GHz
m7
m8
ADS
dB(S(4,1))[::,m10_index,::]
dB(S(3,1))[::,m10_index,::]
-4.4
-4.6
-4.8
-5.0
-5.2
-5.4
-5.6
-5.8
35
40
45
50
55
60
65
freq, GHz

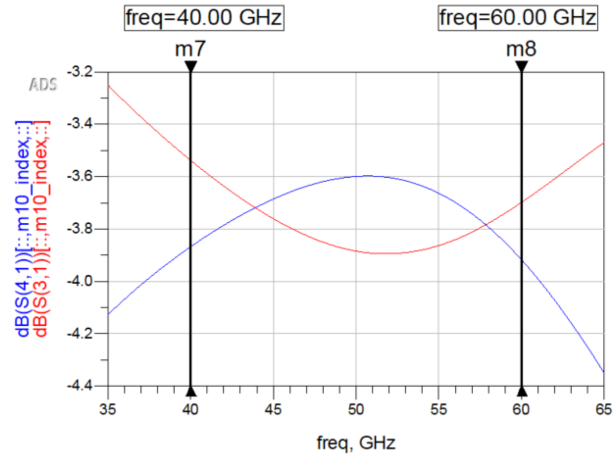

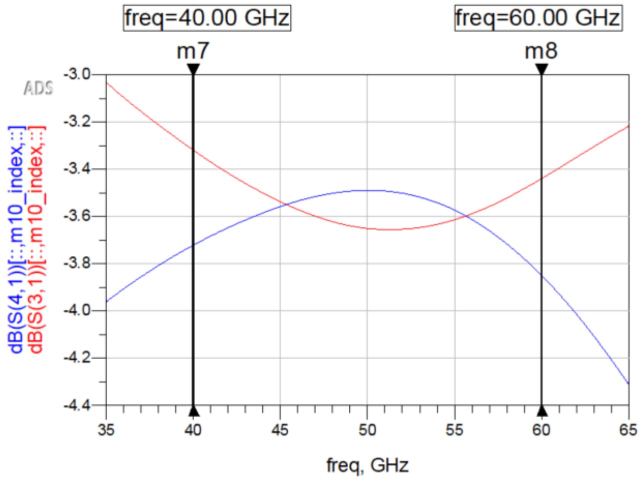

Figure 70 - Insertion loss over three different track thicknesses. Top – 0.1 um. Middle - 0.4 um. Bottom - 1

5.2 Alternative Integration Topologies of the LNA and SHIRM

An assessment of integration and miniaturisation options was carried out early in this project for WP1 to inform the subsequent design of the LNA+SHIRM and provide direction for future projects. We investigated how the RF LNA can be integrated with the RF section of the SHIRM. Figure 71 shows block diagrams of three options of topologies for this integration, including the chosen topology, and Table 13 summarises their main attributes. The three options were:

1. Waveguide RF Hybrid: Maintain the LNA followed by the RF waveguide hybrid coupler (a). This was chosen for this project, as discussed in section 3.1.
2. On-chip RF Hybrid: Maintain the LNA and follow it with an on-chip RF hybrid coupler in place of the waveguide structure (b). This is discussed in section 5.2.1.

3. Balanced Approach: Insert the LNA MMICs inside the SHIRM structure in the RF paths of the Schottky diode mixers (c). This is discussed in section 5.2.2.

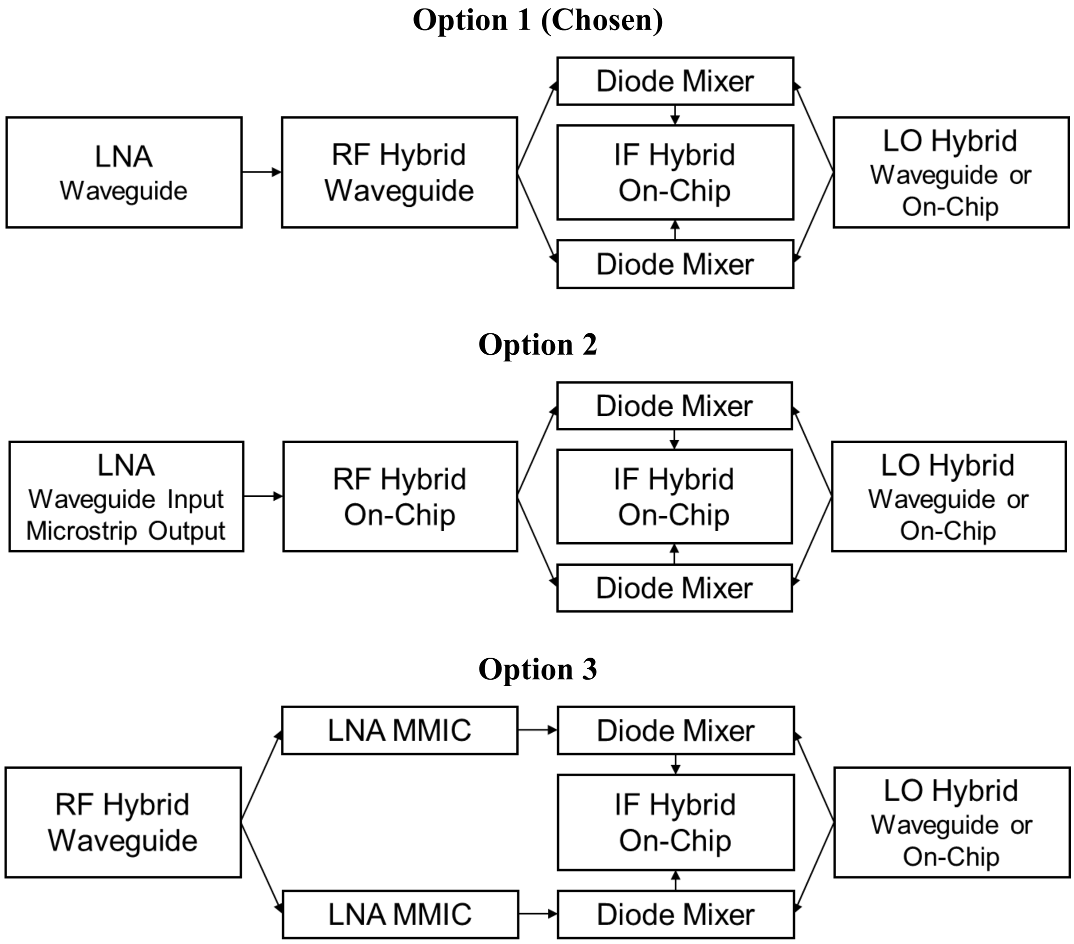

Figure 71 - Block diagrams for each of the integration options identified for this *TASER* project

5.2.1 On-Chip Hybrid Couplers (Option Two)

The RF waveguide hybrid structure discussed above has a fixed size and shape that limits further miniaturization and integration, especially on-chip integration. Using a waveguide structure also requires a transition from microstrip to waveguide between the output of the LNA and the input of the RF hybrid and then another opposite direction transition at the outputs of the hybrid. As explained in section 5.1 each transition introduces unwanted losses and reflections. Replacing the RF waveguide hybrid coupler with an on-chip component offers more potential benefits from the integration of the LNA and SHIRM, and offers a clear path towards future integration of multiple components onto the same chip. However, the performance of the RF on-chip hybrid coupler needs to be investigated to understand better the potential performance trade off that would need to be made to allow for this integration.

In terms of the integration of an RF on-chip coupler, although it is likely that there will be more insertion loss then an equivalent waveguide structure, as the coupler is located after the LNAs the effect of this on the noise performance of the receiver should be minimized. Using a quartz substrate for the RF coupler would also allow for possible future integration with the two mixer sections in the SHIRM which are also fabricated on quartz substrates. Due to the smaller size of the RF coupler, there is also potential that it can be integrated directly onto the output of the LNA MMIC, this would need further investigation to understand the performance implications.

5.2.2 The Balanced Topology (Option Three)

The third integration option takes a more holistic approach to the integration of the LNA and SHIRM components. An integrated design approach allows for the adjustment of the topology of the entire LNA+SHIRM structure to optimise its performance. A pair of LNA MMICs could be inserted after the RF hybrid and in-front of the Schottky diodes within the SHIRM structure. The benefits of this approach are the introduction of a balanced amplifier structure into the design, potentially offering improvements in the reflection coefficient of the RF input of the LNA+SHIRM. This adjacent location of the LNA and mixer also opens potential for future on-chip integration of these components, which may be attractive when translating this LNA+SHIRM technology to higher frequencies.

For integration option three, it is possible to take advantage of integrating all of the LNA and SHIRM components into a single package and rearrange the architecture of the SHIRM to include a LNA MMIC directly in front of the Schottky diode mixers. This combination of RF hybrid coupler followed by parallel LNA MMICs forms the input for a balanced amplifier architecture, which is often used as a way to improve the input reflection coefficient of an amplifier. Typically, an isolator would be required between LNA gain stages to prevent gain ripples. However, with the improvements in input reflection coefficient of the LNA+SHIRM offered by the balanced amplifier structure, the isolator may no longer be necessary. Considering a first stage RF LNA in front of the LNA+SHIRM would also reduce the effect of the RF hybrid losses on the overall system noise, allowing the hybrid to be implemented in either a waveguide structure or on-chip component. This choice of hybrid implementation is essentially the same consideration that was studied for integration options 1 and 2 described earlier in the report; the waveguide structure would offer the best performance, but the on-chip component would offer better miniaturization and further integration options. This consideration is dependent on the RF of the LNA+SHIRM: as the frequency increases the size of the waveguide hybrid will reduce and the difficulty of implementing an on-chip hybrid with acceptable performance increases.

The main disadvantage of this approach is that twice the number of LNA MMICs are required. At a system level this will have both technical and cost implications, especially for FPA systems where multiple individual receiver pixels (and therefore multiple LNA+SHIRM components) are being used. It is typical that all the transistor stages in the LNAs are biased independently to have the most control over the gain and noise performance. However, in receivers with large numbers of LNAs and receiver pixels, this strategy leads to a very large number of bias cables that need to be assembled in the cryostat and to pass through its vacuum case, increasing the complexity of the system. The increase in the number of MMICs will also result in a corresponding increase in the power and therefore heat dissipation from the LNAs in the cryostat, something that will be exacerbated as the number of pixels is increased for larger FPA or PAF receivers. Another drawback is that a second MMIC bias circuit must be contained within the LNA+SHIRM, which would require careful design to keep the size of the integrated LNA+SHIRM block within the acceptable envelope for FPA and PAF receivers.

However, for the most part, these challenges are well understood or can be quantified during the design of the components and receiver pixel(s). For example, the cost of the required MMICs and heat dissipation can be factored into the design of a receiver, and steps can be taken to bias multiple LNA stages from a single set of bias lines, reducing the number of cables required in the cryostat and the size of the bias PCBs required for the MMICs.

The remaining unknown to this integration approach is whether the inclusion of the LNA MMICs within the SHIRM structure would adversely affect its operation. Specifically, it will be important to understand how the gain and phase difference introduced by the MMICs varies between nominally identical units. If the difference between the two MMICs is too great to be controlled by the bias conditions, this may disrupt the balance of the SHIRM and reduce the performance, affecting the sideband separation rejection ratio and causing an imbalance between the upper and lower sideband outputs. It may therefore be necessary to perform on-wafer pre-screening phase and gain measurements of the MMICs and to select suitable pairs for the LNA+SHIRM.

5.2.3 Summary of LNA+SHIRM Integration Options

A summary of the three integration options for an LNA+SHIRM are presented in Table 13, which lists a selection of the important design and performance considerations. These considerations are highlighted for each option depending on if they are a positive, negative, or need more investigation.

	1	2	3
W-Band Hybrid	Waveguide	On-Chip^	Waveguide
LNA MMIC	Single MMIC	Single MMIC	Two MMICs*
Bias PCB	No issues	No issues	Space constraints&
MMIC Phase	No issues	No issues	Possible phase difference#
Integration	Least Integration	More Integration	More Integration
Future on-chip integration	No	Yes	Yes

^ Performance of on-chip w-band hybrids will need to be investigated
* Two MMICs would lead to twice power dissipation, bias PCBs, connectors and cables
& Careful design will be needed to fit the PCB for the second MMIC in the layout
\# Concern if possible phase difference between MMICs could affect SHIRM performance

Table 13 - Summary of integration options presented in Figure 69.

5.3 Integration of the Tripler

The RAL diode based tripler used in the LO chain was the most repeatable part in the *CARUSO* receiver chain and had no production issues. A problem with modularity is that individual part failures inside an integrated block are much harder to diagnose and fix. The tripler is therefore low risk from a production standpoint, giving it good integration potential. Integrating the tripler would also remove the need for an LO waveguide interface, increasing the potential for future integration and miniaturisation with an on-chip LO hybrid coupler.

The downside of integrating the tripler would be that it could interact with other parts of the receiver, such as the mixer, complicating the design and requiring more simulation time. As such this LO tripler and on-chip coupler integration would make a good subject for a future development project.

5.4 Integration of the IF Amplifier

In the *CARUSO* receiver, the outputs of the SHIRM were connected straight through the bulkhead of the cryostat and into the room temperature section of the receiver. Including a cryogenic IF LNA straight after the SHIRM would have been beneficial for receiver performance. This gives another option for future integration, including two IF LNA MMICs (one per sideband) inside the SHIRM package would increase the receiver gain at a critical point in the signal path before the losses of the cryostat interface. UoM have designed several LNA MMICs that would be suitable for this purpose using a commercially available GaAs pHEMT process. Over a band from 4 to 20 GHz these have an average room temperature noise of between 80 and 100 K with a gain of >30 dB. While not as low noise as an InP device, they should perform well enough at this stage of the receiver where gain is the main consideration in achieving the best receiver performance. Using a commercial process leads to several benefits in this application, including providing high volume, high yield, high repeatability MMICs that will simplify the integration process; and also, an order of magnitude or more decrease in MMIC cost for high volume supply.

To enable this IF LNA integration, a new MMIC design will be needed to implement a couple of design changes. Firstly, the new design should concentrate on minimising the number of transistor stages to reduce the power dissipation of each MMIC. Secondly, the design should limit the number of bias lines required for each LNA, ideally to the point where each IF MMIC needs only a single bias. Both of these factors will reduce the number of bias lines required for the IF LNA, an essential improvement for FPAs.

5.5 Integration of the Initial LNA Stage

Another option for further integration would be to include both stages of LNA along with the SHIRM in a single package. There are some significant challenges that would need to be overcome to achieve this while still ensuring optimum receiver performance can be achieved.

Firstly, it is common to use an isolator between the first and second stage of LNAs in order to reduce the effect of reflected power between the LNAs and reduce the ripple in the receiver gain that this can cause. The isolators used for *CARUSO* can be supplied in a format suitable for integration into custom packaging, this presents an option to integrate an LNA, an isolator, a second LNA, and the SHIRM into a single package. However, there are well known downsides of isolators, and it would be beneficial to remove it from the receiver entirely if possible. The reflections that cause gain ripple are a result of an impedance mismatch at the input match of the second stage LNA: improving this could remove the need for the isolator completely. As described in section 5.2.2 a balanced amplifier topology achieves much better input matching then a typical LNA MMIC. Integrating LNA MMICs into the SHIRM structure and using the RF hybrid coupler to form a balanced amplifier at their input (as shown in Figure 71) could provide a good enough match that no isolator is needed between the first and second stage LNAs.

Secondly, there is an additional challenge around LNA MMIC selection. One of the biggest disadvantages of integrating both LNAs into a single package is the loss of the ability to select the first stage LNA to achieve the best overall receiver noise performance. Ideally, all of the LNA MMICs would be pre-measured as dice on a cryogenic probe station to assess their gain and noise performance, this would allow for the optimum selection of MMICs for assembly into an integrated package. Currently we do not have this capability, UoM have a cryogenic probe station suitable for use up to 67 GHz (50 GHz with current measurement equipment). The probe station utilises stainless steel coaxial cables for the RF signals, it could be possible to upgrade this for up to ~116 GHz but these stainless-steel cables are unlikely to perform well for much higher frequencies due to the high losses. Instead, a waveguide solution would be preferred but this brings its own implementation challenges. On-wafer measurements at room temperature are considerably easier to implement, and commercial solutions already exist that enable this up to over 1 THz with VNA extender modules. However, the noise performance of an LNA MMIC at room temperature does not necessarily give an indication of how well the MMIC will perform at cryogenic temperature. It would however allow for basic functionality tests that would prevent faulty MMICs being assembled into an integrated package. This is also a service that can commonly be provided by commercial MMIC foundries, often at an extra cost. In addition, this kind of on-wafer testing leaves a (best case) small amount of pad damage which can affect how the bond wires are attached to the pads of the MMICs.

Finally, if there is no option to pre-measure the MMICs using a probe station then they will need to be ‘blind’ picked from those available. Our detailed analysis of the devices from our NGC run shows that those devices closer to the centre of the wafer typically provide their expected performance with an increased likelihood of MMIC damage or impaired functionality towards the edge of the wafer. Using a MMIC process with high yield and repeatability would be critical in this case to minimize the number of non-functioning MMICs being assembled into integrated packages. Still, extra packages and assemblies are needed to account for inevitability. In addition, picking the MMICs in such a way will mean there is little control over the noise performance of the first stage LNA, which is critical to achieving optimum receiver performance. A high repeatability process with minimal performance variation would help to counter this somewhat, but it is still a risk when a large number of integrated blocks are required.

In summary, it is foreseeable to integrate the first stage LNA and the use of a balanced second stage LNA may alleviate the need for the isolator. Testing the concept of a balanced second stage LNA should be a high priority for future projects to establish if this is indeed the case. If this is a feasible solution, then the ability to pre-measure MMICs before assembly will be critical for future integrated receiver packaging.

5.6 Triple Cascode Mixers

One of the downsides to a passive Schottky diode-based mixer, such as the one used in *TASER* is the associated conversion loss of the mixer that degrades the performance of the receiver. One possible alternative is the Triple Cascode Mixer (TCM) [23] [24] [25] [26], which is an active mixer utilising transistors rather than Schottky diodes. This offers strong potential for combining with existing LNA technology, integrating both functionalities in one MMIC chip. The benefits of this in relation to *TASER* become clear when looking at integration option 3 in section 5.2 that positions the LNA MMIC next to the Schottky diode mixers. In future it will be possible to replace both components with a single LNA+TCM MMIC. The rest of this section presents some consideration of integrating an LNA and TCM onto a single chip. In this case we are just considering a single DSB type mixer and not a sideband separating topology.

The advantages of combining the LNA and mixer into one MMIC are:

- The integration of the LNA and TCM onto a single chip will allow both components to be designed together, removing the usual need to provide a 50 Ω match at the output of the LNA and input of the TCM and also critically will remove the need for bond wires to connect separate chips. It has already been shown in work package 1 that integrating an LNA and mixer into the same package can reduce the overall size of the integrated package through removing the need for a waveguide flange.
- An active mixer provides conversion gain instead of loss. Compensating for the loss and noise contribution of the mixer requires a large amount of LNA gain before the mixer in the signal chain and significantly reducing these losses or even providing gain at this stage could reduce the amount of gain required from the LNAs. As we look towards higher frequency LNA based receivers, this will be critical as the amount of gain available is limited by the transistor technology.
- Having just one MMIC instead of two will reduce the testing and assembly time, which especially becomes an advantage the more receivers are required for a project.

However, there are several disadvantages to this approach

- Combining more components onto a single MMIC will naturally increase the size of the chip, resulting in less chips per fabrication run and potentially an associated cost increase depending on the number of chips required for a project.

- The increased number of components on a single chip result in a more complex design process and potentially increased design process time. This increase in component numbers also increases the chances of fabrication problems, resulting in poor performance from the chip
- The increased size of the chips could also lead to mechanical problems and failures of the chips when they are cooled to cryogenic temperatures. Further study would be needed in future projects to establish where the limits of chip sizes lie. Although the ultimate aim would be to integrate all the gain stages with the mixer section of a receiver onto a single chip, it is likely that two stages of LNA will be required to provide sufficient gain for the receiver, even with the gain provided by the TCM device. Therefore, a separate first stage LNA MMIC could be utilised in the receiver which could be selected for best noise performance and then followed by a second stage LNA+TCM MMIC to increase the gain and down convert the signal.

As a first step towards this LNA+TCM integration a TCM MMIC has been developed at the UoM. It covers 32-52 GHz RF, with an IF of 4-14 GHz and LO of 28, 33, and 38 GHz. Two variants have been created with slightly different performance characteristics with the intention of increasing our understanding of this TCM circuit topology. The simulation results are presented in Figure 73 and Figure 74. The design uses the WIN Semiconductors PP10-20 100 nm gate length gallium arsenide pHEMT process, which offers the benefits of a commercial process and is ideally suited to prototyping new devices in these frequency ranges. Once we understand more about the TCM circuit, this design could be taken to higher frequencies by using a shorter gate length process such as the NGC 35 or 25 nm gate length InP processes. However, we still need to learn more about the design of the TCM circuit, and the transistor models required for the design process. The Win TCM MMICs have been manufactured and have arrived in Manchester, see Figure 72, and we are in the process of upgrading our systems to be able to measure mixer devices. Two options have been identified:

1. Using the cryogenic probe station would allow for these MMICs to be measured without the need for packaging, however this requires upgrading the probe station with an addition RF port. This would also allow for relatively straight forward cryogenic testing.
2. An in-house, custom designed package – in a similar manner to LNA measurements, a custom gold plated, brass package can be designed and fabricated. This approach would allow for cryogenic measurements in a typical cryostat (the UoM cryostat is currently undergoing modification to allow mixer measurements). However, this is a more expensive option and will likely take longer to produce but does offer a packaged device that would be compatible with LNAs MMICs we have also developed in the 30-52 GHz frequency band (using both Win Semiconductors GaAs pHEMTs and NGC's 35nm InP processes).

In addition, we have also begun working with the Academia Sinica Institute of Astronomy and Astrophysics (ASIAA) who have been leading the research on this type of TCM topology, and we have jointly applied for grants that would allow us to begin further collaboration to develop the TCM devices. We have identified the area of transistor modelling as requiring particular attention: being able to model accurately the transistors their operating state in a circuit is essential for producing circuits with good performance. Through this collaboration with ASIAA, we will develop the modelling techniques that will be needed, as well as begin to investigate how we can push the design of the TCM circuit to higher frequencies in the future.

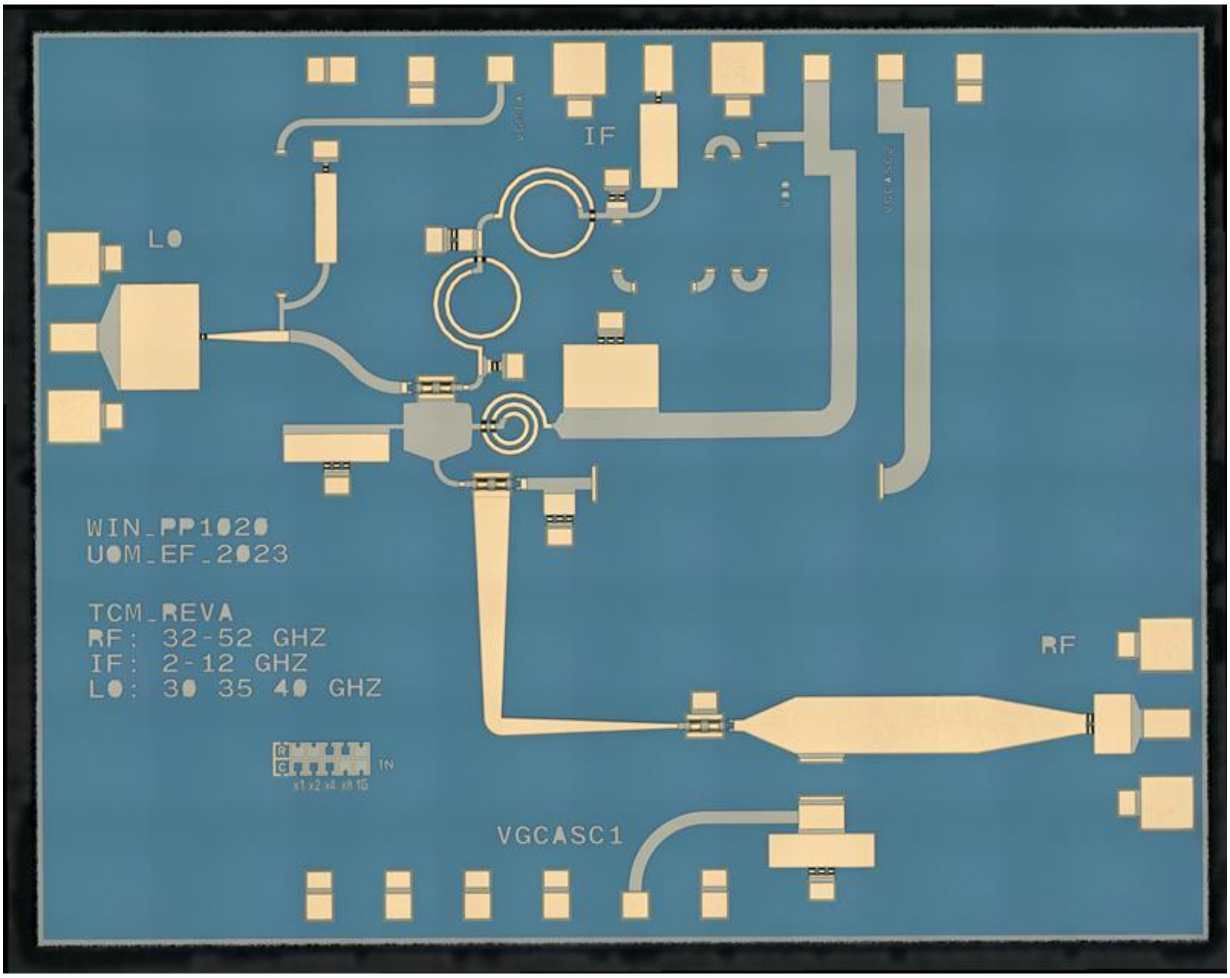

Figure 72 - UoM TCM MMIC Probe Optimised Variant

5.6.1 Simulations

Figure 73 shows the reflection coefficients of the two input and one output ports of the TCM. The RF matching is below -10 dB for the majority of the band, crossing below down to -7.6 dB after 50 GHz. The IF matching is below -8 dB across the band, with a large portion of it below -10 dB. LO matching has been sacrificed by design for the conversion gain characteristics show in Figure 74. The conversion gain shows better than 3 dB flatness across the band for each LO frequency, and a total variance across all three bands between approximately 2.9 dB and 9.4 dB. The power dissipation simulated was 20.8 mW.

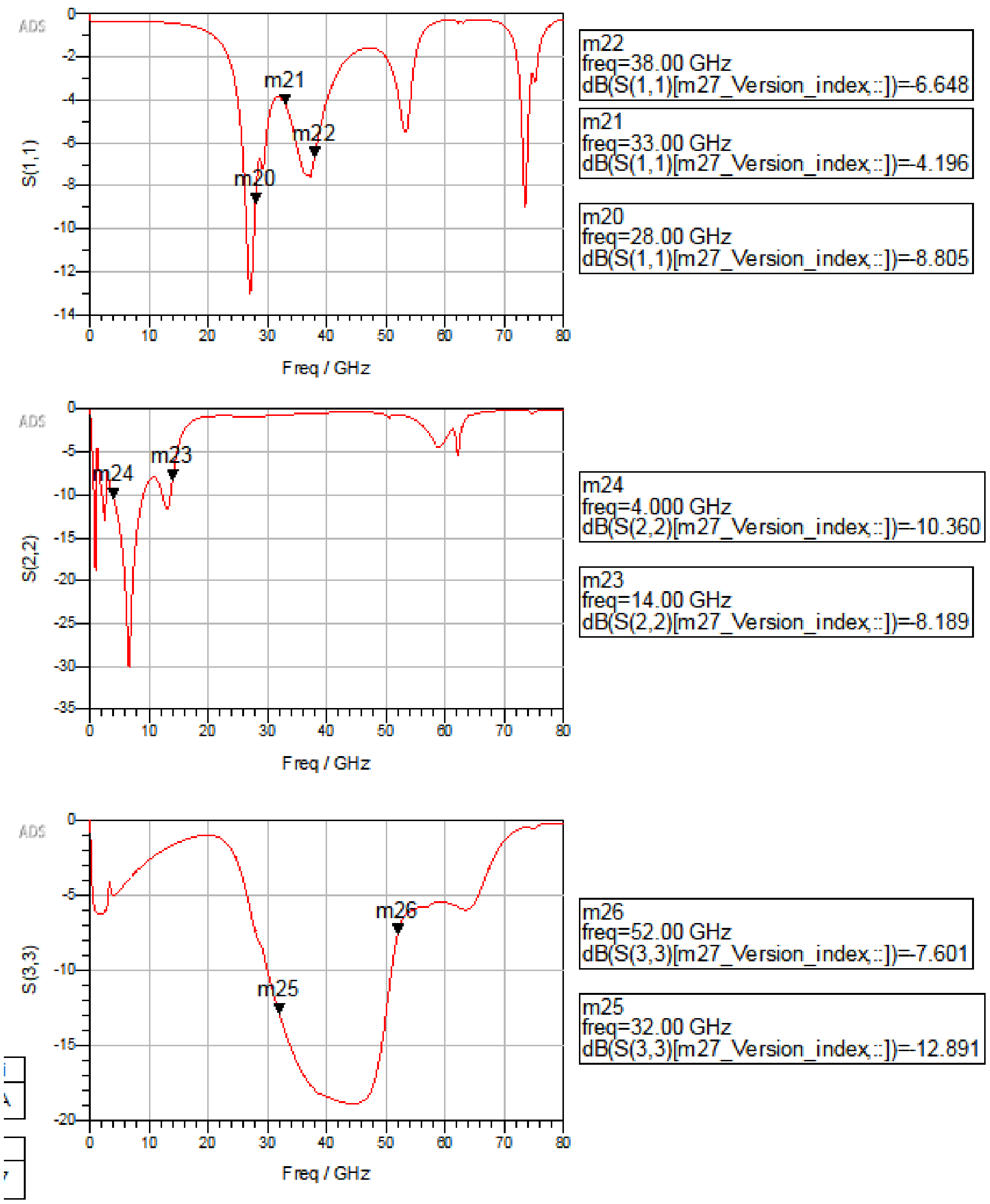

Figure 73 - TCM 32-52 GHz Mixer MMIC's Simulated S-Parameters. Top: LO, Middle: IF, Bottom: RF

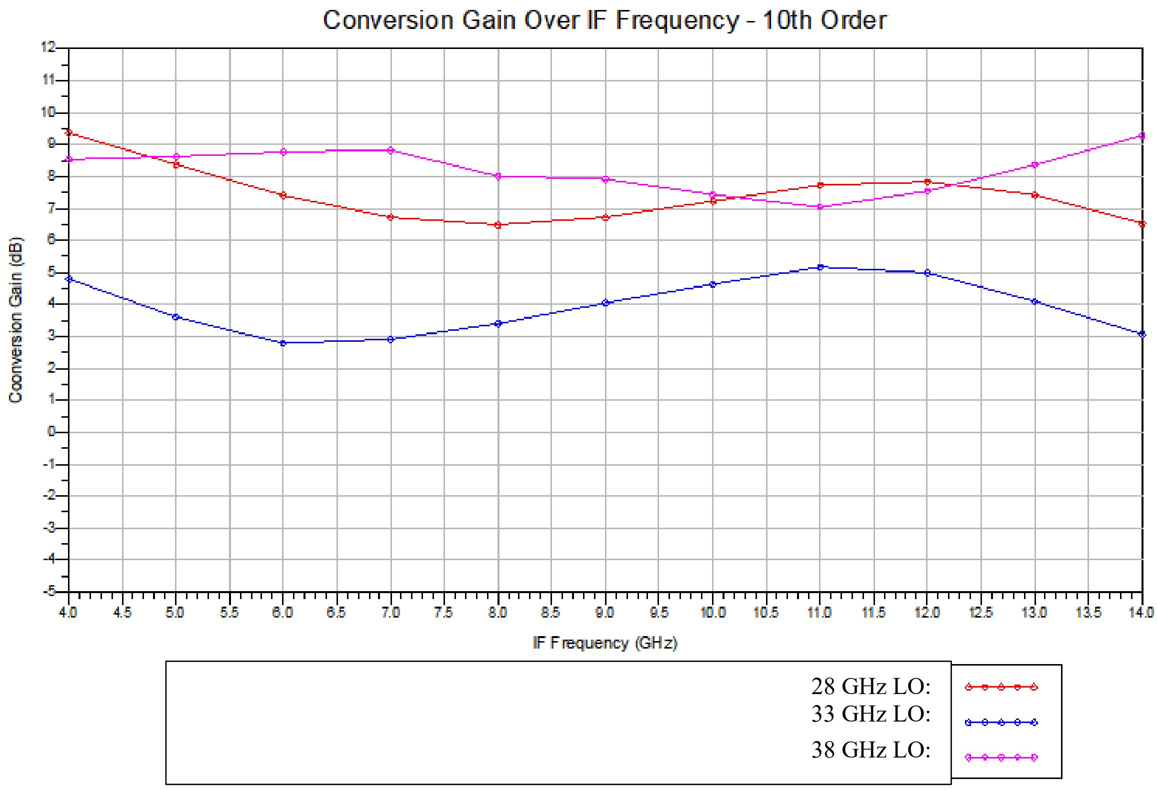

Figure 74 - TCM 32-52 GHz Mixer MMIC's Simulated Conversion Gain

5.7 Summary

In this section three broad areas have been considered for receiver integration in order to inform the future direction of this research. The potential of on-chip couplers has been shown, with a design and simulation given for both a 30-50 GHz and 40-60 GHz Lange coupler in section 5.1. The main concerns are the track thickness possible during manufacture, see Figure 70. On-chip couplers have been shown to be feasible, despite being difficult to produce, which is backed up by [19] [19].

Alternative integrated LNA+SHIRM topologies have been explored through various options as shown in and summarised in Table 13. The first option kept the waveguide coupler and was the one utilised in WP1, the second changed the RF coupler into an on-chip coupler, drastically reducing package size, as mentioned in section 5.2.1, and the final is the balanced amplifier approach as detailed in section 5.2.2.

Other parts have been considered for package integration, such as the tripler, which has historically shown to be a very reliable part. The downside to tripler integration is that it would complicate the mixer design with possible interference between the tripler and the mixer. Additionally, integration of an IF amplifier has been considered, which would provide additional gain at a critical point of the receiver chain, with the downside of increasing power dissipation from the block substantially. Finally, thought has been given to integration of an initial LNA stage, which when coupled with the balanced amplifier approach, could be used to eliminate the need for an isolator between each of these LNA stages. The drawback would be that pre-selection of the LNA MMICs would be important, as the ability to easily pair packaged amplifiers by performance would be removed. This would require good probe station capabilities.

Adopting a balanced approach, as seen in section 5.2.2 and placing an LNA MMIC with each of the diode mixers within the SHIRM structure, offers some attractive upsides such as the potential for on-chip integration of LNA MMIC and mixer. Introducing the balanced amplifier topology to the LNA+SHIRM should provide very good input reflection coefficient on the RF port. The implementation of the RF hybrid coupler in this option will consider the findings of the first two integration options of this study. A waveguide hybrid will offer the best performance but will limit the miniaturization potential. This will be less of a factor at higher frequencies as the size of the hybrid is reduced. An on-chip hybrid will reduce the size of the LNA+SHIRM integration and offer the possibility for future on-chip integration, however the performance trade off to enable this may become prohibitive at higher frequencies.

Finally, the TCM has been shown to have promise for on-MMIC integration of a mixer and LNA. Good simulation results have been shown, with approximately 3 to 9.5 dB of conversion gain. Chips have been fabricated and are ready for testing.

6. Forward Look

Based on the work during this project it is clear that the route towards an integrated receiver is heavily dependent on aspects such as the operating frequencies and whether a single pixel or multi-pixel receiver is desired. In this section, the need for MMIC pre-selection is discussed, followed by suggestions on two routes forward for this research, one with the end goal of an integrated single pixel receiver for higher frequencies (such as ALMA Band 4+5), and a second with a focus on FPA receivers.

Looking at the outcome of WP1, section 3, the need for good MMIC pre-selection techniques is very clear should a fully integrated front end be a goal. As can be seen in Figure 3, a cascaded pair of UoM 3 stage ALMA Band 2 LNAs at 15 K can achieve a noise temperature of 26.02 K. The noise temperatures of the LNA+SHIRM achieved in WP1, measured at 20 K, were approximately 50 K and 80 K, reducing to 27 K and 27.6 K when a 26 K LNA is used as a first stage. In each of these cases the noise will be largely dominated by the initial LNA stage; however, it should be noted that the mixer will have a much higher contribution to the noise temperature than a second LNA stage would have, so directly comparing the results in Figure 3 with those in section 3.4 is unfair. The results in section 3.4 show a large amount of variance, which presents a challenge to overcome when integrating the initial LNA stage, since with integrated design, high performing MMICs cannot be chosen post-packaging. Any route forward for further receiver integration will have to address this issue. Some possible options include analysis to find areas of a given wafer which MMICs can be taken from giving higher chances of good performance; probing of individual MMICs prior to packaging on a cryogenic probe station could give more confidence whether a MMIC will perform well when packaged; possible simulation using results of MMICs measured on a cryogenic probe station could also be a way towards better packaged performance.

For ALMA Band 4+5, receiver integration can provide an increase in performance, as the spacing between components can be smaller and therefore there are fewer losses. With a modular approach, each package has a minimum size due to waveguide flanges, which at lower frequencies are less of an issue, but as frequencies increase and wavelengths get shorter, these can start to look relatively large. Through integration into a single package, spaces between components can be reduced, and loss can be reduced with it. UoM have already designed MMIC amplifiers covering the range 125 – 211 GHz (corresponding to ALMA Band 4+5) in a project funded through the ESO Development programme. These have been manufactured, Figure 75, and promising room temperature performance has been demonstrated. Cryogenic measurements are scheduled for winter 2025/2026. With the completion of WP2, it would be a very natural progression to make an ALMA Band 4+5 LNA+SHIRM.

For an ALMA Band 4+5 LNA+SHIRM, waveguide couplers are likely still the best option, as they exhibit lower insertion loss than on-chip couplers, and the space they take up inside the package is less of a problem. This is because as frequencies get higher, the waveguide structures are smaller, and with, for example, ALMA Band 4+5, the RF and LO frequencies will both be high enough that the space saving from on-chip couplers is not substantial enough to warrant any drop in performance. As an ALMA Band 4+5 upgrade would be a single pixel, the size of the package which the receiver parts are integrated within is less of an issue.

Additionally, further work towards on-MMIC integration, through technologies such as the TCM, can reduce the number of required bond wires, which at ALMA Band 4+5 frequencies are a large source of loss, even when kept short.

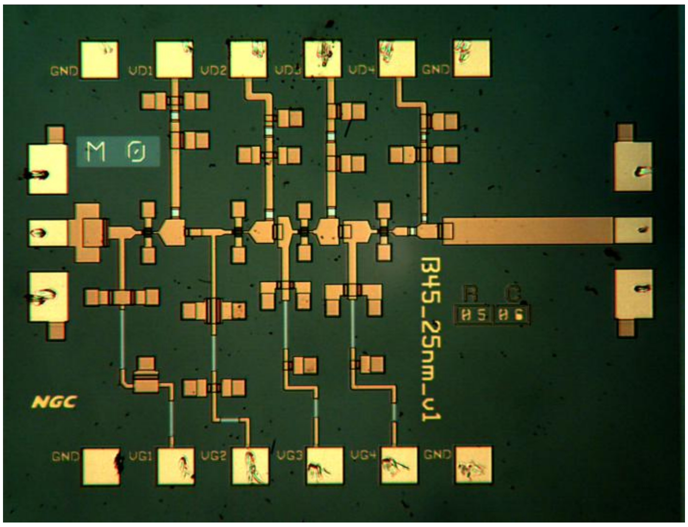

Figure 75 - Photo of a UoM designed ALMA Band 4+5 LNA MMIC

Another route for this research is receiver integration for multi-pixel receivers, PAFs or FPAs. For both of these, many receiver chains are required, often in as small of a package as possible due to size limitations for optimal positioning of the feedhorns, as outlined in section 2. In these cases, the space saving is imperative. As described in section 5.1, on-chip couplers would be a priority going forwards. Additionally, the balanced amplifier approach, as detailed in section 5.2.2, could remove the need for isolators between LNAs due to the increase in input matching performance, saving further space. Furthermore, integration of the on-chip couplers with a balanced amplifier could move this area closer to a SHIRM on-chip, with potential to merge a balanced amplifier setup with a TCM topology, leading to a balanced TCM. A balanced TCM would have the potential of very good input reflection coefficients, alongside exhibiting conversion gain instead of loss, and minimal mismatches between stages.

7. Summary

The *TASER* project has successfully demonstrated the feasibility and benefits of integrating receiver components, with considerations to both multi and single pixel receivers. Two hardware deliverables, an ALMA Band 2 LNA+SHIRM and a Band 4–5 SHIRM, were designed, manufactured, and tested at RAL. The integrated ALMA Band 2 LNA+SHIRM units maintained excellent noise performance, with Block A and Block B achieving noise temperatures of approximately 80 K and 50 K respectively during cryogenic tests. When paired with a UoM 3 stage ALMA Band 2 first stage LNA (taking 17 dB of gain and 26 K noise temperature as representative), system noise temperature are 27 K and 28 K, showing that the *TASER* LNA+SHIRMs only add 1 or 2 K of noise. These results confirm that integration does not compromise receiver performance, offering a clear pathway towards miniaturisation. MMIC pre-selection as discussed in section 6 is very important moving forward should an initial LNA stage wish to be integrated, considering the variance in LNA performance.

The Band 4–5 SHIRM showed consistent behaviour across devices and LO frequencies with balanced sideband performance and predicted improvements at cryogenic temperatures. Its compact design and low LO power requirement show promise, with future work on integrating it with UoM's ALMA Band 4+5 LNAs planned.

Beyond hardware, the feasibility study explored integration strategies, including on-chip couplers, alternative LNA+SHIRM topologies, and additional component integration such as triplers and IF amplifiers. Additionally, on-chip LNA and mixer integration was shown to be promising through the TCM topology, which has been simulated, fabricated, and is awaiting testing. Simulated performance showed 3 to 9.5 dB of conversion gain. While each approach presents trade-offs in complexity, performance, power dissipation, and manufacturability, the findings highlight multiple viable routes for further receiver integration.

Overall, *TASER* has delivered both practical hardware and a clear roadmap for next-generation receiver development. Continued research should focus on MMIC pre-selection techniques, refining on-chip integration techniques, optimising balanced amplifier architectures, and addressing manufacturing challenges to enable compact, high-performance solutions for future radio astronomy instrumentation.

8. Bibliography

[1] University of Manchester and STFC Rutherford Appleton Laboratory, "TASER: Towards ALMA System on Chip European Receivers," 2023.

[2] J. Carpenter, D. Iono, F. Kemper and A. Wootten, "The ALMA Development Program: Roadmap to 2030," *Monthly Newsletter of International URSI Commission J Radio Astronomy,* 29 January 2020.

[3] P. Yagoubov, T. Mroczkowski, V. Belitsky, D. Cuadrado-Calle, F. Cuttaia, G. A. Fuller, J.-D. Gallego, A. Gonzalez, K. Kaneko, P. Mena, R. Molina, R. Nesti, V. Tapia, F. Villa, M. Beltrán, F. Cavaliere, J. Ceru, G. E. Chesmore and K. Coughl, "Wideband 67−116 GHz receiver development for ALMA Band 2," *Astronomy & Astrophysics,* vol. 634, no. A46, 2020.

[4] M. A. McCulloch, M. D'Cruze, K. Grainge, M. Keith and S. Melhuish, "An S-band cryogenic phased array feed for radio astronomy," *RAS Techniques and Instruments,* vol. 2, no. 1, pp. 432-440, 2023.

[5] D. Cuadrado-Calle, D. George, G. A. Fuller, K. Cleary, L. Samoska and P. Kangaslahti, "Broadband MMIC LNAs for ALMA Band 2+3 With Noise Temperature Below 28 K," *IEEE Transactions on Microwave Theory and Techniques,* vol. 65, no. 5, pp. 1589-1597, 2017.

[6] N. Daghestani, H. Wang, B. Alderman, N. Brewster, E. Gallagher and A. Obeed, "Extended-W-band Single Pixel for Cryogenic Array Receiver for Users of the Sardinia Observatory (CARUSO) Astronomical Instrument," in *4th URSI Atlantic Radio Science Meeting (AT-RASC)*, Meloneras, 2024.

[7] N. Estella, L. Bui, E. Camargo and J. Schellenberg, "35nm InP HEMT LNAs at E/W-Band Frequencies," in *IEEE Compound Semiconductor Integrated Circuit Symposium (CSICS)*, Austin, 2016.

[8] Marki Microwave, "MQS-0418CH," Marki Microwave, San Jose, 2018.

[9] J. Carpenter, C. Brogan, D. Iono and T. Mroczkowski, "The ALMA2030 Wideband Sensitivity Upgrade," arXiv e-prints, 2022.

[10] Marki Microwave, "MQS-0218CH," Marki Microwave, 01 08 2018. [Online]. Available: https://shop.markimicrowave.com/products/detail/mqs0218ch-marki-microwave/693009/. [Accessed 14 10 2025].

[11] M. Leffel and R. Daniel, “The Y Factor Technique for Noise Figure Measurements,” Rhode and Schwarz, 2021.

[12] A. R. Kerr, S. K. Pan and J. E. Effland, “ALMA Memo 357,” 2001 March 2001. [Online]. Available: https://legacy.nrao.edu/alma/memos/html-memos/alma357/memo357.pdf. [Accessed 14 October 2025].

[13] M. Pospieszalski, A. Kerr and J. Mangum, “On the Instantaneous SIS Receiver Bandwidth,” National Radio Astronomy Observatory, Charlottesville, USA, 2016.

[14] J. Carpenter, D. Iono, L. Testi, N. Whyborn, A. Wootten and N. Evan, “The ALMA Development Road Map,” ALMA, 2018.

[15] E. Alfonso, A. Zaman and E. Pucci, “Gap waveguide components for millimeter-wave systems. Couplers, filters, antennas, MMIC packaging,” in *International Symposium on Antennas and Propagation, ISAP* , Nagoya, Japan, 2012.

[16] N. M. Giang and L. D. Manh, “A Simple Approach for Improving Bandwidth and Isolation of Wilkinson Power Divider,” *Radioengineering,* vol. 31, pp. 224-230, 2022.

[17] L. H. Chua, A. C. Ng, G. I. Ng, H. Wang, J. Zhou and H. Nakamura, “Design and analysis of coplanar Lange coupler for millimetre-wave applications up to 90 GHz,” in *Asia-Pacific Microwave Conference Proceedings*, Sydney, Australia, 2000.

[18] Keysight Technologies, Discrete and Microstrip Coupler Design, Santa Rosa: Keysight Technologies, 2021.

[19] C. M. Cooke, M. Duffy, M. Fordham, M. Eller, A. Escorcia and W. Deal, “On-Chip Hybrid Couplers Enabling Highly Integrated MMIC Components at Millimeter and Submillimeter Wave Frequencies,” in *IEEE/MTT-S International Microwave Symposium - IMS 2024*, Washington, DC, USA, 2024.

[20] W. McGenn, E. Franks, G. A. Fuller and D. George, “Development of Broadband On-Chip Hybrid Couplers for Millimetre and Submillimetre-Wave Receivers,” in *ISSTT*, Berlin, 2025.

[21] Keysight, “MLANG (Microstrip Lange Coupler),” Keysight, Santa Rosa, CA, USA, 2024.

[22] R. Hesper, A. Khudchenko, A. Baryshev, J. Bharkhof and F. Mena, “A new high-performance sideband-separating mixer,” in *Proceedings of SPIE - The International Society for Optical Engineering*, Cologne, Germany, 2017.

[23] J.-C. Kao, K.-Y. Lin, C.-C. Chiong, C.-Y. Peng and H. Wang, "A W-band High LO-to-RF Isolation Triple Cascode Mixer With Wide IF Bandwidth," *IEEE Transactions on Microwave Theory and Techniques,* vol. 62, no. 7, pp. 1506-1514, 2014.

[24] S.-H. Weng, C.-C. Chiong, C.-C. Chang, H.-L. Wu, Y.-D. Huang and Y.-J. Hwang, "A 35–50 GHz triple cascode mixer module with intermediate frequency of 4–12 GHz based on low noise GaAs PHEMT process," in *IEEE International Symposium on Radio-Frequency Integration Technology*, Taipei, 2016.

[25] J.-C. Kao, C.-F. Chou, C.-C. Chiong, C.-C. Chuang and H. Wang, "A high LO-to-RF isolation 32–52 GHz triple cascode down-conversion mixer with 2–12 GHz IF bandwidth for ALMA band-1," in *Asia-Pacific Microwave Conference*, Sendai, 2014.

[26] C.-N. Chen, Y.-H. Lin, Y.-C. Chen, C.-C. Chiong and H. Wang, "A High LO-to-RF Isolation 34–53 GHz Cascode Mixer for ALMA Observatory Applications," in *IEEE/MTT-S International Microwave Symposium*, Philadelphia, 2018.

[27] D. White, W. McGenn, D. George, G. A. Fuller, K. Cleary, A. Readhead, R. Lai and G. Mei, "125 - 211 GHz low noise MMIC amplifier design for radio astronomy," *Experimental Astronomy,* vol. 48, pp. 137 - 143, 2019.